Taylor meshless method for thin plates

Haitao Tian

HESAM UNIVERSITÉ

Arts et Métiers Sciences et Technologies

2019-ENAM-0036

École doctorale n° 432 : Science des Métiers de l'ingénieur

Doctorat

T H È S E

pour obtenir le grade de docteur délivré par

l'École Nationale Supérieure d'Arts et Métiers

Spécialité " Mécanique - matériaux "

présentée et soutenue publiquement par

Haitao TIAN

le 06 décembre 2019

Taylor Meshless Method for Thin Plates

Directeur de thèse : **Farid ABED-MERAIM**

Co-encadrement de la thèse : **Michel POTIER-FERRY**

Jury

M. Hamid ZAHROUNI, Professeur, Université de Lorraine, France	Président
M. Fan XU, Professeur, Fudan University, Shanghai, China	Rapporteur
M. Noureddine DAMIL, Professeur, Université Hassan II de Casablanca, Maroc	Rapporteur
M. Yao KOUTSAWA, Chercheur (HDR), LIST, Luxembourg	Examinateur
M. Farid ABED-MERAIM, Professeur, Arts et Métiers, France	Examinateur
M. Michel POTIER-FERRY, Professeur, Université de Lorraine, France	Examinateur

Arts et Métiers ParisTech - Campus de Metz

Laboratoire d'Étude des Microstructures et de Mécanique des Matériaux (LEM3)

UMR CNRS 7239

T H È S E

Acknowledgments

I would like to express my sincere appreciation to my supervisor Professor Michel POTIER-FERRY for his great patience and continuous guidance on my PhD study. His immense knowledge and support light up my research career in difficult days. I deeply thank my supervisor Professor Farid ABED-MERAIM for his responsible supervision and valuable suggestions and encouragement. Without his guidance and persistent help this dissertation would not have been possible.

Many thanks to the organization China Scholarship Council (CSC). The funding from my country supports my study and living in France.

I really appreciate the help from my colleagues Peng WANG, Jie YANG, Hocine CHALAL, Mohamed BEN BETTAIEB, Holanyo Koffi AKPAMA, etc. I also thank my Chinese friends for the memorable days we have had together in the past few years.

Last but not the least, I would like to express my gratitude to my parents and my girlfriend for their sacrifices and spiritual support. The encouragement from them is the strength that sustains me thus far.

I would like to thank all the people who helped me all the way.

Contents

Contents ..... **i**

List of Tables and Figures ..... **iii**

Chapter 1 Literature review on meshless methods **1**

1.1 Research background 1

1.1.1 Finite difference method 2

1.1.2 Finite element method 3

1.1.3 Boundary element method 5

1.2 Meshless methods 5

1.2.1 Approximation approaches of field functions 6

1.2.2 Galerkin formulation and collocation formulation 10

1.2.3 Taylor Meshless Method 14

1.3 Organization of the thesis 15

Chapter 2 Techniques of Taylor Meshless Method **17**

2.1 Introduction 17

2.2 Resolution of partial differential equations 17

2.3 Treatment of boundary and interface conditions 20

2.4 Application to 2D Laplace equation 22

2.5 Application of TMM to Kirchhoff plate problems 24

2.5.1 Calculation of the shape functions 25

2.5.2 Kirchhoff plate problem with a circular domain 29

2.5.3 Kirchhoff plate problem with a rectangular domain 31

2.6 Application of TMM to sandwich plates 35

2.6.1 The loading and the governing equation 35

2.6.2 Exact solution 35

2.6.3 The properties of each case 35

2.6.4 Results 37

2.7 Conclusion 41

Chapter 3 Application of TMM to large deflection of thin plates 42

3.1 Introduction 42

3.2 Governing equations 44

3.3 Combination of TMM and ANM 45

3.3.1 The procedure of ANM 45

3.3.2 TMM formulation 48

1.1.1 Treatment of boundary and interface conditions 50

3.4 Results and discussion 54

3.4.1 Buckling of a square plate with movable edges 55

3.4.2 Bending of a square plate with immovable edges 57

3.4.3 Buckling of a square plate with immovable edges under uniaxial compression 59

3.5 Conclusion 63

Chapter 4 Application of TMM to wrinkling of membranes under shear loading 64

4.1 Introduction 64

4.2 Modelling of the membrane boundary value problem 65

4.3 Numerical Results 69

4.3.1 Generation of membrane wrinkles 69

4.3.2 Sensitivity with respect to the number of subdomains 71

4.3.3 Sensitivity with respect to tension loads 72

4.3.4 Imperfection sensitivity 79

4.4 Conclusion 80

Conclusions and future works 82

References 84

Résumé en français de la thèse 94

List of Tables and Figures

Table 2.1 Organization of the computation 28

Table 2.2 Deflection and moment of the center of a rectangular plate, clamped edges, uniform load..... 34

Table 3.1 Deflection and membrane stress at the center of plate vs. load $\bar{p}$ 58

Table 3.2 Displacement load values when the displacement of center point $\bar{w} = 1$, convergence with mesh refinement and with the degree 62

Table 4.1 Material property 67

Table 4.2 Sensitivity of the response (number of wrinkles) to the number of sub-domains. Pre-tension $\delta v = 0.02$ mm, imperfection 0.001mm. 72

Table 4.3 Number of wrinkles with different tension loads. 73

Table 4.4 The maximum displacements and amplitudes of center wrinkles, shear load 0.15mm, imperfection 0.001mm..... 74

Table 4.5 Sensitivity of the response (number of wrinkles) to the imperfection. Pre-tension $\delta v = 0.02$ mm, number of sub-domains: 33×11. 80

Figure 1.1 The procedure of scientific computation 1

Figure 1.2 The cover of the domain by kernel functions 7

Figure 1.3 Background grid of EFGM for integration 12

Figure 1.4 Domains and boundaries in MLPG 13

Figure 2.1 One domain with Dirichlet and Neumann boundary conditions 20

Figure 2.2 Multidomains and the interface 21

Figure 2.3 Distribution of collocation points 23

Figure 2.4 The influence of the number of collocation points for Eq.(2.25), N=10, 20, 30 24

Figure 2.5 The influence of the degree N for Eq.(2.25), $M = 4N$ 24

Figure 2.6 A circular Kirchhoff plate with clamped edges 29

Figure 2.7 The influence of the number of collocation points on the convergence for circular Kirchhoff plate..... 30

Figure 2.8 The convergence of TMM for circular Kirchhoff plate 31
Figure 2.9 Rectangular domain and collocation points on the boundaries 31
Figure 2.10 The distribution of the deflection from Eq.(2.42) 32
Figure 2.11 The influence of the number of collocation points on the convergence for rectangular Kirchhoff plate 33
Figure 2.12 The convergence of TMM for rectangular Kirchhoff plate 33
Figure 2.13 The distribution of the deflection of a clamped Kirchhoff plate 34
Figure 2.14 Fiber directions and thickness of each case 37
Figure 2.15 The coordinate system and expansion point 37
Figure 2.16 The influence of the degree on the convergence, Case1 38
Figure 2.17 The influence of the number of collocation points on the convergence, N = 16, Case1 38
Figure 2.18 The influence of the degree on the convergence, Case2 39
Figure 2.19 The influence of the number of collocation points on the convergence, N = 16, Case2 39
Figure 2.20 The influence of the degree on the convergence, Case3 40
Figure 2.21 The influence of the number of collocation points on the convergence, N = 16, Case3 40
Figure 2.22 The influence of expand point on the convergence 41
Figure 3.1 A square and simply supported plate with boundary collocation points 50
Figure 3.2 A square plate with immovable edges 51
Figure 3.3 Effect of small perturbations on the buckling of a simply supported square plate. The ANM-TMM algorithm is compared with a commercial finite element code. On the ANM-TMM curve, each point corresponds to one ANM step 55
Figure 3.4 A zoom of Figure 3.3. One sees that the ANM-TMM method permits to compute easily quasi-perfect bifurcations. On the ANM-TMM curve, each point corresponds to one ANM step. 56
Figure 3.5 h-convergence: decimal logarithm of the error on the bifurcation stress, according to the degree P and to the number of subdomains. 56

Figure 3.6 Deflection at the center of plate vs. load $\bar{p}$ 57
Figure 3.7 A square plate with immovable edges 59
Figure 3.8 Displacement of center point of the plate vs. load, degree of TMM 8, order of ANM 10 60
Figure 3.9 The deformation of the plate at point A, B, C, D in Figure 3.8 60
Figure 3.10 Comparison of results by FEM and TMM with degree 8 and 10 61
Figure 3.11 The deformation of the plate at point E in Figure 3.10 61
Figure 3.12 Displacement load values when the displacement of center point is 1... 62
Figure 4.1 Rectangular membrane with tension δv and shear load δu 67
Figure 4.2 Steps of the algorithm 67
Figure 4.3 An imperfection sample 68
Figure 4.4 Imperfection of the membrane for wrinkling, tension load 0.02mm, imperfection 0.001mm. 70
Figure 4.5 Full wrinkled membrane, 33×11 domains, tension load 0.02mm, imperfection 0.001mm. 70
Figure 4.6 Full wrinkled membrane. Subdomains: 21×11, tension load 0.02mm, imperfection 0.001mm, shear load 0.15mm. 72
Figure 4.7 Wrinkle patterns with different tension loads. 73
Figure 4.8 Shear load vs maximum displacement, tension loads from 0.0005mm to 0.08mm, imperfection 0.001mm. 74
Figure 4.9 A zoom of the buckling curve, tension load 0.05mm. 75
Figure 4.10 Deformations of the membrane with different shear loads, tension load 0.05mm. 76
Figure 4.11 A zoom of the buckling curve, tension load 0.001mm. 77
Figure 4.12 Deformations of the membrane with different shear loads, tension load 0.001mm. 77
Figure 4.13 A zoom of the buckling curve, tension load 0.0005mm. 78
Figure 4.14 Deformations of the membrane with different shear loads, tension load 0.0005mm. 79

Chapter 1 Literature review on meshless methods

1.1 Research background

Numerical simulation on computers has become an important tool to study and predict the behavior of physical systems, especially for those who cannot provide analytical solutions, as in most nonlinear systems [1]. The procedure of scientific computation and solving technical problems consists of several steps, as shown in Figure 1.1.

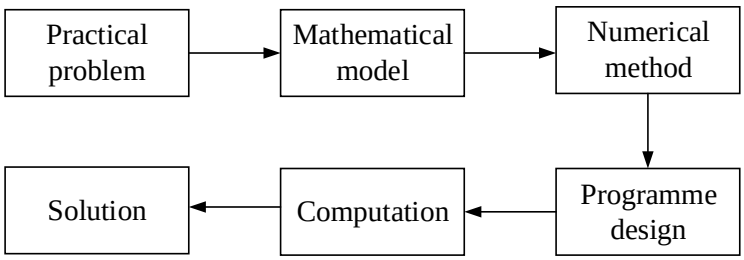

Figure 1.1 The procedure of scientific computation

The premise and basis of scientific computation is modeling practical problems based on scientific theory, mathematical theory and some reasonable assumptions. However, the key of the procedure is to obtain solutions of mathematical models which can meet accuracy requirements using computers. This is a new branch of mathematics - Numerical Analysis, including function interpolation, numerical differentiation and integration, solving systems of linear and nonlinear equations, calculation of matrix eigenvalues and eigenvectors, computational methods for optimization problems, numerical solutions of ordinary differential equations and partial differential equations, etc. It also involves theoretical research on reliability of computational methods, such as convergence, stability and error estimation.

Numerical analysis is applied widely in fundamental industrial production and researches of the most advanced science and technology. It provides an alternative way of scientific investigation besides theoretical solutions and expensive,

time-consuming experiments, becoming essential in optimization design of mechanical and electrical products, geological exploration and oilfield development, weather forecast and earthquake prediction, development of cutting-edge weapons and aerospace. Furthermore, it has infiltrated into different science fields, generating interdisciplinary subjects such as computational physics, digital image processing and econometrics.

On this background, computational mechanics is formed by the interdisciplinary of numerical analysis and mechanics, which deals with the use of computational methods in engineering practices to study physical phenomena governed by the principles of mechanics [2]. Over the past few decades, it has shown huge potential for the application on physical and biological systems based on classical mechanics, quantum mechanics and biology. The computational mechanics are extended to the areas of mechanics, mathematics, computer science, making a significant contribution in the design and simulation of new products because of the advantages of convenience, effectiveness and high efficiency. The computational method has become one of the most important tools in engineering and science, covering various topics including thermal, fluid, solid mechanics, vibration, and vehicle dynamics.

Among numerous computational methods in computational mechanics, the most popular ones are finite difference methods (FDM), finite element methods (FEM) and boundary element methods (BEM). They are widely used for solving engineering problems, especially finite element methods. However, despite of widespread applications, they have their own shortcomings and limitations. The advantages and disadvantages of these methods are introduced and detailed in this section.

1.1.1 Finite difference method

The finite difference methods (FDM) is one of the most traditional and simplest methods for solving differential equations by approximating them with difference equations, in which finite differences approximate the derivatives [3].

FDM solves the original linear or nonlinear differential equations by converting them into a linear system, which can be solved by matrix techniques. The finite difference approximation began to develop rapidly with the widespread use of computers. The accuracy, stability and convergence of FDM are well studied during the last few decades. The calculation format and program design are intuitive and simple, making it an important tool in computational mathematics and computational physics.

In FDM, one pays attention to the corresponding functional values of the discrete independent variables, neglecting the feature that independent variables are continuous in differential equations. The derivatives in the equations are replaced by differential quotients. For the one-dimensional case, the derivative of a function u at a point $x \in R$ is defined as

$$u'(x) = \lim_{h \to 0} \frac{u(x+h) - u(x)}{h} \tag{1.1}$$

Nevertheless, the desirable computational accuracy can still be obtained by reducing the interval of discrete variables or interpolating the functional values of discrete points. In other words, the approximation can be improved by using a smaller h. The discretization error of the approximate solution comes from the error that is committed by going from a differential operator to a difference operator.

Despite of the simplicity of FDM, it needs a regular mesh of grids, which limits the application to problems with regular geometry and simple boundary conditions. The treatment quickly becomes complicated when adding some complexities like moving boundaries or adaptive mesh grid. Researchers have improved FDM by proposing Generalized Finite Differences, making it possible for problems with irregular node distribution. However, the bad conditioning is still a problem for dense meshes [4].

1.1.2 Finite element method

Finite element method is a very efficient tool for solving complex differential

equations. The fundamental principle of finite element analysis is to discretize the continuous domain into a family of discrete subdomains by mesh discretization. In 1960, Clough proposed “Finite Element Method” and used it to solve plane elastic problem [5, 6]. In 1967 Zienkiewicz and Cheung published the first book on finite element analysis [7]. FEM was used to solve nonlinear and large deformation problems after 1970. With the development of computer technology, many computational software have been developed based on the principle of finite element method, some famous of which are ABAQUS, ANSYS, MSC/NASTRAN and IDEAS.

In FEM, a continuous domain is discretized into finite elements. Then, the relation of forces and displacements on all nodes is obtained by element and integral analysis. Stress, strain and other fields of each element are computed by introducing boundary conditions. FEM does not require high continuity of the interpolation functions due to the weak form of the equivalent integral of differential equations. Because of the computational stability and high applicability, FEM can deal with complex geometry, boundary conditions and material properties.

Although FEM has many advantages and has been applied in many scientific fields, it has some inherent shortcomings:

(1) FEM has difficulties in dealing with some complex problems. These problems mainly include: extremely large deformation problems; dynamic crack propagation problems; high-speed impact and geometric distortion problems; material fission problems; metal material forming problems; multi-phase transformation problems, etc. When analyzing these problems with FEM, large mesh distortion or element splitting may bring difficulties or even failure in numerical computation.

(2) In finite element analysis, meshing consumes too much time. In addition, FEM needs complex post processing because it adopts low-order shape functions, which leads to relatively lower accuracy.

1.2 Meshless methods

Classical numerical methods have some troubles when dealing with some practical problems, such as high velocity impact, material molding, dynamic crack propagation, discontinuity problems, fluid-solid coupling and adaptive problems. In recent decades, new generation of computational methods - meshless methods - have been developed as they are expected to be better than mesh-based FDM and FEM in many applications[8]. Similar to conventional FEM, FDM and finite volume methods, meshless methods are actually a tool for solving partial differential equations that govern physical phenomena [9].

In the finite difference method and the finite element method, the spatial domain is discretized by predefined grids and meshes, providing a relationship between the nodes. The PDEs defined in the domain are discretized by a system of algebraic equations based on the grids and meshes. In meshless methods, the solving process consists of two steps: the approximation of field functions and the discretization of governing equations. The approximation functions and their derivatives, depending on the location of discretized points in the domain, are built up without the use of grids or meshes, which means that the relationship between the points is not required. This main advantage makes meshless methods suitable for problems involving large deformation and adaptive meshes, such as high velocity impact, crack propagation and fluid-solid coupling [10].

Gingold and Monaghan [11] applied smooth particle hydrodynamics (SPH) to polytropic stellar models. Lucy [12] used SPH to solve the fission problem for optically thick protostarts. These two papers are considered to be the earliest work on meshless methods. In the past decades, a number of meshless methods have been developed and applied to the corresponding engineering practice based on their own characteristics. They can be classified in terms of different approximation approaches of field functions such as moving least-square (MLS), radial basis function (RBF), kernel particle (KP), point interpolation (PI) and partition of unity

(PU). They can be also classified according to different approaches to discretize the governing equations: the weak-form formulation and the strong-form formulation. One can assemble various types of meshless methods by combining different approximation and discretization approaches.

The basic idea and research status of meshless methods will be introduced hereafter around the approximation approaches of field functions and the discrete approaches of algebraic equations.

1.2.1 Approximation approaches of field functions

The first and most important step in meshless methods is to approximate the field functions and create shape functions of the problem from a cloud of points. The shape functions constructed should be stable, consistent, efficient and independent of the nodal distribution, so that the implementation and the accuracy of the method can be ensured. In this section, various approximations for meshless methods will be recalled.

Kernel particle and reproducing kernel particle approximation

The kernel methods approximate the field function $u(\boldsymbol{x})$ with a kernel function in a domain Ω [13]:

$$u^h(\boldsymbol{x}) = \int_\Omega w(\boldsymbol{x}-\boldsymbol{s},h)u(\boldsymbol{s})d\Omega \tag{1.2}$$

where $u^h(\boldsymbol{x})$ is the approximation, $\boldsymbol{x}$ is a vector in 2D and 3D problems, $\boldsymbol{s}$ is the integral variable, $w(\boldsymbol{x}-\boldsymbol{s},h)$ is the kernel interpolation function. The kernel functions should satisfy the following conditions (see Figure 1.2):

$$\begin{cases} w(\boldsymbol{x}-\boldsymbol{s},h) \geq 0 & \text{in } \Omega_i \\ w(\boldsymbol{x}-\boldsymbol{s},h) = 0 & \text{out of } \Omega_i \\ \int_\Omega w(\boldsymbol{x}-\boldsymbol{s},h)d\Omega = 1 \end{cases} \tag{1.3}$$

Besides, $w(\|\boldsymbol{x}-\boldsymbol{s}\|,h)$ should be a monotonically decreasing function as well as $w(\|\boldsymbol{x}-\boldsymbol{s}\|,h)\to\delta(\|\boldsymbol{x}-\boldsymbol{s}\|)$ when $h\to 0$, where δ is the Dirac-δ function. Common kernel functions include exponential form, cubic spline form and quartic spline form. The integral term on the right side of Eq.(1.2) is discretized with function values on each collocation point satisfying differential equations and boundary conditions.

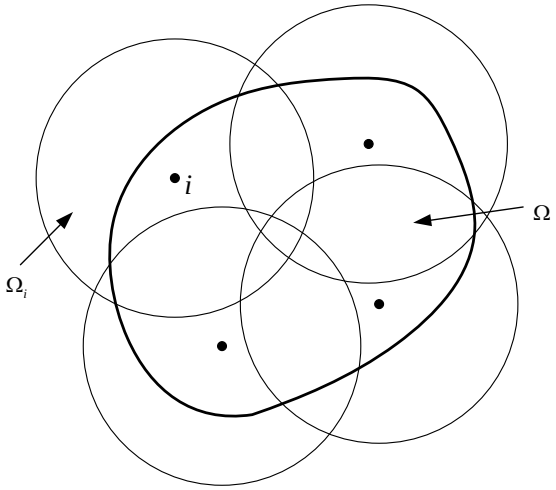

Figure 1.2 The cover of the domain by kernel functions

In 1970s, the kernel approximation was invoked for the first time by Lucy in the smoothed particle hydrodynamics (SPH), which is also the oldest meshless method [12]. This method is successfully applied to the astrophysical field. In 1980s, Monaghan developed SPH to simulate the shocktube phenomena, binary star interactions and magnetohydrodynamics [13-18]. Despite of its versatility and simplicity, the disadvantage of SPH is its limited accuracy that needs plenty of nodes to improve the situation. Nevertheless, the superiority of SPH in fields such as high velocity impact makes it one of the few meshless methods that has been applied in engineering practice.

Liu developed reproducing kernel particle method (RKPM) based on SPH, in which the kernel particle interpolation function consists of a flexible window function and a continuous correction function [19]. It gives more accurate results because of the addition of the correction function. He also proposed multiscale reproducing kernel particle method based on reproducing kernel and wavelet analysis,

implementing adaptive analysis by RKPM [20, 21]. Chen studied hyper-elasticity and elasto-plasticity problems based on RKPM [22]. The results indicated that RKPM is more effective and accurate than FEMs when dealing with large material distortion because of the smoother shape functions. Lin solved time-space fractional diffusion equations in 2D regular and irregular domains using RKPM [23]. Wang proposed a quasi-convex reproducing kernel meshless method, which has better accuracy compared with the conventional RKPM [24].

Moving least-squares approximation

Another approach to construct shape functions in meshless methods is moving least-square (MLS) approximation that was proposed by Lancaster for data fitting [25]. In the domain Ω, the approximation function $u^h(\boldsymbol{x})$ of field function $u(\boldsymbol{x})$ is

$$u^h(\boldsymbol{x})=\sum_{i=1}^{m} b_i(\boldsymbol{x})a_i(\boldsymbol{x})=\boldsymbol{b}^T(\boldsymbol{x})\boldsymbol{a}(\boldsymbol{x}) \tag{1.4}$$

where m is the number of terms in the basis functions $b_i(\boldsymbol{x})$ and $a_i(\boldsymbol{x})$ are the corresponding coefficients. The basis functions should satisfy the following requirements:

$$\begin{cases} b_1(\boldsymbol{x})\equiv 1 \\ b_i(\boldsymbol{x})\in C^l(\Omega)(i=1,2,\cdots,m;l=0,1,\cdots,m) \\ \{b_i(\boldsymbol{x})\}(i=1,2,\cdots,m)\text{ are linearly independent} \end{cases} \tag{1.5}$$

Commonly used bases are the linear basis of complete polynomials. For example, a quadratic basis in 2D is $\boldsymbol{b}^T(\boldsymbol{x})=(1,x,y,x^2,xy,y^2)$. In [26], the trigonometric function was selected as the basis function to solve some 2D elastostatic problems. For singular problems, the characteristic function near the singular point can be used as the basis function [27].

From Eq.(1.4), the quadratic form by a weighted least-square fit with respect to coefficients $a_i(\boldsymbol{x})$ can be obtained:

$$J = \sum_j w\left(\boldsymbol{x} - \boldsymbol{x}_j\right)\left[\sum_{i=1}^{m} b_i\left(\boldsymbol{x}\right) a_i\left(\boldsymbol{x}\right) - u_j\right]^2 \tag{1.6}$$

The coefficients $a_i\left(\boldsymbol{x}\right)$ are obtained by calculating the derivative of *J*. Because $u^h\left(\boldsymbol{x}_j\right) \neq u_j$, the weighted function is smooth and continuous, which brings difficulty to introduce Dirichlet boundary condition. To get MLS approximation with point-passing interpolation character, one can choose singular weighted functions that satisfy $u^h\left(\boldsymbol{x}_j\right) = u_j$.

Nayroles et al proposed the diffuse element method (DEM) firstly using moving least-square approximations in 1992 [28]. By improving DEM, Belytschko et al proposed the famous element-free Galerkin method (EFGM) [29]. With the use of Lagrange multipliers, a large number of quadrature points and modified derivatives of the interpolants, EFGM has a better performance in accuracy and stability than DEM. EFGM was successfully applied to the numerical simulation of crack propagation as it overcame the drawback of FEM in remeshing [30-36]. In the next few years, EFGM was developed and applied to various fields such as contact [37, 38], vibration analysis [39], hydromechanics [40] and heat transfer [41].

Onate and Idelsohn proposed the finite point method (FPM) in 1996, which has been applied to hydromechanics and aerodynamics successfully [42-45]. However, the application of FPM in solid mechanics is limited due the high requirement of point symmetry next to boundary segments [46]. Other meshless method using MLS to construct shape functions include hp-clouds method [47-49] and Meshless Local Petrov-Galerkin Method (MLPG) [50, 51].

Polynomial and radial point interpolation approximation

In MLS approximation, the number of nodes in the neighborhood of point $\boldsymbol{x}$ is larger than the number of basis functions. In general case, the least-square fitting does not pass the points with continuous and nonsingular weighted functions. This brings difficulty for the introduction of Dirichlet boundary conditions. The point

interpolation method (PIM) uses the same number of basis functions and nodes in the neighborhood of point $\boldsymbol{x}$. The shape functions satisfy $u^h\left(\boldsymbol{x}_j\right)=u_j$ on the nodes, making it easy to introduce Dirichlet boundary conditions.

There are two types of basis functions that are used in PIM. Liu and Gu [52] developed PIM by using polynomial basis functions. The interpolation coefficients are constant while they are functions in MLS. Despite of its simplicity, the polynomial PIM may lead to singular moment matrix. Wang and Liu used radial basis functions (RBF) as the interpolation functions and they called it radial point interpolation method (RPIM) [53]. In the conventional RBF meshless method [54-56], the radial basis functions are defined on the global domain and the formed system matrix is full, thus it is not suitable for large scale problems. The algebraic model in RPIM is banded, which is very important for solving partial differential equations. However, the h-convergence of RPIM depends on the selection of RBF's shape parameters.

Other meshless approximation methods include partition of unit approximation [57, 58] and Taylor series [4].

1.2.2 Galerkin formulation and collocation formulation

The second important step in meshless methods is to build the algebraic equations of the discretized model on the basis of approximation functions. There are three typical realizing ways: global Galerkin integration, local Galerkin integration and collocation formulation, where the first two formulations are weak form and the third one is strong form.

Global Galerkin formulation

A weak form formulation requires weaker consistency on the approximation functions for variables compared with a strong form formulation [10]. Formulation based on weak forms produces a stable set of algebraic equations and leads to more accurate results with the discretized system.

Consider the plane elasticity problem in the domain Ω:

$$\begin{cases} \nabla \cdot \boldsymbol{\sigma} + \boldsymbol{f} = 0 & \boldsymbol{x} \in \Omega \\ \boldsymbol{u} = \bar{\boldsymbol{u}} & \boldsymbol{x} \in \Gamma_u \\ \boldsymbol{\sigma} \cdot \boldsymbol{n} = \bar{\boldsymbol{t}} & \boldsymbol{x} \in \Gamma_t \end{cases} \tag{1.7}$$

where $\boldsymbol{\sigma}$ is the stress tensor, $\boldsymbol{f}$ is the volume force tensor, $\bar{\boldsymbol{u}}$ is the given displacement boundary condition, $\bar{\boldsymbol{t}}$ is the given stress boundary condition, $\boldsymbol{n}$ is the normal vector on the boundary. The equivalent integral form of the equilibrium equation and the stress boundary condition in Eq.(1.7) is

$$\delta\Pi(u_i) = \int_\Omega \delta u_i \left(\sigma_{ij,j} + \bar{f}_i\right) d\Omega - \int_{\Omega_t} \delta u_i \left(\sigma_{ij} n_j - \bar{t}_i\right) d\Gamma_t = 0 \tag{1.8}$$

By using the variation $\delta u_i\big|_{\Gamma_u} = 0$ and the symmetric property of the stress tensor σ_{ij}, Eq.(1.8) is integrated by parts and becomes

$$\delta\Pi(u_i) = \int_\Omega \left(-\delta\varepsilon_{ij}\sigma_{ij} + \delta u_i \bar{f}_i\right) d\Omega + \int_{\Gamma_t} \delta u_i \bar{t}_i d\Gamma_t = 0 \tag{1.9}$$

which is the equivalent integral weak form of Eq.(1.7). The matrix form of Eq.(1.9) is

$$\delta\Pi(\boldsymbol{u}) = \int_\Omega \left(-\delta\boldsymbol{\varepsilon}^T\boldsymbol{\sigma} + \delta\boldsymbol{u}^T\bar{\boldsymbol{f}}\right) d\Omega - \int_{\Gamma_t} \delta\boldsymbol{u}^T\bar{\boldsymbol{t}} d\Gamma_t = 0 \tag{1.10}$$

where

$$\begin{aligned} &\boldsymbol{u} = [u_1, u_2]^T,\ \bar{\boldsymbol{f}} = \left[\bar{f}_1, \bar{f}_2\right]^T,\ \bar{\boldsymbol{t}} = [\bar{t}_1, \bar{t}_2]^T \\ &\boldsymbol{\varepsilon} = \left[\varepsilon_{xx}, \varepsilon_{yy}, 2\varepsilon_{xy}\right]^T,\ \boldsymbol{\sigma} = \left[\sigma_{xx}, \sigma_{yy}, \sigma_{xy}\right]^T \\ &\boldsymbol{\sigma} = D\boldsymbol{\varepsilon} \end{aligned} \tag{1.11}$$

By substituting the approximation function into Eq.(1.10), one can obtain the final discrete algebraic equations. The domain in meshless methods is discretized by nodes and in general, the approximation functions are not polynomials. Therefore, the integral in Galerkin meshless methods is achieved in the ways that differ from FEM. In EFGM [29], the integral for the domain Ω is converted to the integral for each cell of a regular grid that covers the domain, in which Gauss integration is applied (see

Figure 1.3). Even though the cells are simple and arbitrary, EFGM is not a pure meshless method due to the presence of background grid. As Gauss integration is time consuming in dealing with complex problems, Beissel [59] adopted the nodal integration mode, in which the value of the integrand in a neighborhood equals to the value at the node. Compared with the approach in EFGM, the nodal integration largely improves the computational efficiency. However, the accuracy and the stability are decreased in the meantime. Carpinteri [60] proposed the partition of unity quadrature, in which the compact support domain is used as the domain of integration

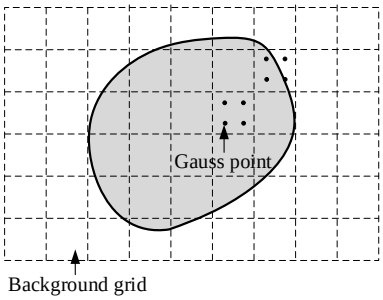

Figure 1.3 Background grid of EFGM for integration

Local Petrov-Galerkin formulation

The implementation of global Galerkin formulation is based on the integration on the whole domain. In general cases, it is difficult to satisfy the equation over the entire problem domain. In the meshless local Petrov-Galerkin (MLPG) originated by Atluri [51], the equation is satisfied point by point and the integration is implemented in a local domain. The equivalent integral weak form of local Petrov-Galerkin at the integration point $\boldsymbol{x}_I$ is

$$\int_{\Omega_{te}^I}\left(\sigma_{ij,j}+f_i\right)\upsilon_i d\Omega-\alpha\int_{\Gamma_{su}^I}\left(u_i-\bar{u}_i\right)\upsilon_i d\Gamma=0 \tag{1.12}$$

where Γ_{su}^I is the intersection of the displacement boundary and Ω_{te}^I (see Figure 1.4), α is the penalty factor for the essential boundary condition.

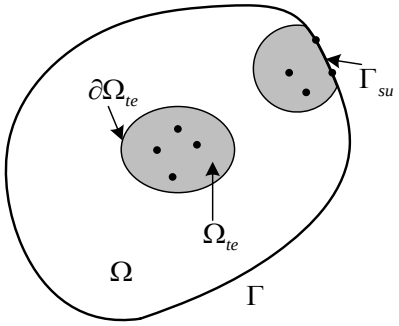

Figure 1.4 Domains and boundaries in MLPG

Collocation formulation

The system of equations developed with Galerkin and local Petrov-Galerkin formulations are weak form system. The integral process and the introduction of the displacement boundary condition are complicated in practical operation. In contrast, the collocation-based meshless methods have no any background grids and are very efficient, making them pure meshless methods. In the collocation formulation, the residual of the PDEs and boundaries on a group of discrete points is forced to be 0:

$$\begin{cases} \nabla\cdot\boldsymbol{\sigma}\left(\boldsymbol{x}_I\right)+\boldsymbol{f}\left(\boldsymbol{x}_I\right)=0 & \boldsymbol{x}_I\in\Omega \\ \boldsymbol{u}\left(\boldsymbol{x}_I\right)=\bar{\boldsymbol{u}}\left(\boldsymbol{x}_I\right) & \boldsymbol{x}_I\in\Gamma_u \\ \boldsymbol{\sigma}\left(\boldsymbol{x}_I\right)\cdot\boldsymbol{n}=\bar{\boldsymbol{t}}\left(\boldsymbol{x}_I\right) & \boldsymbol{x}_I\in\Gamma_t \end{cases} \tag{1.13}$$

The number of collocation points should be larger than the number of algebraic equations as the result might be instable if the two numbers are equal. The error in collocation methods is mainly from the introduction of Neumann boundary condition. Zhang [61] adopted a number of auxiliary points that satisfied the equilibrium conditions to stabilize the solution and improve the accuracy. Liu [62] proposed meshfree weak-strong form method (MWS) by combining the strong form and the weak form, in which the Neumann boundary condition was introduced by local Petrov-Galerkin method. Sadeghirad [63] improved the stability and accuracy of collocation methods by implementing integration on the segments of Neumann boundary.

1.2.3 Taylor Meshless Method

Taylor Meshless Method (TMM) is a boundary type meshless method that is proposed by Zézé et al [64] in 2010. The field equations are approximated with Taylor series and only boundaries are discretized. This method converges fast and requires much less degrees of freedoms than finite element method.

Tampango evaluated the convergence properties of Taylor series [65] and introduced the technique of subdomains in the case of a complex domain [66]. Yang tested both least-square collocation and Lagrange multipliers to account for boundary conditions and solved large-scale 3D problems with TMM [67]. TMM is combined with Newton method to solve non-linear elliptic PDEs in [68].

The approximation method of the field function in TMM is similar to that in point collocated Trefftz methods using general polynomial solutions as shape functions. For constant coefficients linear partial differential equations that have general solutions, the approximation forms of the field function are the same in TMM and Trefftz methods. However, for nonlinear partial differential equations, it is difficult to find the general solution that can satisfy the equations exactly. This is the limitation of Trettfz methods. In TMM, a truncated interruptive Taylor series is introduced into partial differential equations, then the non-independent coefficients are eliminated in the approximate solution. The independent coefficients in the reduced approximate solution are much less than that in the original Taylor series. This is the key advantage of TMM. Although the solution obtained in this way is not the exact solution, the residuals of the equations can be reduced to a very small value by increasing the degree of Taylor series. This treatment can be applied to any kind of elliptic partial differential equations. The governing equation is satisfied by an approximate solution, thus only boundary discretization is needed to obtain the independent coefficients in the approximate solution.

1.2.4 Boundary element method

Boundary element method (BEM) is an efficient numerical analysis method for engineering and scientific problems developed after FEM [69]. Taking the boundary integral equations as the mathematical basis and drawing on the discrete element technique, BEM becomes an important supplement to the FEM in some areas. The discretization is proposed only on boundaries instead of the whole domain. Boundary conditions are approximated with functions that satisfy the governing equations. The dimension of the problem is reduced and the boundary geometry is simulated with simple elements. The analytic fundamental solution of differential operators is used as the kernel function of boundary integral equations.

BEM has some main disadvantages. For complex partial differential equations, it is difficult to obtain the fundamental solution. Boundary singular integral is another tough problem. The coefficient matrix established in BEM is an asymmetric full array, which may limit the extension of problem dimension.

1.3 Organization of the thesis

In this work, a boundary collocation meshless method based on Taylor series – Taylor Meshless Method – is applied to solve linear and nonlinear thin plate problems. The objective is to extend the application of TMM to large deflection problems and study the influence of key parameters, proposing a fast and reliable method for practical engineering. The thesis is structured into five chapters, which are described as follows:

In Chapter 2, the construction of approximate functions and boundary discretization of TMM are introduced. The accuracy and the stability are verified by studying a 2D Laplace equation. Then, TMM is used to solve Kirchhoff plate problems and bidirectional sandwich plate problems, what has not been done before.

In Chapter 3, a new numerical technique for post-buckling analysis is presented by combining the Asymptotic Numerical Method (ANM) and TMM. The accuracy

and efficiency are verified by solving Föppl-von Karman plate problems. The bending and buckling of thin plates are studied with various boundary conditions.

In Chapter 4, the wrinkling of a rectangular membrane is studied. The generation of membrane wrinkles is simulated with a three-step loading procedure. The sensitivity to imperfection, tension load and number of subdomains is tested to find the contribution of each parameter on the wrinkling results.

In Chapter 5, the main conclusions of the current work and some prospects for future work are drawn.

Chapter 2 Techniques of Taylor Meshless Method

2.1 Introduction

The solution process of TMM consists of two basic steps: 1) approximation of the unknown field function; 2) introduction of boundary conditions. By using a Taylor series expansion, the governing equation is satisfied in the domain. The system is largely simplified and solved by applying boundary conditions.

In a previous study by Yang [70], Lagrange multiplier method and least-square collocation were tested to account for boundary conditions. These two methods work well and converge about in the same way. As least-square method is more convenient and efficient to bring exponential convergence, it is used to discretize boundary conditions in this thesis.

TMM solves problems in their strong form in the area without any background mesh. The shape functions are built up with high degree polynomials. With the treatment of partial differential equations, the degrees of freedom are reduced significantly, which can help to increase the degree of polynomials easily. In this chapter, the construction of approximate functions and boundary discretization are detailed introduced in detail. A 2D Laplace equation is solved by TMM to test the efficiency, robustness and sensitivity to parameters. Then, TMM is used to study Kirchhoff plates and bidirectional sandwich plates.

2.2 Resolution of partial differential equations

To introduce the techniques of TMM, we consider the Laplace equation:

$$\begin{cases} \Delta u = 0 & \text{in } \Omega \\ u(x,y) = u^d(x,y) & \text{on } \partial\Omega \end{cases} \tag{2.1}$$

The shape functions are determined by a quasi-exact resolution of the PDE in the

domain. The approximate solution of Eq.(2.1) is expressed in the form of the Taylor series of degree N expanded at a point $X_0 = (x_0, y_0)^T$ near the domain.:

$$u(x,y) = \sum_{m=0}^{N} \sum_{n=0}^{N-m} u(m,n)(x-x_0)^m (y-y_0)^n \tag{2.2}$$

To facilitate understanding, the approximate solution is supposed to be expanded at point (0, 0) with fourth degree polynomial:

$$\begin{aligned} u(x,y) \quad &= u(0,0) + u(0,1)y + u(0,2)y^2 + u(0,3)y^3 + u(0,4)y^4 \\ &+ u(1,0)x + u(1,1)xy + u(1,2)xy^2 + u(1,3)xy^3 \\ &+ u(2,0)x^2 + u(2,1)x^2y + u(2,2)x^2y^2 \\ &+ u(3,0)x^3 + u(3,1)x^3y \\ &+ u(4,0)x^4 \end{aligned} \tag{2.3}$$

where $u(m,n), 0 \le m \le 4, 0 \le n \le 4-n$ are the coefficients of the Taylor series. For the complete polynomial Eq.(2.2), there are 15 coefficients to be found. The second partial derivatives of Eq.(2.3) are given as:

$$\begin{aligned} \frac{\partial^2 u}{\partial x^2}(x,y) &= 2u(2,0) + 2u(2,1)y + 2u(2,2)y^2 \\ &+ 6u(3,0)x + 6u(3,1)xy + 12u(4,0)x^2 \end{aligned} \tag{2.4}$$

$$\begin{aligned} \frac{\partial^2 u}{\partial y^2}(x,y) &= 2u(0,2) + 6u(0,3)y + 12u(0,4)y^2 \\ &+ 2u(1,2)x + 6u(1,3)xy + 2u(2,2)x^2 \end{aligned} \tag{2.5}$$

Eq.(2.4) and Eq.(2.5) can be summarized as:

$$\frac{\partial^2 u}{\partial x^2}(x,y) = \sum_{m=0}^{2} \sum_{n=0}^{2-m} (m+2)(m+1)u(m+2,n)x^m y^n \tag{2.6}$$

$$\frac{\partial^2 u}{\partial y^2}(x,y) = \sum_{m=0}^{2} \sum_{n=0}^{2-m} (n+2)(n+1)u(m,n+2)x^m y^n \tag{2.7}$$

From Eq.(2.1) one knows that the sums of the relevant parts for $x^m y^n$ in Eq.(2.6) and Eq.(2.7) should be zero respectively:

$$(m+2)(m+1)u(m+2,n)+(n+2)(n+1)u(m,n+2)=0 \tag{2.8}$$

where $0 \le m \le 2$, $0 \le n \le 2-m$. Eq.(2.8) indicates that all coefficients are not independent. With initial items $u(0,0)$, $u(0,1)$, $u(0,2)$, $u(0,3)$, $u(0,4)$, $u(1,0)$, $u(1,1)$, $u(1,2)$, $u(1,3)$, the remaining coefficients can be obtained by the recurrence:

$$u(m,n)=-\frac{(n+2)(n+1)}{m(m-1)}u(m-2,n+2) \tag{2.9}$$

In this way, the number of independent coefficients for the PDE is reduced from 15 to 9, which is the amount of initial items. Each initial item α_i corresponds to an independent shape function P_i . The approximate solution is the linear combination of shape functions:

$$u^h=\sum_{k=1}^{9}\alpha_k P_k \tag{2.10}$$

In other words, the equation $\Delta u=0$ has been solved in the sense of Taylor series by vanishing the Taylor coefficients of the residual Δu . Eq.(2.10) is the general form of solution for a homogeneous equation. Vector α is determined by boundary conditions. For inhomogeneous equations, consider Poisson equation for example:

$$\Delta u = f \tag{2.11}$$

The approximate solution for Eq.(2.11) includes two parts: the general solution and a particular solution. To find a particular solution, the right side f is expanded with Taylor series at the degree of $N-2$, which is consistent with Δu .

$$f(x,y)=\sum_{m=0}^{N-2}\sum_{n=0}^{N-m-2} f(m,n)x^m y^n \tag{2.12}$$

From Eq.(2.8) and Eq.(2.12) it can be concluded that:

$$(m+2)(m+1)u(m+2,n)+(n+2)(n+1)u(m,n+2)= f(m,n) \tag{2.13}$$

where $0 \le m \le N-2, 0 \le n \le N-m-2$. The particular solution for Eq.(2.11) can be chosen arbitrarily by setting any initial items satisfied by Eq.(2.13):

$$P_s(x,y) = \sum_{m=0}^{N} \sum_{n=0}^{N-m} u_s(m,n) x^m y^n \tag{2.14}$$

The approximate solution for Poisson equation is in the form:

$$u = \sum_{k=1}^{2N+1} \alpha_k P_k(x,y) + P_s(x,y) = \boldsymbol{P}\{\alpha\} + P_s \tag{2.15}$$

2.3 Treatment of boundary and interface conditions

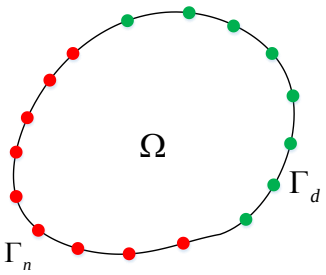

Figure 2.1 One domain with Dirichlet and Neumann boundary conditions

The simplest collocation technique is to choose as many points as shape functions. However, the pure boundary collocation may lead to numerical instabilities. Yang has applied Lagrange multiplier method to account for boundary conditions, which requires additional parameters for radial functions. The least-square collocation is validated as an efficient and robust method in most of the cases that were tested, bringing exponential convergence with few degrees of freedom [65, 67]. That's why least-square is chosen as the collocation method in this thesis.

A set of points is collocated on the boundary of the domain. With M_d points on the Dirichlet boundary Γ_d and M_n points on the Neumann boundary Γ_n, the error between approximate solution and exact solution for the problem in Figure 2.1 is:

$$\begin{aligned} J(\alpha) &= \frac{1}{2} \sum_{\boldsymbol{x}_i \in \Gamma_d} \left\| u^h(\boldsymbol{x}_i) - u^d(\boldsymbol{x}_i) \right\|^2 + \frac{1}{2} \sum_{x_j \in \Gamma_n} \left\| \frac{\partial u^h}{\partial n}(\boldsymbol{x}_j) - g^n(\boldsymbol{x}_j) \right\|^2 \\ &= \frac{1}{2} \sum_{\boldsymbol{x}_i \in \Gamma_d} \left\| \boldsymbol{P}\{\alpha\} + P_s - u^d \right\|^2 + \frac{1}{2} \sum_{x_j \in \Gamma_n} \left\| \boldsymbol{Q}\{\alpha\} + Q_s - g^n \right\|^2 \end{aligned} \tag{2.16}$$

The first part of the right side in Eq.(2.16) corresponds to Dirichlet boundary and the second part corresponds to Neumann boundary. $\boldsymbol{Q}$ is the first derivative of $\boldsymbol{P}$ and Q_s is the first derivative of P_s. The principle is to minimize Eq.(2.16) by making the first partial derivatives of the function zero:

$$\begin{aligned}\frac{\partial J}{\partial \alpha} = &\{\boldsymbol{P}\}^T\{\boldsymbol{P}\}\{\alpha\}+\{\boldsymbol{P}\}^T\{P_s\}-\{\boldsymbol{P}\}^T\{u^d\}+\\ &\{\boldsymbol{Q}\}^T\{\boldsymbol{Q}\}\{\alpha\}+\{\boldsymbol{Q}\}^T\{Q_s\}-\{\boldsymbol{Q}\}^T\{g^n\}=0\end{aligned} \tag{2.17}$$

Eq.(2.17) leads to a linear system:

$$[K]\{\alpha\}=\{F\} \tag{2.18}$$

where

$$[K]=\{\boldsymbol{P}\}^T\{\boldsymbol{P}\}+\{\boldsymbol{Q}\}^T\{\boldsymbol{Q}\} \tag{2.19}$$

$$\{F\}=\{\boldsymbol{P}\}^T\left(\{u^d\}-\{P_s\}\right)+\{\boldsymbol{Q}\}^T\left(\{g^n\}-\{Q_s\}\right) \tag{2.20}$$

The coefficient vector $\{\alpha\}$ can be obtained by solving the linear system Eq.(2.18).

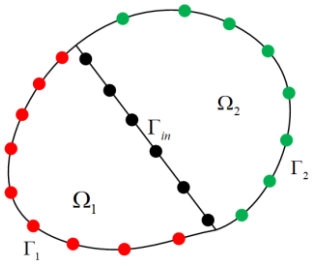

Figure 2.2 Multidomains and the interface

Limited to the convergence radius, one Taylor series is not sufficient to describe a complex problem. Even though one can increase the degree of polynomials to a high level, it is time consuming and may lead to ill conditioning. A better approach is to split the whole domain into several subdomains, in which the equations are approximated with independent Taylor series. The subdomains are coupled by interface conditions that are introduced with a least square collocation[64].

In Figure 2.2, two subdomains Ω_1 and Ω_2 are connected with the interface Γ_{in}. Boundary conditions for each subdomain are introduced independently with the

formulation Eq.(2.16). The interface is collocated with M_{in} points satisfying the following continuity condition:

$$\begin{cases} u^1\left(\boldsymbol{x}_j\right)=u^2\left(\boldsymbol{x}_j\right) \\ \dfrac{\partial u^1}{\partial n}\left(\boldsymbol{x}_j\right)=\dfrac{\partial u^2}{\partial n}\left(\boldsymbol{x}_j\right) \end{cases} \quad \boldsymbol{x}_j \in \Gamma_{in} \tag{2.21}$$

Now the quadratic sum of the error consists of three parts: the boundary conditions for each domain and the continuity condition:

$$J\left(\alpha_1,\alpha_2\right)=J_1\left(\alpha_1\right)\big|_{\Gamma_1}+J_2\left(\alpha_2\right)\big|_{\Gamma_2}+J_{in}\left(\alpha_1,\alpha_2\right)\big|_{\Gamma_{in}} \tag{2.22}$$

where

$$J_{in}\left(\alpha_1,\alpha_2\right)=\frac{1}{2}\sum_{\boldsymbol{x}_j\in\Gamma_{in}}\left\|u^1\left(\boldsymbol{x}_i\right)-u^2\left(\boldsymbol{x}_i\right)\right\|^2+\frac{1}{2}\sum_{x_j\in\Gamma_{in}}\left\|\frac{\partial u^1}{\partial n}\left(\boldsymbol{x}_j\right)-\frac{\partial u^2}{\partial n}\left(\boldsymbol{x}_j\right)\right\|^2 \tag{2.23}$$

To compute the coefficient vector $\{\alpha_1\}$ and $\{\alpha_2\}$, one can minimize Eq.(2.23) by making the first partial derivatives of the function zero respectively:

$$\begin{cases} \dfrac{\partial J}{\partial \alpha_1}\left(\alpha_1,\alpha_2\right)=\dfrac{\partial J_1}{\partial \alpha_1}\left(\alpha_1\right)+\dfrac{\partial J_{in}}{\partial \alpha_1}\left(\alpha_1,\alpha_2\right)=0 \\ \dfrac{\partial J}{\partial \alpha_2}\left(\alpha_1,\alpha_2\right)=\dfrac{\partial J_2}{\partial \alpha_2}\left(\alpha_2\right)+\dfrac{\partial J_{in}}{\partial \alpha_2}\left(\alpha_1,\alpha_2\right)=0 \end{cases} \tag{2.24}$$

2.4 Application to 2D Laplace equation

To test the convergence and the robustness of the method, we consider the Dirichlet problem in a circular domain: $x^2+y^2\le 1$.

$$\begin{cases} \Delta u=0 & \text{in } \Omega \\ u^d\left(x,y\right)=\dfrac{x-x_0}{\left(x-x_0\right)^2+\left(y-y_0\right)^2} & \text{on } \partial\Omega \end{cases} \tag{2.25}$$

The exact solution for the problem is: $\underline{u}^e\left(x,y\right)=\left(x-x_0\right)\Big/\left[\left(x-x_0\right)^2+\left(y-y_0\right)^2\right]$.

To avoid the influence of the singularity, $X_0=\left(x_0,y_0\right)$ is chosen as (1.5, 0.2). The error is the difference between the exact solution and the approximate solution divided by

the maximum value of the solution:

$$Error = \frac{\left|u^e - u^h\right|}{\max\left(\left|u^e\right|\right)} \tag{2.26}$$

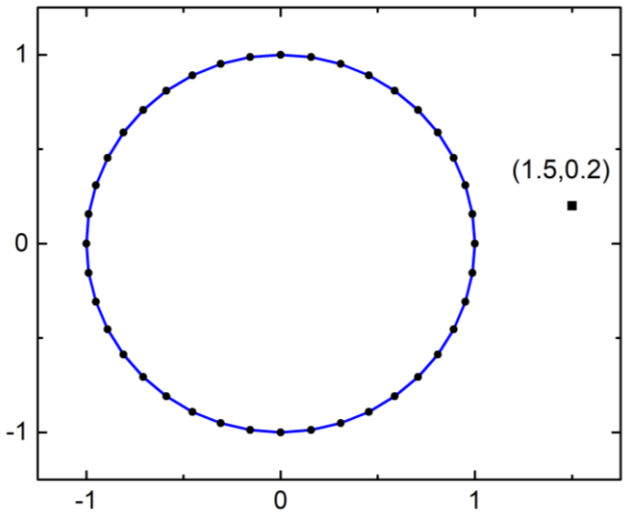

Figure 2.3 Distribution of collocation points

Uniformly distributed collocation points are chosen for the calculation (see Figure 2.3). The Taylor series for this problem are developed at point $(0,0)$. Figure 2.4 is the influence of the number of collocation points for degree N=10, 20 and 30. It can be seen that the results may fluctuate and are not accurate enough if the collocation points are too few. The results become stable if the number of collocation points M is large enough. The degrees of freedom for Eq.(2.25) are $2N$+1, thus M should be more than $2N$+1 because collocation points should be more than the dimension of the vector α in least-square method.

Figure 2.5 shows that the results get accurate with the increase of the degree. The maximal error becomes stable when the degree is more than 85. After that the accuracy stands under 10^{-14}.

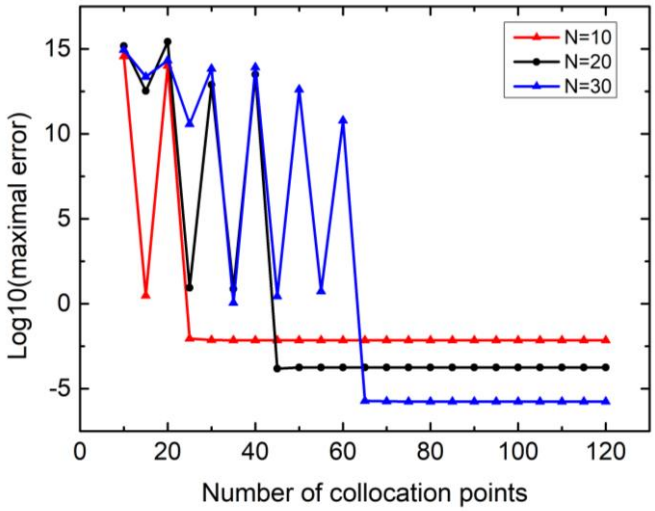

Figure 2.4 The influence of the number of collocation points for Eq.(2.25), *N*=10, 20, 30

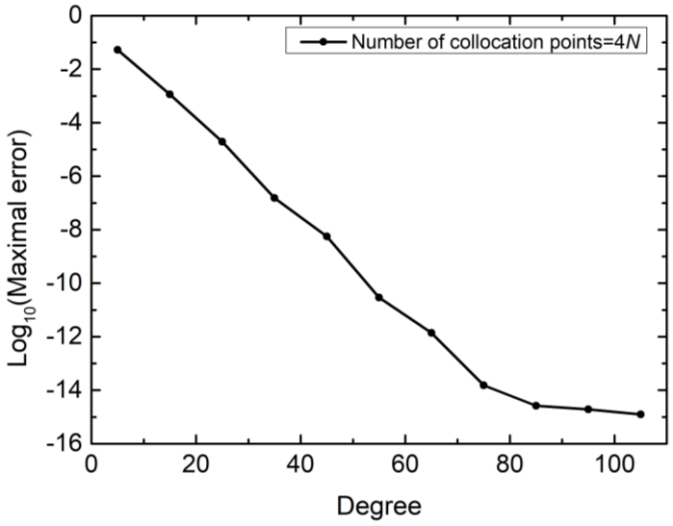

Figure 2.5 The influence of the degree *N* for Eq.(2.25), $M = 4N$

2.5 Application of TMM to Kirchhoff plate problems

The Kirchhoff-Love theory of plates is a two-dimensional model for thin plates with small deflections. It was developed by extending Euler-Bernoulli beam theory in 1888 [71]. This theory makes the following assumptions:

1) The linear strain perpendicular to the middle plane can be disregarded;

2) The middle plane of the plate remains neutral during the deformation;

3) Stress components τ_{xz}, τ_{yz} and σ_z are much less than the other three components,

therefore the deformation from them can be disregarded.

The governing equation for a Kirchhoff-Love plate under transverse load is a fourth order partial differential equation that has no analytical solution except for a few plates of simple regular shapes. Thus numerical methods are used to approximately solve these problems. The formation of TMM for Kirchhoff plate will be introduced. Several cases are studied and results are discussed in the following part of this section.

2.5.1 Calculation of the shape functions

The governing differential equation for plates in the Kirchhoff plate theory is [72]:

$$D_0\nabla^4 w(x,y)=p(x,y)\quad (x,y)\in\Omega \tag{2.27}$$

where $w(x,y)$ is the lateral deflection, $p(x,y)$ is the lateral load, $D_0=Eh^3/12(1-\mu^2)$ is the flexural rigidity of the plates, E and μ are Young's modulus and Poisson's ratio respectively and h is the plate thickness.

If one can obtain a solution $w(x,y)$, satisfying Eq.(2.27) and the given boundary conditions, bending moments, twisting moment and shear forces may be defined in terms of a function w by:

$$\begin{cases} M_x=-D\left(\dfrac{\partial^2 w}{\partial x^2}+\mu\dfrac{\partial^2 w}{\partial y^2}\right)\\ M_y=-D\left(\dfrac{\partial^2 w}{\partial y^2}+\mu\dfrac{\partial^2 w}{\partial x^2}\right)\\ M_{xy}=-D(1-\mu)\dfrac{\partial^2 w}{\partial x\partial y}\end{cases}$$
$$Q_x=-D\frac{\partial}{\partial x}\nabla^2 w, Q_y=-D\frac{\partial}{\partial y}\nabla^2 w \tag{2.28}$$
$$\begin{cases} Q_x^*=-D\left(\dfrac{\partial^3 w}{\partial x^3}+(2-\mu)\dfrac{\partial^3 w}{\partial x\partial y^2}\right)\\ Q_y^*=-D\left(\dfrac{\partial^3 w}{\partial y^3}+(2-\mu)\dfrac{\partial^3 w}{\partial x^2\partial y}\right)\end{cases}$$

Eq.(2.27) and bending moments in Eq.(2.28) can be written in the form of second order derivatives:

$$\frac{\partial^2 M_x}{\partial x^2}+2\frac{\partial^2 M_{xy}}{\partial x\partial y}+\frac{\partial^2 M_y}{\partial y^2}+p=0\Rightarrow\frac{\partial^2 M_{\alpha\beta}}{\partial x_\alpha\partial x_\beta}+p=0 \tag{2.29}$$

$$\{M\}=\begin{Bmatrix}M_x\\M_y\\M_{xy}\end{Bmatrix}=\begin{bmatrix}D_{11}&D_{12}&D_{16}\\D_{12}&D_{22}&D_{26}\\D_{16}&D_{26}&D_{66}\end{bmatrix}\begin{Bmatrix}-\dfrac{\partial^2 w}{\partial x^2}\\-\dfrac{\partial^2 w}{\partial y^2}\\-\dfrac{\partial^2 w}{\partial x\partial y}\end{Bmatrix}=[D]\{K\} \tag{2.30}$$

where $[D]$ is the elastic matrix. $D_{ij}(i, j = 1, 2, 6)$ together are called flexural rigidity which are determined by the material of the plates. For Kirchhoff plates with isotropic materials, the elastic matrix is:

$$[D]=D_0\begin{bmatrix}1&\mu&0\\\mu&1&0\\0&0&1-\mu\end{bmatrix} \tag{2.31}$$

Now we have three equations with second order derivatives:

$$\begin{cases}\dfrac{\partial^2 M_{\alpha\beta}}{\partial x_\alpha\partial x_\beta}+p=0\\[2ex] k_{\alpha\beta}=-\dfrac{\partial^2 w}{\partial x_\alpha\partial x_\beta}\\[2ex] \{M\}=[D]\{K\}\end{cases} \tag{2.32}$$

The unknowns $\{M\}$ and $\{K\}$ are split into two parts:

$$\begin{cases}\{M\}=\begin{Bmatrix}M_x\\\overline{M}\end{Bmatrix},\overline{M}=\begin{Bmatrix}M_y\\M_{xy}\end{Bmatrix}\\[2ex] \{K\}=\begin{Bmatrix}k_x\\\overline{k}\end{Bmatrix},\overline{k}=\begin{Bmatrix}k_y\\k_{xy}\end{Bmatrix}\end{cases} \tag{2.33}$$

This splitting is motivated by the procedure established in [64]and [67] to solve

the differential equation: one assumes that the dependence with respect to *y* is known and one considers the equation as a differential equation in *x*. The last equation in Eq.(2.32) can be represented with $\overline{M}$ and $\bar{k}$:

$$\begin{Bmatrix} M_x \\ \overline{M} \end{Bmatrix} = \begin{Bmatrix} M_x \\ M_y \\ M_{xy} \end{Bmatrix} = \begin{bmatrix} D_{11} & D_{12} & D_{13} \\ D_{12} & D_{22} & D_{23} \\ D_{13} & D_{23} & D_{33} \end{bmatrix} \begin{Bmatrix} k_x \\ k_y \\ k_{xy} \end{Bmatrix} = \begin{Bmatrix} D_{11}k_x + D_{12}k_y + D_{13}k_{xy} \\ \begin{Bmatrix} D_{12} \\ D_{13} \end{Bmatrix} k_x + \overline{D}.\bar{k} \end{Bmatrix} \tag{2.34}$$

With the technique in Chapter 2.2, Eq.(2.32), Eq.(2.33) and Eq.(2.34) can be expanded with complete polynomials of order *N*. It can be concluded at the that equations at *rank*(*m*, *n*) are:

$$k_x = -\frac{\partial^2 w}{\partial x^2} \Rightarrow k_x(m,n) = -(m+2)(m+1)\,w(m+2,n) \tag{2.35}$$

$$\bar{k} = -\begin{Bmatrix} \dfrac{\partial^2 w}{\partial y^2} \\ \dfrac{\partial^2 w}{\partial x \partial y} \end{Bmatrix} \Rightarrow \bar{k}(m,n) = -\begin{Bmatrix} (n+2)(n+1)\,w(m,n+2) \\ (m+1)(n+1)\,w(m+1,n+1) \end{Bmatrix} \tag{2.36}$$

$$\overline{M} = \begin{Bmatrix} D_{12} \\ D_{13} \end{Bmatrix} k_x + \overline{D}.\bar{k} \Rightarrow \overline{M}(m,n) = \begin{Bmatrix} D_{12} \\ D_{13} \end{Bmatrix} k_x(m,n) + \overline{D}.\bar{k}(m,n) \tag{2.37}$$

$$\begin{aligned} &\frac{\partial^2 M_x}{\partial x^2} + 2\frac{\partial^2 M_{xy}}{\partial x \partial y} + \frac{\partial^2 M_y}{\partial y^2} + p = 0 \Rightarrow \\ &\begin{Bmatrix} (m+2)(m+1)M_x(m+2,n) + 2(m+1)(n+1)M_{xy}(m+1,n+1) \\ +(n+2)(n+1)M_y(m,n+2) + p(m,n) \end{Bmatrix} \end{aligned} \tag{2.38}$$

Eq.(2.35) - Eq.(2.38) give the recurrence formulae for the elements of TMM, as is shown in Table 2.1.

Table 2.1 Organization of the computation

Equation	Derivation
$k_x = -\dfrac{\partial^2 w}{\partial x^2}$	(1) $w(m,n) = \dfrac{1}{m(m-1)} k_x(m-2,n)$
$\bar{k} = -\begin{Bmatrix} \dfrac{\partial^2 w}{\partial y^2} \\ \dfrac{\partial^2 w}{\partial x \partial y} \end{Bmatrix}$	(2) $\bar{k}(m,n) = -\begin{Bmatrix} (n+2)(n+1)w(m,n+2) \\ (m+1)(n+1)w(m+1,n+1) \end{Bmatrix}$
$\overline{M} = \begin{Bmatrix} D_{12} \\ D_{13} \end{Bmatrix} k_x + \overline{D}.\bar{k}$	(3) $\overline{M}(m,n) = \begin{Bmatrix} D_{12} \\ D_{13} \end{Bmatrix} k_x(m,n) + \overline{D}.\bar{k}(m,n)$
$\dfrac{\partial^2 M_x}{\partial x^2} = -2\dfrac{\partial^2 M_{xy}}{\partial x \partial y} - \dfrac{\partial^2 M_y}{\partial y^2} - p$	(4) $M_x(m,n) = \dfrac{-1}{m(m-1)} \begin{Bmatrix} p(m-2,n) + 2(m-1)(n+1)M_{xy}(m-1,n+1) \\ +(n+2)(n+1)M_y(m-2,n+2) \end{Bmatrix}$
$k_x = \dfrac{1}{D_{11}} \left\{ M_x - D_{12} k_y - D_{13} k_{xy} \right\}$	(5) $k_x(m,n) = \dfrac{1}{D_{11}} \left\{ M_x(m,n) - D_{12} k_y(m,n) - D_{13} k_{xy}(m,n) \right\}$

With the initial data $w(0,n), w(1,n), k_x(0,n), k_x(1,n)$, the approximate solution can be obtained as $w = \sum_{j=0}^{4N-3} P_j \alpha_j$, where

$$\alpha_j = \begin{cases} w(0,j) & 0 \le j \le N \\ w(1,j-N-1) & N+1 \le j \le 2N \\ k_x(0,j)-2N-1 & 2N+1 \le j \le 3N-1 \\ k_x(1,j-3N) & 3N \le j \le 4N-3 \end{cases}$$

To calculate the i^{th} shape function P_i, $\alpha_j \left(0 \le j \le 4N-3\right)$ are chosen to be equal to 1 successively. The algorithm to choose α_j is encoded as

```
for i = 0  to 4N − 3
  for j = 0  to  4N − 3  do
      if  j == i  then
      (α_j)_i = 1
      else
      (α_j)_i = 0
      end if
  end for
end for
```

With the data $\left(\alpha_j\right)_i$, all terms of w, $\{M\}$ and $\{K\}$ can be calculated using equations in Table 2.1.

Data : $w(0,n),\quad w(1,n),\quad k_x(0,n),\quad k_x(1,n)$

Initialisation

- Step 1: $\left(k_x(0,n), k_x(1,n)\right) \overset{(1)}{\Leftrightarrow} \left(w(2,n), w(3,n)\right)$
- Step 2: $\left(w(0,n),\ w(1,n), w(2,n)\right) \overset{(2)}{\Rightarrow} \left(\bar{k}(0,n),\ \bar{k}(1,n)\right) \overset{(data)}{\Rightarrow} \left(K(0,n),\ K(1,n)\right)$
- Step 3: $\left(K(0,n),\ K(1,n)\right) \overset{Constitutive\ law}{\Rightarrow} \left(M(0,n),\ M(1,n)\right)$

Iteration, $\left(K(m,n),\ M(m,n), w(m,n),\ w(m+1,n)\right)$ being given.

- Step 1: $K(m-1,n), K(m,n) \overset{(1)}{\Rightarrow} w(m+1,n), w(m+2,n) \overset{(2)}{\Rightarrow} \bar{k}(m+1,n)$
- Step 2: $M(m,n) \overset{(4)}{\Rightarrow} M_x(m+1,n) \overset{(5)}{\Rightarrow} k_x(m+1,n)$
- Step 3: $\bar{k}(m+1,n), k_x(m+1,n) \Rightarrow \mathrm{K}(m+1,n)$
- Step 4: $\mathrm{K}(m+1,n), \mathrm{M}_x(m+1,n) \overset{(3)}{\Rightarrow} \mathrm{M}(m+1,n)$

2.5.2 Kirchhoff plate problem with a circular domain

Now we consider a circular Kirchhoff plate with clamped edges in Figure 2.6:

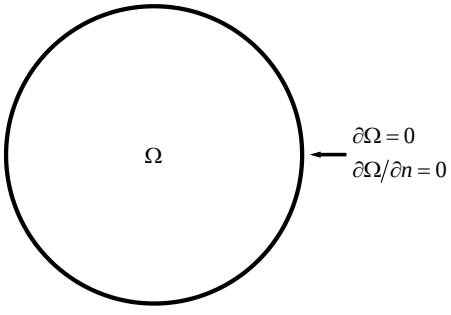

Figure 2.6 A circular Kirchhoff plate with clamped edges

For a circular plate with clamped edge, the problem can be described as:

$$\begin{cases} D_0\nabla^4 w = p \\ w(a) = 0 \\ \left.\dfrac{\partial w}{\partial n}\right|_{r=a} = 0 \end{cases} \tag{2.39}$$

where a is the radius of the plate. With these boundary conditions, the theoretical solution is [15]:

$$w = \frac{p}{64D}\left(a^2 - r^2\right)^2 \tag{2.40}$$

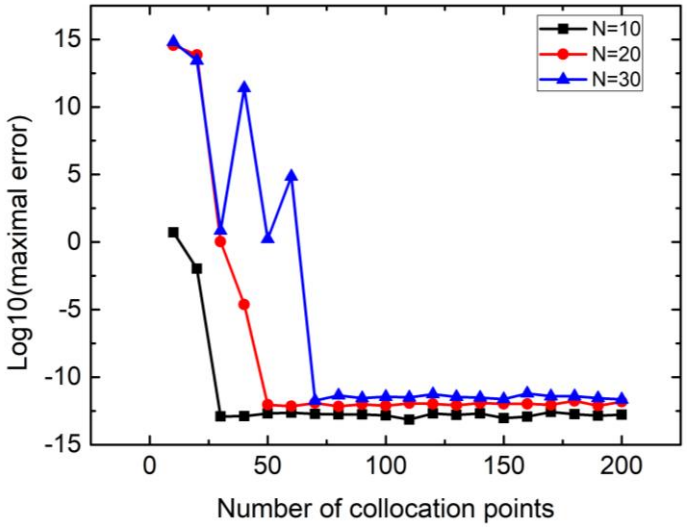

Figure 2.7 The influence of the number of collocation points on the convergence for circular Kirchhoff plate

Figure 2.7 is the convergence of TMM along with the increase of the collocation points when $N = 10$, 20 and 30. The theoretical solution is a polynomial of degree four, hence the numerical solution can be very accurate. When the collocation points are more than $4N$, the error is stable and less than 10^{-10}.

Figure 2.8 is the convergence of TMM along with the increase of the degree of the polynomial. The results get less accurate by increasing the degree. Due to the degree of the theoretical solution, the most accurate result is obtained at degree 4. However, the accuracy still stands less than 10^{-11} after degree 4.

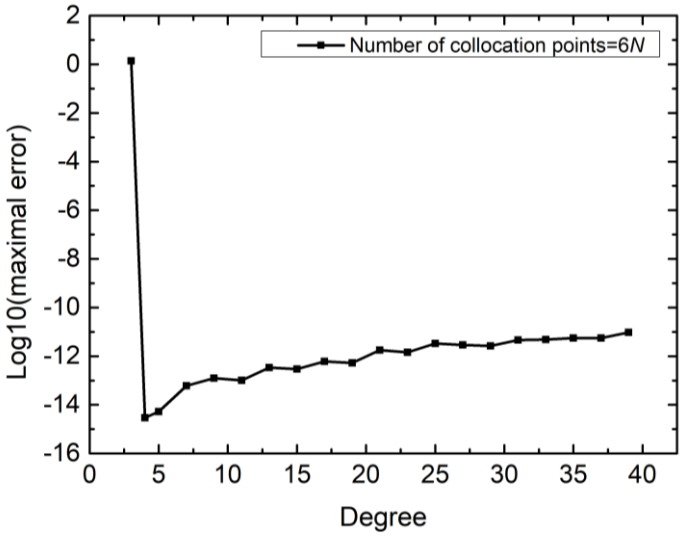

Figure 2.8 The convergence of TMM for circular Kirchhoff plate

2.5.3 Kirchhoff plate problem with a rectangular domain

The domain is a square with the width 1. One chooses a uniformly distributed cloud (see Figure 2.9).

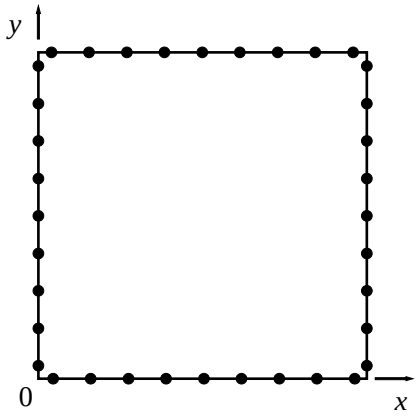

Figure 2.9 Rectangular domain and collocation points on the boundaries

1) Rectangular plate, simply supported, uniform load

For a rectangular plate, when it is simply supported, the problem can be described as:

$$\begin{cases} D_0\nabla^4 w = p \\ w = 0 \qquad \text{on } \partial\Omega^d \\ \dfrac{\partial^2 w}{\partial n^2} = 0 \qquad \text{on } \partial\Omega^n \end{cases} \tag{2.41}$$

An approximate solution for the problem is:

$$w(x,y)=\sum_{m=1}^{\infty}\sum_{n=1}^{\infty}\frac{16p}{(2m-1)(2n-1)\pi^6 D_0}\left[\frac{(2m-1)^2}{a^2}+\frac{(2n-1)^2}{b^2}\right]^{-2}\times \sin\frac{(2m-1)\pi x}{a}\sin\frac{(2n-1)\pi y}{b} \tag{2.42}$$

where a and b are the side lengths of the plate.

In the computation, a and b are set to 1, m and n are set to 200 that is enough to ensure the accuracy of the result. The result from Eq.(2.42) can be seen in Figure 2.10.

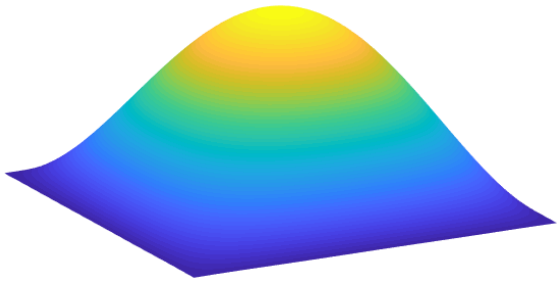

Figure 2.10 The distribution of the deflection from Eq.(2.42)

Figure 2.11 is the convergence for rectangular plate with the degree of the polynomial $N=10$, 30 and 50. The maximal error becomes stationary if the collocation points are enough when the degree is 10. The figures indicate that the accuracy becomes better by increasing the degree of the polynomials from 10 to 30. The maximal error cannot be reduced when the degree is increased from 30 to 50, but the results become more stable from this process.

Figure 2.12 is the convergence of TMM along with the increase of the degree of the polynomial. The maximal error decreases significantly by increasing the degree of the polynomial from 10 to 20. Next, from N=20 to 70, the error stands around 10^{-3} with a small infection.

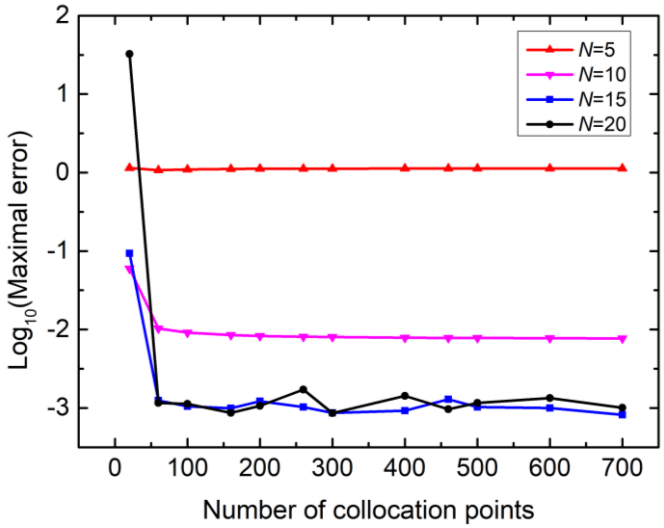

Figure 2.11 The influence of the number of collocation points on the convergence for rectangular Kirchhoff plate

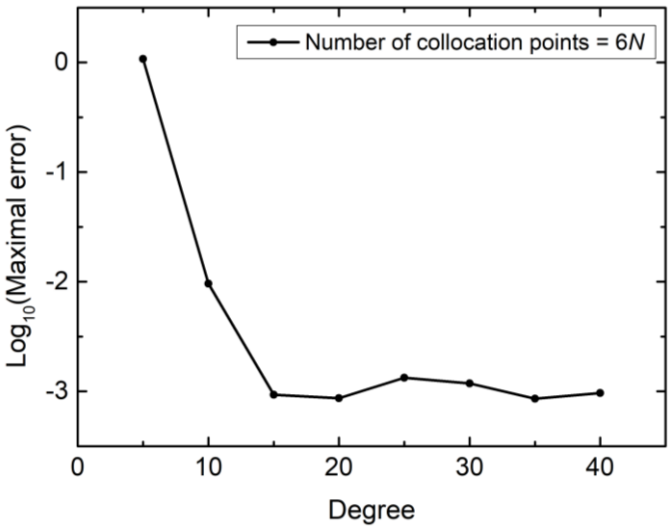

Figure 2.12 The convergence of TMM for rectangular Kirchhoff plate

2) Rectangular plate, clamped edges, uniform load

A rectangular Kirchhoff plate with clamped edges and uniform load can be described as:

$$\begin{cases} D_0\nabla^4 w = p & \\ w = 0 & \text{on } \partial\Omega^d \\ \dfrac{\partial w}{\partial n} = 0 & \text{on } \partial\Omega^n \end{cases} \tag{2.43}$$

Table 2.2 shows the deflection of the plate center obtained with different

methods. Theoretically, M_x should equal to M_y. Figure 2.13 is the deflection of the whole domain, with the boundary conditions $w=0$ and $\partial w/\partial n=0$. One can find that the accuracy of TMM is on the same level as with other methods.

Table 2.2 Deflection and moment of the center of a rectangular plate, clamped edges, uniform load

	Degree	Collocation points	w_{max} $(\times D_0/pa^4)$	M_x $(\times 1/pa^2)$	M_y $(\times 1/pa^2)$
TMM	10	40	0.00126519	0.0228932	0.0228932
		80	0.00126465	0.0228862	0.0228862
		120	0.00126451	0.0228842	0.0228842
	20	80	0.00126532	0.0229046	0.0229056
		160	0.00126532	0.0229043	0.0229058
		240	0.00126530	0.0229025	0.0229061
	30	120	0.00126529	0.0229047	0.0229048
		240	0.00126522	0.0229041	0.0229037
		360	0.00126558	0.0229072	0.0229074
MLPG [73]			0.001258	0.02288	0.02288
BEM [74]			0.001260	0.02290	0.02290
Theoretical Solution [75]			0.001260	0.02310	0.02310

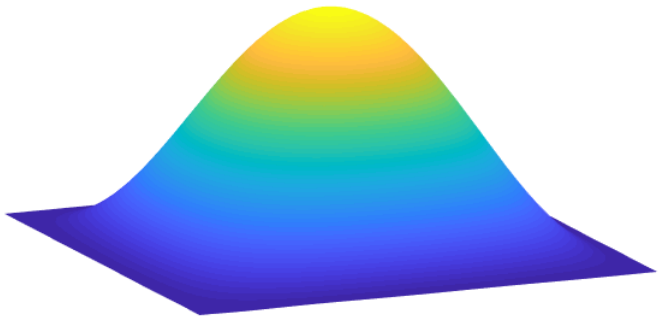

Figure 2.13 The distribution of the deflection of a clamped Kirchhoff plate

2.6 Application of TMM to sandwich plates

2.6.1 The loading and the governing equation

Distributed loading:

$$q_0(x,y) = \sigma \sin px \sin qy \tag{2.44}$$

where $p = p(n) = n\pi/a$, $q = q(m) = m\pi/b (n, m = 1, 2, 3\cdots)$, σ is a constant value.

We let $m = n = 1, \mathrm{a} = \mathrm{b} = 1, \sigma = 1$, the loading becomes:

$$q_0(x,y) = \sin \pi x \sin \pi y \tag{2.45}$$

The governing equation can be simplified as:

$$D_{11} w_{,xxxx} + (D_{12} + D_{21} + 4D_{66}) w_{,xxyy} + D_{22} w_{,yyyy} = q_0 \tag{2.46}$$

2.6.2 Exact solution

From the loading Eq.(2.44) and the governing equation Eq.(2.46) one can conclude that the exact solution is:

$$w_e = C \sin px \sin qy \tag{2.47}$$

where C is a constant. It is determined by bending stiffness D_{ij} and the loading q_0.

$$C = \frac{\sigma}{\left(D_{11}p^4 + 2(D_{12} + 2D_{66})p^2q^2 + D_{22}q^4\right)} \tag{2.48}$$

2.6.3 The properties of each case

The layer material coefficients are:

$$\begin{aligned} &E_L = 25\times10^6\,\text{psi} \qquad E_T = 10^6\,\text{psi} \\ &G_{LT} = 0.5\times10^6\,\text{psi} \quad G_{TT} = 0.2\times10^6\,\text{psi} \\ &\nu_{LT} = \nu_{TT} = 0.25 \end{aligned} \tag{2.49}$$

where L signifies the direction parallel to the fibers, T the transverse direction, and v_{LT} is the Poisson ratio measuring strain in the T-direction under uniaxial normal stress in the L-direction.

The normalized quantities are defined with respect to this data:

$$\begin{aligned} &\left(\bar{\sigma}_x, \bar{\sigma}_y, \bar{\tau}_{xy}\right) = \frac{1}{\sigma S^2}\left(\sigma_x, \sigma_y, \tau_{xy}\right) \\ &\left(\bar{\tau}_{xz}, \bar{\tau}_{yz}\right) = \frac{1}{\sigma S}\left(\tau_{xz}, \tau_{yz}\right) \\ &\bar{w} = \frac{100E_T w}{\sigma h S^4}, S = \frac{a}{h}, \bar{z} = \frac{z}{h} \end{aligned} \tag{2.50}$$

The stiffness coefficients can be expressed in terms of the engineering constants:

$$\begin{aligned} &Q_{11} = \frac{1-\nu_{yz}\nu_{zy}}{E_{yy}E_{zz}\Delta}, Q_{12} = \frac{\nu_{yx}+\nu_{zx}\nu_{yz}}{E_{yy}E_{zz}\Delta}, Q_{13} = \frac{\nu_{zx}+\nu_{yx}\nu_{zy}}{E_{yy}E_{zz}\Delta} \\ &Q_{22} = \frac{1-\nu_{xz}\nu_{zx}}{E_{xx}E_{zz}\Delta}, Q_{23} = \frac{\nu_{zy}+\nu_{xy}\nu_{zx}}{E_{xx}E_{zz}\Delta}, Q_{33} = \frac{1-\nu_{yx}\nu_{xy}}{E_{xx}E_{yy}\Delta} \\ &\mathrm{Q}_{44} = G_{yz}, \mathrm{Q}_{55} = G_{zx}, \mathrm{Q}_{66} = G_{xy} \\ &\Delta = \frac{1-\nu_{xy}\nu_{yx}-\nu_{yz}\nu_{zy}-\nu_{xz}\nu_{zx}-2\nu_{yx}\nu_{zy}\nu_{xz}}{E_{xx}E_{yy}E_{zz}} \end{aligned} \tag{2.51}$$

Three problems are considered for laminates (see Figure 2.14). Case 1 and Case 2 are constructed of the material described by Eq.(2.49):

Case 1: a symmetric 3-ply laminate with a=b and layers of equal thickness – the L direction coincides with x in the outer layers, while T is parallel to x in the central layer.

Case 2: the same laminating geometry as in Case 1, but in this case we take b=3a.

Case 3 is a square (a=b) sandwich plate under the distributed loading considered

in the previous cases. The material of the face sheets is that defined by Eq.(2.49). The thickness of each face sheet is *h*/10. The core material is transversely isotropic with respect to *z* and is characterized by the following properties:

$$\begin{aligned} &E_{xx} = E_{yy} = 0.04\times10^6\,\text{psi} \quad E_{zz} = 0.5\times10^6\,\text{psi} \\ &G_{xz} = G_{yz} = 0.06\times10^6\,\text{psi} \quad G_{xy} = 0.016\times10^6\,\text{psi} \\ &\nu_{zx} = \nu_{zy} = \nu_{xy} = 0.25 \end{aligned} \tag{2.52}$$

Case 1 Case 2 Case3

Figure 2.14 Fiber directions and thickness of each case

2.6.4 Results

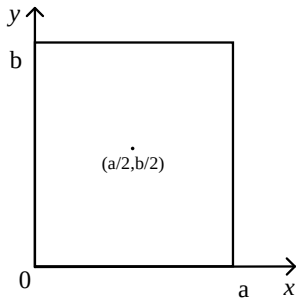

Figure 2.15 The coordinate system and expansion point

The Taylor series is expanded at the center of the plates, (a/2, b/2) (see Figure 2.15).

(1) Stresses in Square Sandwich Plate, Case 1

The convergence of Case 1 is illustrated in Figure 2.16 and Figure 2.17. From Figure 2.16 it can be seen that all errors of the stresses decrease with the degree *N* until it is around 15. After that, the errors fluctuate at a higher level of accuracy. Compared with Figure 2.16 (b), in which 10*N* collocation points have been distributed, Figure 2.16 (b) shows that all the stresses get their best solution at degree 16 and they have smaller errors. However, less collocation points lead to larger errors after degree

16.

In Figure 2.17, one can obtain locally optimal solution with about 100 collocation points when the degree is 16. The errors increase with 0.5 magnitude and then decrease to a stable status.

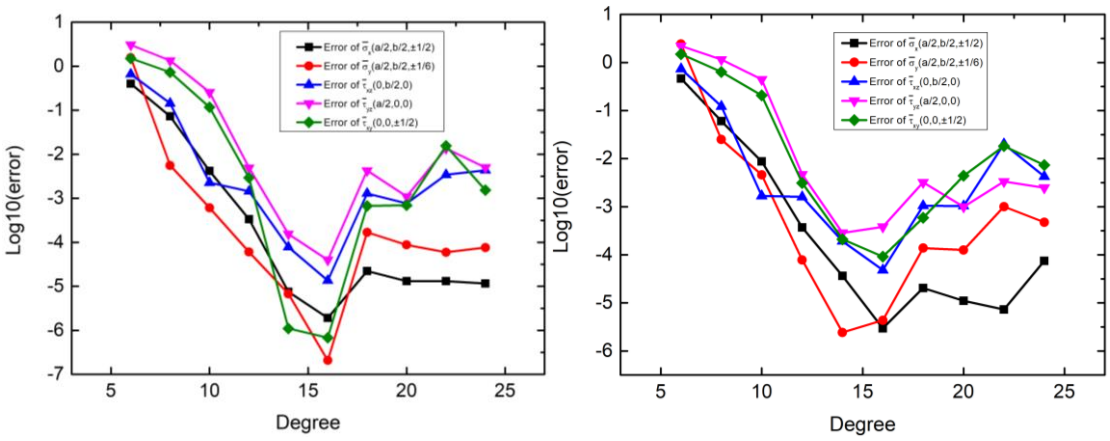

(a) Number of collocation points = 6N (b) Number of collocation points = 10N

Figure 2.16 The influence of the degree on the convergence, Case1

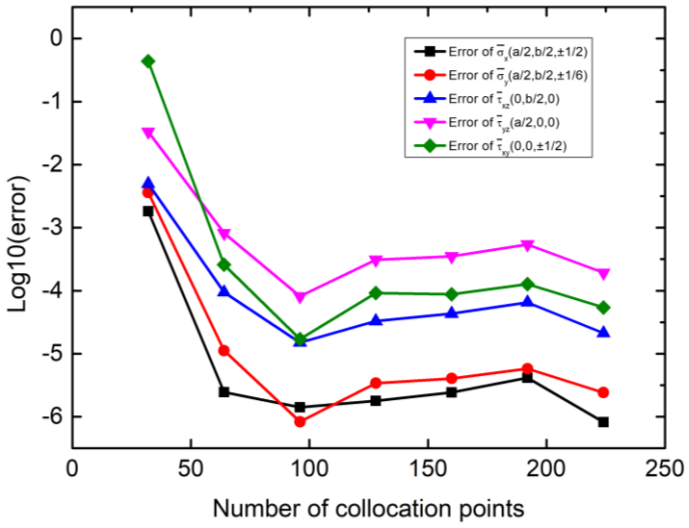

Figure 2.17 The influence of the number of collocation points on the convergence, N = 16, Case1

(2) Stresses and Deflection in Rectangular (b=3a) Laminate, Case 2

Figure 2.18 and Figure 2.19 are the convergence of the rectangular laminate plate (b=3a). Figure 2.18 clearly shows that at degree 16, stresses and deflection get their best solution, while the deflection has the smallest error, which is about 10^{-7}. The normal stresses $\bar{\sigma}_x, \bar{\sigma}_y$ and shear stress $\bar{\tau}_{xy}$ have larger errors since they are in direct

proportion to the second derivatives of the deflection. The shear stress $\overline{\tau}_{xz}, \overline{\tau}_{yz}$ have the largest errors since they are in direct proportion to the third derivatives of the deflection.

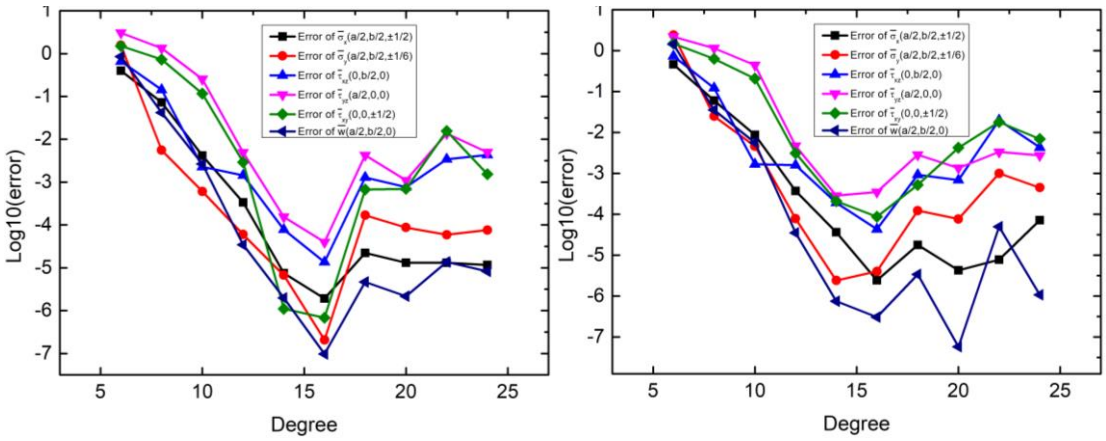

(a) Number of collocation points = 6N (b) Number of collocation points = 10N

Figure 2.18 The influence of the degree on the convergence, Case2

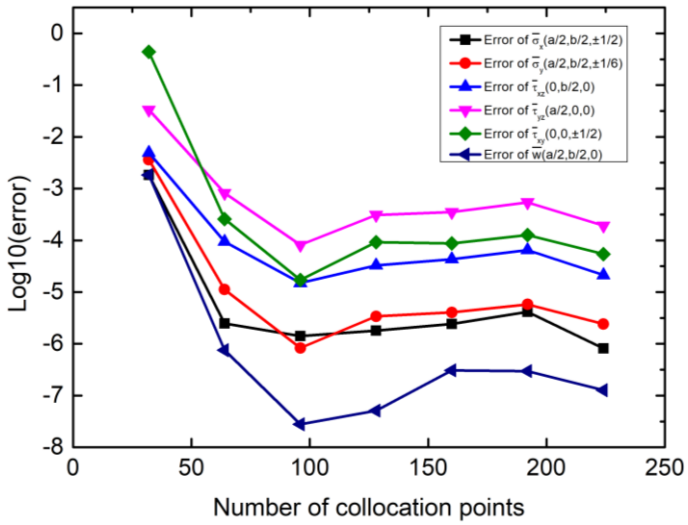

Figure 2.19 The influence of the number of collocation points on the convergence, N = 16, Case2

(3) Stresses in Square Sandwich Plate, Case 3

Figure 2.20 and Figure 2.21 are the convergence of a square sandwich plate with two kinds of materials. From Figure 2.20 one checks that the method fails if the number of collocation points is too small. The maximal error decreases with the number of collocation points until an optimal number where it becomes stable. A number of about 4N can already lead to good results. However, the degree of freedom

for this problem is $6N-2$. To ensure the best convergence, the number is recommended to be larger than $6N-2$.

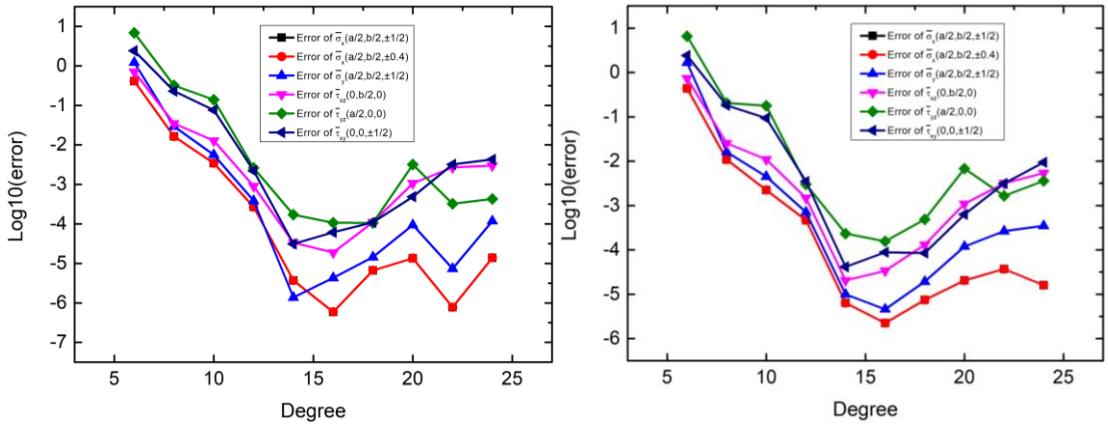

(a) Number of collocation points = 6N (b) Number of collocation points = 10N

Figure 2.20 The influence of the degree on the convergence, Case3

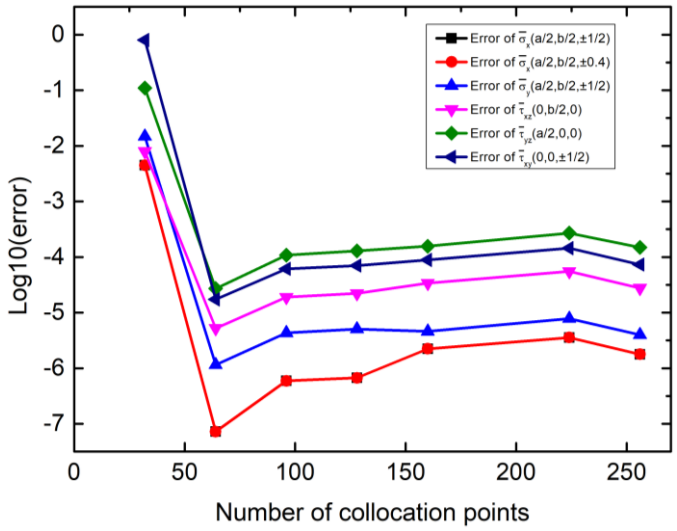

Figure 2.21 The influence of the number of collocation points on the convergence, N = 16, Case3

We take the normal stress $\bar{\sigma}_y$ in Case 3 for example. Figure 2.22 is the influence of expand point on the convergence. One can see that the results when the polynomial is expanded at (a/2, b/2) are better than that at (0, 0) at each degree. It is because Taylor series are suitable for a neighborhood, while point (a/2, b/2) is closer than (0, 0) to the whole domain. The technique of subdomains can be applied to get more accurate results.

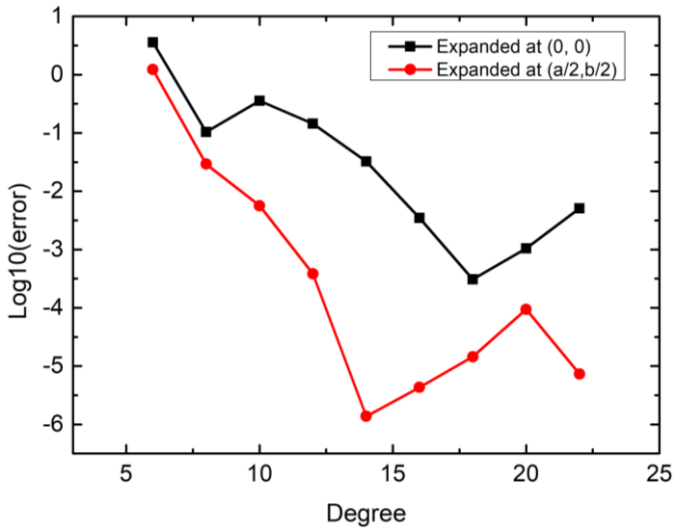

Figure 2.22 The influence of expand point on the convergence

2.7 Conclusion

A new meshless method – Taylor meshless method has been introduced in this chapter. TMM solves quasi-exactly the partial differential equations by using Taylor series. This technique reduces the degree of freedom for the problem significantly so that one can increase the degree of the polynomials to a very high level. Only collocation points on the boundary are needed, which makes TMM a true meshless method. In the cases that have been studied, this method is robust and effective. Only one domain has been used in this chapter, which is sufficient to solve boundary value problems. In the case of rectangular plate with clamped edges, the absence of an exponential convergence may be due to the singularity of the exact solution.

The convergence cannot be guaranteed in some other cases due to the developing point of Taylor series and the single domain. In next chapter, multidomain technique will be considered to solve nonlinear problems with collocation points on boundaries and interfaces.

Chapter 3 Application of TMM to large deflection of thin plates

3.1 Introduction

In the problem of large deflection of a thin plate, the deflection does not linearly depend on the external load. The membrane stresses acting in the plane of the plate have an effect on the bending or buckling of the plate, which become non-negligible as they are not small in comparison with bending stresses. A large deflection theory should be employed for these kinds of problems. The nonlinear partial differential equations describing large deflection of thin plates usually have no analytical solutions, which must be solved by numerical methods. Generally, researchers try to solve these problems using finite element method or finite difference method. These methods have some inherent weaknesses like mesh distortion, computational efficiency or complexity of pretreatment.

Many progresses have been made over the last forty years concerning the numerical computation of bifurcation problems. A first way is to solve the "extended system" characterizing the bifurcation points [76]. A simpler technique is to solve a continuation problem with an arc-length control for passing limit points [77]. Nowadays this standard procedure is available in many existing codes, especially in extensively used commercial packages. Note that this continuation technique requires the introduction of a perturbation to capture the bifurcation path in a secure manner and a balance between a sufficiently large perturbation and a sufficiently small step length is required for capturing the post-bifurcation response. This difficulty is partially removed with the Asymptotic Numerical Method (ANM), where each step is a Taylor series with respect to a control parameter, [78, 79], the key point being an adaptive step length related to the radius of convergence of the Taylor series. This adaptivity permits to compute the post-bifurcation curves with a very small perturbation. Moreover, as underlined in [80], one observes an accumulation of small

ANM-steps close to a bifurcation point because the radius of convergence is strongly connected with the distance to a neighbor bifurcation point. So an accumulation of small ANM-steps is a simple criterion for detecting bifurcations, but there are other techniques to analyze bifurcation problems within ANM, for instance by computing a bifurcation indicator [81, 82] or by identifying a geometric progression in the computed Taylor series [83]. More generally, ANM is an efficient path following technique able to solve a number of non-linear problems, including unilateral contact or plasticity problems [84].

A discretization method has to be associated with a non-linear solver as ANM and, in most of the cases, this was the finite element method. Nevertheless one can mention several papers where ANM was coupled with a meshless discretization method [85-87]. Benefits and drawbacks of meshless techniques are well known and will not be re-discussed here. In this chapter, we aim to combine ANM with TMM. The latter belongs to the large family of Trefftz methods that use exact solutions of the PDE as shape functions, see for example [88]. The Method of Fundamental Solution (MFS) is likely the most used Trefftz method [89]. The main advantage of Trefftz method and MFS is a strong reduction of the number of unknowns: for instance in [65] a problem was solved with only 90 DOFs while it needs more than 5000 with quadratic finite elements and much more with linear interpolation. The main drawback of Trefftz-type methods is matrix ill-conditioning that prevents solving large-scale problems [90, 91] , even if there were many works to try to improve this condition number, see for instance [92, 93]. Nevertheless, splitting in subdomains is a simple manner to control the ill-conditioning and several procedures are available [66], what allowed to solve large-scale problems in the Taylor meshless framework [67].

The treatment of non-linear problems is not straightforward within Trefftz methods, because it is not possible to get exact solutions of non-linear or nonhomogeneous problems by inverting the exact tangent operator. Thus, one generally re-introduces a discretization of the domain by radial functions that are

combined with fundamental solutions of a reference operator. Typical applications concern Poisson problem [94], Newtonian fluids [95] or plasticity [96] and the non-linear problem is solved by Picard iterations, but also by ANM [85, 86]. One can avoid the spatial discretization when using the method of Taylor series, in which case one can moreover obtain accurately the general solution of the homogeneous tangent problem. In the latter paper, the polynomial shape functions were computed via an Automatic Differentiation procedure [97], what could permit a wide range of applications.

In the present chapter, ANM will be combined with the Taylor meshless method: in other words, we shall perform together Taylor series in space and in load parameter. This double Taylor series expansion will be applied to the famous Föppl-von Karman plate model [98].

3.2 Governing equations

The fundamental equations for large elastic deflection of thin plates are known as Föppl-Von Kármán equations, given in the following form:

$$\begin{cases} D\Delta^2 w - \left(\dfrac{\partial^2 w}{\partial x^2}\dfrac{\partial^2 f}{\partial y^2} + \dfrac{\partial^2 w}{\partial y^2}\dfrac{\partial^2 f}{\partial x^2} - 2\dfrac{\partial^2 w}{\partial x \partial y}\dfrac{\partial^2 f}{\partial x \partial y} \right) = p \\ \dfrac{1}{Eh}\Delta^2 f + \dfrac{\partial^2 w}{\partial x^2}\dfrac{\partial^2 w}{\partial y^2} - \left(\dfrac{\partial^2 w}{\partial x \partial y} \right)^2 = 0 \end{cases} \tag{3.1}$$

where w is the vertical displacement out of the middle plane of the plate, E is the Young's modulus, p is the loading per unit area of the plate, h is the thickness of the plate and $D = Eh^3 / 12\left(1-\nu^2\right)$ is the flexural rigidity of the plate. The relations between the stress function f and the in-plane forces are:

$$N_x = \frac{\partial^2 f}{\partial y^2}, N_y = \frac{\partial^2 f}{\partial x^2}, N_{xy} = -\frac{\partial^2 f}{\partial x \partial y} \tag{3.2}$$

3.3 Combination of TMM and ANM

Asymptotic-numerical method (ANM) was proposed by Damil and Potier-Ferry in 1990 [99]. The non-linear branches are expanded in the form of power series. The non-linear problem becomes a series of linear problems, which can be solved efficiently by using recurrence formulas. Compared with some other methods of solving non-linear problem, such as Newton's method, the step length in ANM is determined automatically by a reliable path-following technique. This is a main advantage of ANM dealing with problems when there is a sudden change of direction [79].

In this chapter, ANM is applied to linearize the nonlinear system and TMM is used to solve linear partial differential equations obtained by ANM.

3.3.1 The procedure of ANM

In the isotropic case and with a transversal force $\lambda p(x,y)$, where λ is the load parameter, Eq.(3.1) can be rewritten as:

$$\begin{cases} D\Delta^2 w - [w, f] = \lambda p \\ \dfrac{1}{Eh}\Delta^2 f + \dfrac{1}{2}[w, w] = 0 \end{cases} \tag{3.3}$$

where the bracket operator involves the second derivatives of its arguments:

$$[A, B] = \frac{\partial^2 A}{\partial x^2}\frac{\partial^2 B}{\partial y^2} + \frac{\partial^2 A}{\partial y^2}\frac{\partial^2 B}{\partial x^2} - 2\frac{\partial^2 A}{\partial x \partial y}\frac{\partial^2 B}{\partial x \partial y} \tag{3.4}$$

ANM seeks a family of solutions depending on a scalar parameter "a". The parameter λ is also expressed as a function of "a". First, the variables $w(x,y)$, $f(x,y)$ and the load parameter λ are expanded to the form of power series with respect to the parameter "a" from a starting solution denoted as $w_0(x,y)$, $f_0(x,y)$, λ_0:

$$\begin{Bmatrix} w(x,y) \\ f(x,y) \\ \lambda \end{Bmatrix} - \begin{Bmatrix} w_0(x,y) \\ f_0(x,y) \\ \lambda_0 \end{Bmatrix} = \sum_{K=1}^{N_A} a^K \begin{Bmatrix} w_K(x,y) \\ f_K(x,y) \\ \lambda_K \end{Bmatrix} \tag{3.5}$$

Next, substituting in Eq.(3.3), one derives differential equations for each term of the series $\left(w_K(x,y), f_K(x,y), \lambda_K\right)$. To define the path parameter "a", the linearized arc length parameter is chosen since it permits a secure guiding near bifurcation points [79]:

$$a = \langle w - w_0, w_1 \rangle + \langle f - f_0, f_1 \rangle + (\lambda - \lambda_0)\lambda_1 \tag{3.6}$$

At order one, all the items that have a coefficient a^1 are picked out. A family of linear problems can be obtained as:

$$\begin{cases} D\Delta^2 w_1 - [w_0, f_1] - [w_1, f_0] = \lambda_1 p \\ \dfrac{1}{Eh}\Delta^2 f_1 + [w_0, w_1] = 0 \\ 1 = \langle w_1, w_1 \rangle + \langle f_1, f_1 \rangle + \lambda_1^2 \end{cases} \tag{3.7}$$

At order two:

$$\begin{cases} D\Delta^2 w_2 - [w_0, f_2] - [w_2, f_0] = \lambda_2 p + [w_1, f_1] \\ \dfrac{1}{Eh}\Delta^2 f_2 + [w_0, w_2] = -\dfrac{1}{2}[w_1, w_1] \\ 0 = \langle w_2, w_1 \rangle + \langle f_2, f_1 \rangle + \lambda_2 \lambda_1 \end{cases} \tag{3.8}$$

The items w_1, f_1 in the bracket operator are known after the resolution of Eq.(3.7). The generic form of the linear problems at order K:

$$\begin{cases} D\Delta^2 w_K - [w_0, f_K] - [w_K, f_0] = \lambda_K p + g_K^{nl} \\ \dfrac{1}{Eh}\Delta^2 f_K + [w_0, w_K] = h_K^{nl} \\ 0 = \langle w_K, w_1 \rangle + \langle f_K, f_1 \rangle + \lambda_K \lambda_1 \end{cases} \tag{3.9}$$

where $g_K^{nl} = \sum_{R=1}^{K-1} [w_R, f_{K-R}]$, $h_K^{nl} = -\left(\sum_{R=1}^{K-1} [w_R, w_{K-R}]\right)/2$. Two operators remain at any order:

$$\begin{cases} \mathcal{L}_1(w, f) = D\Delta^2 w - [w_0, f] - [w, f_0] \\ \mathcal{L}_2(w, f) = \dfrac{1}{Eh}\Delta^2 f + [w_0, w] \end{cases} \tag{3.10}$$

Let us start at order one. To solve Eq.(3.7), one supposes that $(\hat{w}, \hat{f})$ is the solution of

$$\begin{cases} D\Delta^2 \hat{w} - [w_0, \hat{f}] - [\hat{w}, f_0] = p \\ \dfrac{1}{Eh}\Delta^2 \hat{f} + [w_0, \hat{w}] = 0 \end{cases} \tag{3.11}$$

The resolution of Eq.(3.11) will be discussed in Section 3.2. Eq.(3.11) is a linear equation, thus the solution of Eq.(3.7) is $w_1(x, y) = \lambda_1 \hat{w}(x, y)$, $f_1(x, y) = \lambda_1 \hat{f}(x, y)$. One can obtain λ_1 from the third equation of Eq.(3.7):

$$\lambda_1^2 = \frac{1}{\langle \hat{w}, \hat{w} \rangle + \langle \hat{f}, \hat{f} \rangle + 1} \tag{3.12}$$

Eq.(3.12) has two solutions because one can move in two directions along the branch of solutions. In the first ANM-step, the user has to define the orientation. In the next ones the orientation can be chosen with respect to the tangent direction at the end of the previous step.

For the generic case at order K, there are two new polynomials g_K^{nl} and h_K^{nl}. The solution for order K is:

$$w_K = \lambda_K \hat{w} + w_K^{nl},\ f_K = \lambda_K \hat{f} + f_K^{nl} \tag{3.13}$$

where (w_K^{nl}, f_K^{nl}) is the solution of:

$$\begin{cases} D\Delta^2 w_K^{nl} - [w_0, f_K^{nl}] - [w_K^{nl}, f_0] = g_K^{nl} \\ \dfrac{1}{Eh}\Delta^2 f_K^{nl} + [w_0, w_K^{nl}] = h_K^{nl} \end{cases} \tag{3.14}$$

3.3.2 TMM formulation

In this part, TMM is used to solve the linear systems with variable coefficients Eq.(3.11) and Eq.(3.14). The principle of TMM is to expand the unknown fields in Taylor series and to solve the PDEs in the sense of Taylor series. The two unknowns of Eq.(3.11) or Eq.(3.14) - the transverse displacement *w* and the stress function *f* are approximated by Taylor series truncated at TMM degree *N*:

$$\begin{Bmatrix} w(x,y) \\ f(x,y) \end{Bmatrix} = \sum_{m=0}^{N} \sum_{n=0}^{N-m} (x-x_0)^m (y-y_0)^n \begin{Bmatrix} w_{m,n} \\ f_{m,n} \end{Bmatrix} \tag{3.15}$$

In these two complete polynomials, there are $(N+1)(N+2)$ coefficients to be found. The equations Eq.(3.11) and Eq.(3.14) are also expanded into series up to the order $N-4$ after substituting Eq.(3.15). For instance, the bending equation in Eq.(3.11) is approximated by:

$$D\left(\Delta^2 \hat{w}\right)_{m,n} - \left[w_0, \hat{f} \right]_{m,n} - \left[\hat{w}, f_0 \right]_{m,n} = p_{m,n}, 0 \le m+n \le N-4 \tag{3.16}$$

The computation of the Taylor coefficients of the bilaplacian is

$$\begin{aligned} \left(\Delta^2 \hat{w}\right)_{m,n} &= (m+4)(m+3)(m+2)(m+1)\hat{w}_{m+4,n} \\ &+2(m+2)(m+1)(n+2)(n+1)\hat{w}_{m+2,n+2} \\ &+(n+4)(n+3)(n+2)(n+1)\hat{w}_{m,n+4} \end{aligned} \tag{3.17}$$

as well as the tensor of the second derivatives

$$\begin{Bmatrix} \partial^2 \hat{w}/\partial x^2 \\ \partial^2 \hat{w}/\partial y^2 \\ \partial^2 \hat{w}/\partial x \partial y \end{Bmatrix}_{m,n} = \begin{Bmatrix} (m+2)(m+1)\hat{w}_{m+2,n} \\ (n+2)(n+1)\hat{w}_{m,n+2} \\ (m+1)(n+1)\hat{w}_{m+1,n+1} \end{Bmatrix} \tag{3.18}$$

For the homogeneous part of Eq.(3.16), all the other coefficients can be deduced from initial data $\hat{w}_{0,n}, \hat{w}_{1,n}, \hat{w}_{2,n}, \hat{w}_{3,n}, \hat{f}_{0,n}, \hat{f}_{1,n}, \hat{f}_{2,n}, \hat{f}_{3,n}$. The dimension of the initial data is $8N-4$. Thus the number of the degrees of freedom for Eq.(3.11) is reduced significantly from $(N+1)(N+2)$ to $8N-4$. These initial data are linearly

independent. The technique is to set them to 1 successively while others are 0. One can obtain $8N-4$ complete polynomials respectively $\left\{P_i^{\hat{w}}(x,y), P_i^{\hat{f}}(x,y)\right\}$, which build up the shape functions of the problem. For the inhomogeneous part, one can easily find a particular solution $\left\{P_s^{\hat{w}}(x,y), P_s^{\hat{f}}(x,y)\right\}$. Finally the solution of each problem Eq.(3.11) and Eq.(3.14) is computed in the form

$$\begin{Bmatrix} w(x,y) \\ f(x,y) \end{Bmatrix} = \sum_{i=1}^{8N-4} \alpha_i \begin{Bmatrix} P_i^w(x,y) \\ P_i^f(x,y) \end{Bmatrix} + \begin{Bmatrix} P_s^w(x,y) \\ P_s^f(x,y) \end{Bmatrix} = \begin{Bmatrix} P^w \\ P^f \end{Bmatrix} \alpha + \begin{Bmatrix} P_s^w \\ P_s^f \end{Bmatrix} \tag{3.19}$$

To solve the linearized PDEs Eq.(3.11) and Eq.(3.14), one has to compute the vector α which is determined by boundary conditions. This will be done by least-square collocation as in Chapter 2.

The auxiliary problems Eq.(3.11) and Eq.(3.14) being solved, one can compute all the terms of the ANM-series Eq.(3.5), after having obtained those of the path parameter λ_K. Last, we have to define the range of validity of the series Eq.(3.5). In conformity with the basic ANM algorithm, one requires that the last term of the series is small with respect to the first one:

$$a_{\max} = \left\{ \delta \frac{\left\| \{ f_1, x_1 \} \right\|}{\left\| \{ f_{N_a}, x_{N_a} \} \right\|} \right\}^{1/N_a - 1} \tag{3.20}$$

This leads to adaptive step lengths and this is very important when dealing with bifurcation problems. The radius of convergence is generally governed by the distance to the nearest bifurcation point [80]. That is why one observes an accumulation of small steps close to the bifurcation: hence, such an accumulation leads to a simple bifurcation criterion by sight. Moreover ANM permits to compute response curve with a very small perturbation force: one just has to choose a sufficiently small accuracy parameter δ.

3.3.3 Treatment of boundary and interface conditions

3.3.3.1 A square plate with movable edges

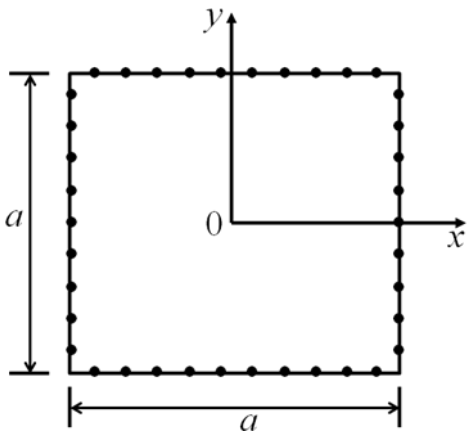

Figure 3.1 A square and simply supported plate with boundary collocation points

We consider a square plate with simply supported boundary conditions as in Figure 3.1. The dimensionless quantities are introduced as: $\bar{x} = x/a$, $\bar{y} = y/a$, $\bar{p} = pa^4/Eh^4$, $\bar{w} = w/h$, $\bar{\sigma} = \sigma a^2/Eh^2$. The load is a uniformly distributed pressure p . The boundary conditions are:

$$\begin{aligned} x = \pm\frac{a}{2} &: w = 0, \frac{\partial^2 w}{\partial x^2} = 0 \\ y = \pm\frac{a}{2} &: w = 0, \frac{\partial^2 w}{\partial y^2} = 0 \end{aligned} \tag{3.21}$$

The boundary conditions for stresses are:

$$\begin{aligned} x = \pm\frac{a}{2} &: \sigma_x = \frac{1}{h}\frac{\partial^2 f}{\partial y^2} = -\lambda, \tau_{xy} = \frac{1}{h}\frac{\partial^2 f}{\partial x \partial y} = 0 \\ y = \pm\frac{a}{2} &: \sigma_y = \frac{1}{h}\frac{\partial^2 f}{\partial x^2} = 0, \tau_{xy} = \frac{1}{h}\frac{\partial^2 f}{\partial x \partial y} = 0 \end{aligned} \tag{3.22}$$

TMM uses Taylor series to approximate the spatial function of the problem. However, a single polynomial is not sufficient if the domain is larger than the radius of the series' convergence. A good idea is to split the whole domain into several elements. Each element, which is called a subdomain, has an independent polynomial

solution. This operation can help to stabilize the global solution and accelerate the convergence. Some additional conditions should be introduced to guarantee the continuity of the displacement and stresses between two neighboring subdomains. The continuity conditions corresponding to bending are:

$$\begin{cases} w^{(1)} = w^{(2)} \\ \dfrac{\partial w^{(1)}}{\partial n} = \dfrac{\partial w^{(2)}}{\partial n} \\ M_n^{(1)} = M_n^{(2)} \\ V_n^{(1)} = V_n^{(2)} \end{cases} \tag{3.23}$$

V_n is an equivalent condition converted by the torque M_{xy} and shear force Q_n:

$$V_n = \frac{\partial^3 w}{\partial n^3} + (2-\nu)\frac{\partial^3 w}{\partial n \partial t^2} \tag{3.24}$$

The continuity conditions corresponding to stresses are:

$$\begin{cases} f^{(1)} = f^{(2)} \\ \dfrac{\partial f^{(1)}}{\partial n} = \dfrac{\partial f^{(2)}}{\partial n} \\ \dfrac{\partial^2 f^{(1)}}{\partial n^2} = \dfrac{\partial^2 f^{(2)}}{\partial n^2} \\ \dfrac{\partial^3 f^{(1)}}{\partial n^3} = \dfrac{\partial^3 f^{(2)}}{\partial n^3} \end{cases} \tag{3.25}$$

3.3.3.2 A square plate with immovable edges

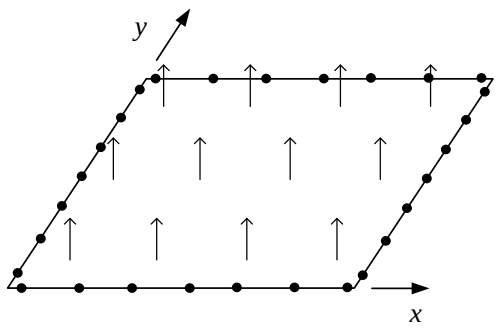

Figure 3.2 A square plate with immovable edges

In the example of Section 3.4.1, the edges can be movable in the plane because the normal stresses and shear stresses on boundaries are set to 0 by conditions Eq.(3.22). To consider immovable edge conditions ($u = v = 0$), one way is to replace the first equation in Eq.(3.3) by two partial differential equations in terms of the in-plane displacements u and v in addition to the transverse displacement w. However, by TMM, the in-plane displacements can be expressed easily by w and stress functions f. The strain components in the middle surface of the plate are given by:

$$\begin{aligned}
\varepsilon_x &= \frac{\partial u}{\partial x} + \frac{1}{2}\left(\frac{\partial w}{\partial x}\right)^2 \\
\varepsilon_y &= \frac{\partial v}{\partial y} + \frac{1}{2}\left(\frac{\partial w}{\partial y}\right)^2 \\
\gamma_{xy} &= \frac{\partial u}{\partial y} + \frac{\partial v}{\partial x} + \frac{\partial w}{\partial x}\frac{\partial w}{\partial y}
\end{aligned} \tag{3.26}$$

After introducing the stress function, the stress components become:

$$\begin{aligned}
\varepsilon_x &= \frac{1}{Eh}\left(\frac{\partial^2 f}{\partial y^2} - \nu\frac{\partial^2 f}{\partial x^2}\right) \\
\varepsilon_y &= \frac{1}{Eh}\left(\frac{\partial^2 f}{\partial x^2} - \nu\frac{\partial^2 f}{\partial y^2}\right) \\
\gamma_{xy} &= -\frac{1}{Gh}\frac{\partial^2 f}{\partial x \partial y}
\end{aligned} \tag{3.27}$$

Using Eq.(3.26) and Eq.(3.27), the partial derivatives of in-plane displacements can be expressed with w and f:

$$\begin{aligned}
\frac{\partial u}{\partial x} &= \frac{1}{Eh}\left(\frac{\partial^2 f}{\partial y^2} - \nu\frac{\partial^2 f}{\partial x^2}\right) - \frac{1}{2}\left(\frac{\partial w}{\partial x}\right)^2 \\
\frac{\partial v}{\partial y} &= \frac{1}{Eh}\left(\frac{\partial^2 f}{\partial x^2} - \nu\frac{\partial^2 f}{\partial y^2}\right) - \frac{1}{2}\left(\frac{\partial w}{\partial y}\right)^2 \\
\frac{\partial u}{\partial y} + \frac{\partial v}{\partial x} &= -\frac{1}{Gh}\frac{\partial^2 f}{\partial x \partial y} - \frac{\partial w}{\partial x}\frac{\partial w}{\partial y}
\end{aligned} \tag{3.28}$$

With the technique in Chapter 2, coefficients of Taylor series of u and v are

related to the coefficients of w and f through the following relations:

$$\begin{aligned}
u(m,n) &= \frac{1}{Eh}\left(\frac{(n+2)(n+1)}{m} f(m-1,n+2) - \nu(m+1) f(m+1,n)\right) - \frac{1}{2m}\theta_{xx}(m-1,n) \\
v(m,n) &= \frac{1}{Eh}\left(\frac{(m+2)(m+1)}{n} f(m+2,n-1) - \nu(n+1) f(m,n+1)\right) - \frac{1}{2n}\theta_{yy}(m,n-1) \\
(n+1)u(m,n+1) &+ (m+1)v(m+1,n) = -\frac{1}{Gh}(m+1)(n+1) f(m+1,n+1) - \theta_{xy}(m,n)
\end{aligned} \tag{3.29}$$

where $\theta_{xx} = (\partial w/\partial x)^2$, $\theta_{yy} = (\partial w/\partial y)^2$, $\theta_{xy} = (\partial w/\partial x)(\partial w/\partial y)$. In ANM, w is expanded in the form of power series with respect to the parameter a as in Eq.(3.5):

$$w = w_0 + a w_1 + a^2 w_2 + \cdots \tag{3.30}$$

The nonlinear part θ_{xx} is expanded as the addition of linear components:

$$\theta_{xx} = \left(\frac{\partial w}{\partial x}\right)^2 = \left(s_0 + a s_1 + a^2 s_2 + \cdots\right)^2 = \begin{pmatrix}
s_0^2 + \\
a(2 s_0 s_1) + \\
a^2\left(s_1^2 + 2 s_0 s_2\right) + \\
a^3\left(s_1 s_2 + s_2 s_1 + 2 s_0 s_3\right) + \\
\vdots \\
a^K\left(\sum_{r=1}^{K\text{-}1} s_r s_{K-r} + 2 s_0 s_K\right) + \\
\vdots
\end{pmatrix} \tag{3.31}$$

where $s_K = \partial w_K / \partial x$. From Eq.(3.31), one can find the generic expression of θ_{xx} at ANM order *K*:

$$(\theta_{xx})_K = \sum_{r=1}^{K\text{-}1} s_r s_{K-r} + 2 s_0 s_K \tag{3.32}$$

Similarly, the generic expressions of θ_{xx} and θ_{xy} are:

$$(\theta_{yy})_K = \sum_{r=1}^{K\text{-}1} t_r t_{K-r} + 2 t_0 t_K \tag{3.33}$$

$$\left(\theta_{xy}\right)_K = \sum_{r=1}^{K-1} s_r t_{K-r} + s_0 t_K + s_K t_0 \tag{3.34}$$

where $t_K = \partial w_K / \partial y$. With Eq.(3.29) and Eq.(3.32)-(3.34), most Taylor series coefficients of u and v at order K can be deduced except $u(0,0)$, $u(0,1)$, $v(0,0)$ and $v(1,0)$, which are corresponding to the in-plane rigid displacement and rotation of the plate. The expansions of u and v need an extra part to consider these three coefficients:

$$\begin{pmatrix} u \\ v \end{pmatrix} = \begin{bmatrix} 1 & 0 & (x-x_0) \\ 0 & 1 & -(y-y_0) \end{bmatrix} \begin{pmatrix} u \\ v \\ \beta \end{pmatrix} \tag{3.35}$$

The continuity conditions corresponding to bending are the same as those in Eq.(3.23). Because of the introduction of in-plane displacements, the continuity conditions corresponding to stresses become

$$\begin{cases} \sigma_n^{(1)} = \sigma_n^{(2)} \\ \tau_{xy}^{(1)} = \tau_{xy}^{(2)} \\ u^{(1)} = u^{(2)} \\ v^{(1)} = v^{(2)} \end{cases} \tag{3.36}$$

3.4 Results and discussion

The numerical method will be assessed by three examples concerning the buckling and bending of a simply supported square plate. Various in-plane boundary conditions have been accounted for. We are interested by the convergence with respect to the degree (p-convergence) and to mesh refinement (h-convergence), as well as its ability to compute bifurcating curves with very small imperfections. Our numerical results will be compared with analytical and numerical results of these examples, mainly from finite element codes.

3.4.1 Buckling of a square plate with movable edges

First, the problem is solved with one domain under conditions in 3.3.3.1. All the boundary conditions are accounted by least-square collocation with 240 collocation points. The parameters of the algorithm are the ANM-degree $K = 20$, the spatial degree $N = 20$, what corresponds to 156 degrees of freedom and the accuracy parameter δ=10^{-8} whose smallness is chosen to ensure the path following for a quasi-perfect bifurcation. This buckling problem will be solved by the method presented here and compared with finite element calculation done with the well-established code ANSYS. In the two calculations, a small symmetry breaking is needed. In ANSYS, this is done by a small modal geometric imperfection measured by the parameter $w_{imperfection}/h$ called "scaling factor".

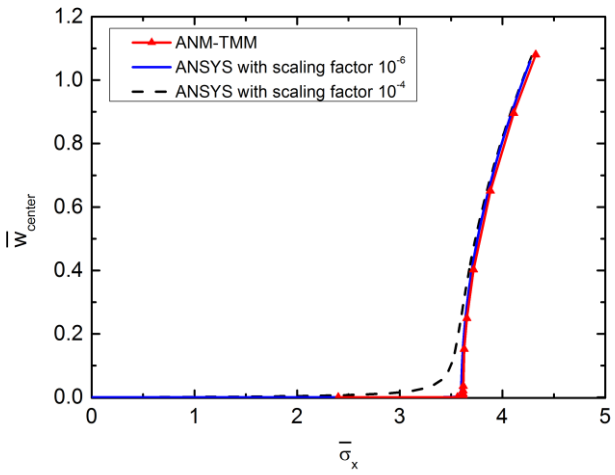

Figure 3.3 Effect of small perturbations on the buckling of a simply supported square plate. The ANM-TMM algorithm is compared with a commercial finite element code. On the ANM-TMM curve, each point corresponds to one ANM step

The obtained bifurcation plots are presented in the Figure 3.3 and Figure 3.4. Within ANSYS, we use a scaling factor of 10^{-4} and 10^{-6} and, within the present method, a dimensionless transversal pressure $\bar{p} = 10^{-6}$. ANSYS was not able to compute the bifurcating curve with a smaller imperfection, even if we suspect that some experts in non-linear calculation should be able to do such a calculation with a commercial package. Clearly the new technique permitted us to compute the

bifurcation plot with a very small imperfection simply by choosing a sufficiently large ANM degree and a sufficiently small accuracy parameter δ .

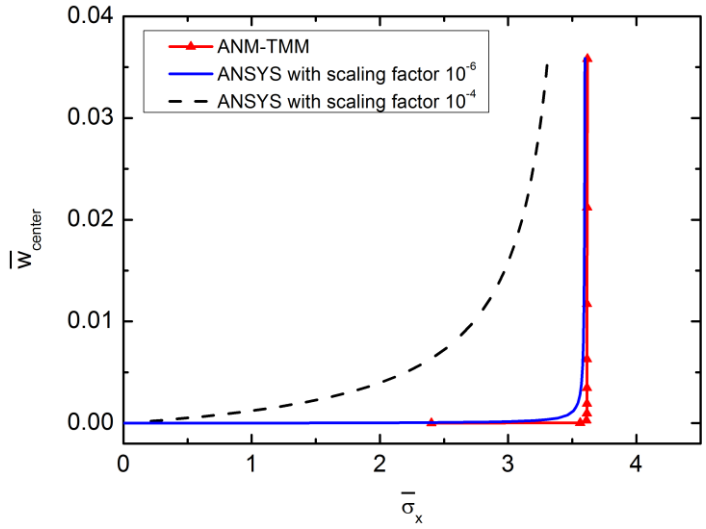

Figure 3.4 A zoom of Figure 3.3. One sees that the ANM-TMM method permits to compute easily quasi-perfect bifurcations. On the ANM-TMM curve, each point corresponds to one ANM step.

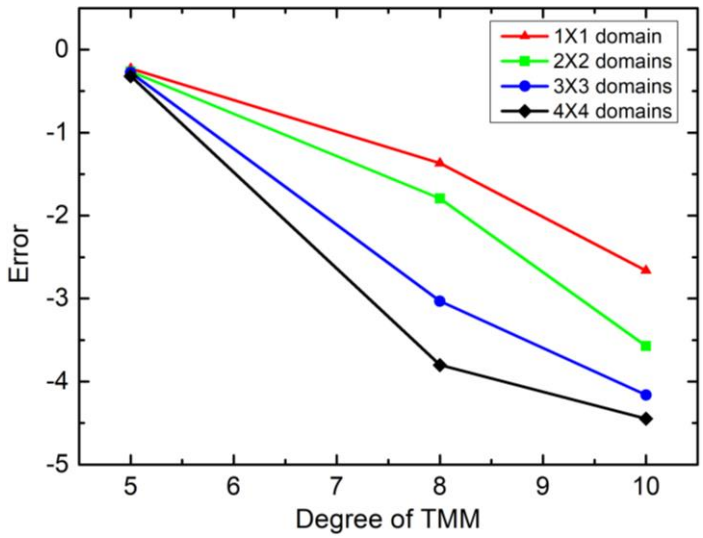

Figure 3.5 h-convergence: decimal logarithm of the error on the bifurcation stress, according to the degree P and to the number of subdomains.

Next one discusses the convergence with the number of subdomains (h-convergence) and with the degree N of the polynomials (p-convergence). The interface and boundary conditions are accounted by the least-square collocation method in a similar way as [68]. One looks at the value of the bifurcation stress $\bar{\sigma}_x$. The analytic value $\bar{\sigma}_x^{analytic}$ is 3.6152. One has applied TMM degrees N = 5, 8, 10 and a

number of subdomains varying from 1 to 16. The results are reported in Figure 3.5. Clearly the method converges with the degree and/or with the number of subdomains, but good results (i.e. error less than 10^{-3}) are obtained with 9 subdomains and $N \geq 8$ or with 4 subdomains and $N \geq 10$.

3.4.2 Bending of a square plate with immovable edges

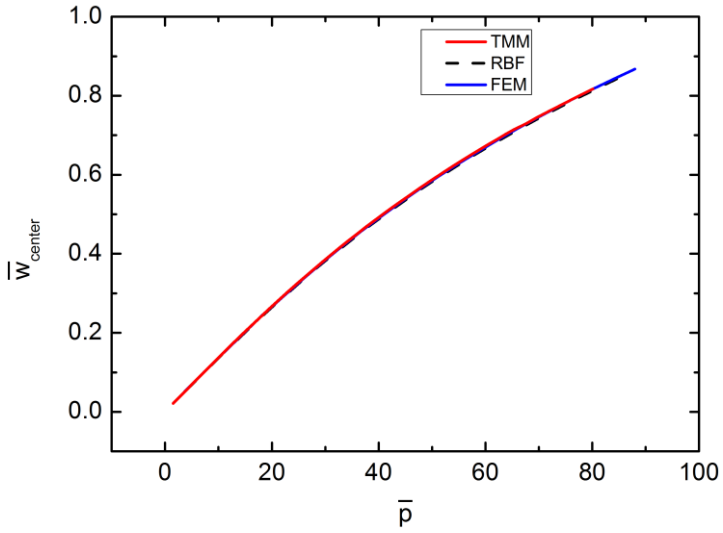

Figure 3.6 Deflection at the center of plate vs. load $\bar{p}$

A bending test of a square plate is studied to check the conditions in 3.3.3.2 and the effectiveness of the method. The plate is split into 5×5 subdomains. The boundary conditions corresponds to a clamped $w = \partial w/\partial n = 0$ and $u = v = 0$. Each subdomain is approximated with a Taylor series of degree 8 and connected with other subdomains using the continuity conditions in 3.3.3.2. The total number of degrees of freedom in this case is 1500. The degree of polynomials in ANM is chosen as 20.

Results are compared with those by FEM and RBF (see Figure 3.2). The RBF solutions are from the reference [100]. The FEM analysis is performed with the commercial software ANSYS using four-node element shell181. The plate is discretized with 50×50 elements and LARGE DISPLACEMENT STATIC option is activated to perform a nonlinear analysis. The number of model degrees of freedom is 15606. Figure 3.6 is the comparison of TMM results with those from FEM and RBF.

It shows that they are very close in the range of $0 < \bar{p} < 90$. Table 3.1 is the detailed comparison of the deflection $\bar{w}$ and the membrane stress $\bar{\sigma}_m$ computed at the center of the plate for different loads between TMM and FEM. The membrane stress $\bar{\sigma}_m$ is defined as the stress at the middle surface of the plate. The load is determined automatically by ANM that is the value after each ANM step. The errors of the center deflection between two methods are at the level of 10^{-3}; while the errors of the membrane stress are at the level of 10^{-4}, indicating that they are in a very good agreement.

Table 3.1 Deflection and membrane stress at the center of plate vs. load $\bar{p}$

$\bar{p}$	$\bar{w}$			$\bar{\sigma}_m$		
	FEM	TMM	ERROR(%)	FEM	TMM	ERROR(%)
2.29	0.0317	0.0316	0.315	0.0033	0.0033	0.000
6.80	0.0937	0.0935	0.213	0.0291	0.0291	0.000
15.96	0.2157	0.2153	0.185	0.1542	0.1543	0.065
25.12	0.3290	0.3285	0.152	0.3581	0.3583	0.056
34.12	0.4304	0.4295	0.209	0.6112	0.6114	0.028
43.06	0.5213	0.5202	0.211	0.8947	0.8946	0.009
51.94	0.6030	0.6017	0.216	1.1942	1.1940	0.013
60.81	0.6771	0.6756	0.222	1.5023	1.5020	0.017
69.61	0.7443	0.7426	0.228	1.8113	1.8109	0.023
78.46	0.8064	0.8046	0.223	2.1222	2.1213	0.040
87.32	0.8640	0.8620	0.231	2.4313	2.4305	0.032
96.10	0.9171	0.9149	0.240	2.7344	2.7331	0.046
104.79	0.9662	0.9638	0.248	3.0305	3.0287	0.058
113.46	1.0123	1.0098	0.247	3.3217	3.3197	0.061

3.4.3 Buckling of a square plate with immovable edges under uniaxial compression

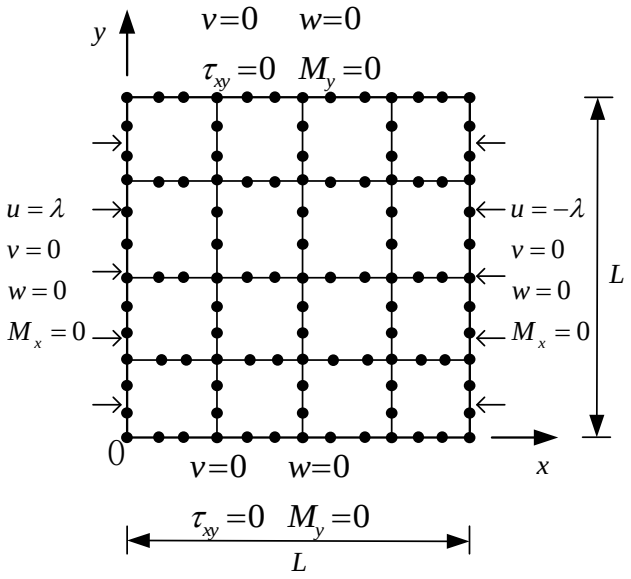

Figure 3.7 A square plate with immovable edges

Consider a simply supported square plate with the same geometric and material data as in Section 3.4.1. The displacement loads are $u = \lambda$ at $x = 0$ and $u = -\lambda$ at $x = L$. All the edges cannot move in y-direction, while the upper and bottom edge can move in x-direction. The plate and boundary conditions can be seen in Figure 3.7.

In this numerical example, the order of ANM is set to 10. The number of degrees of freedom for this problem is $N_e(8N-4)$, where N_e is the number of domains. The accuracy parameter δ is 10^{-8}. Transverse uniform pressure $\bar{p}$ is chosen as a small value 10^{-6} to produce the initial imperfection of the plate. The boundary conditions are accounted by least-square collocation with $32N$ points in one domain, including the boundaries and the interfaces. On the interfaces, two domains share the same collocation points. The distribution of these points is shown in Figure 3.7.

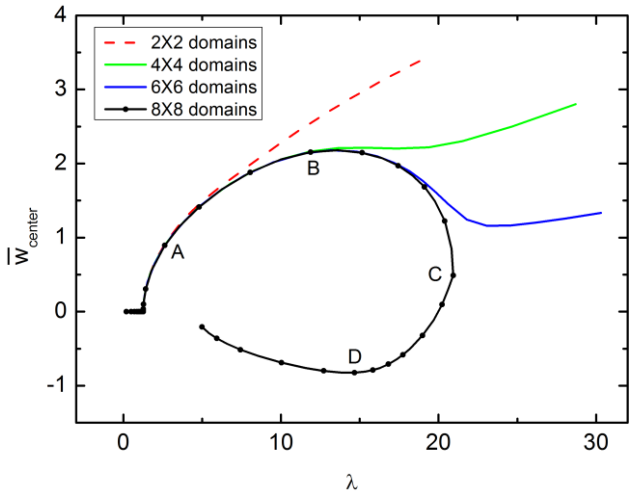

Figure 3.8 Displacement of center point of the plate vs. load, degree of TMM 8, order of ANM 10

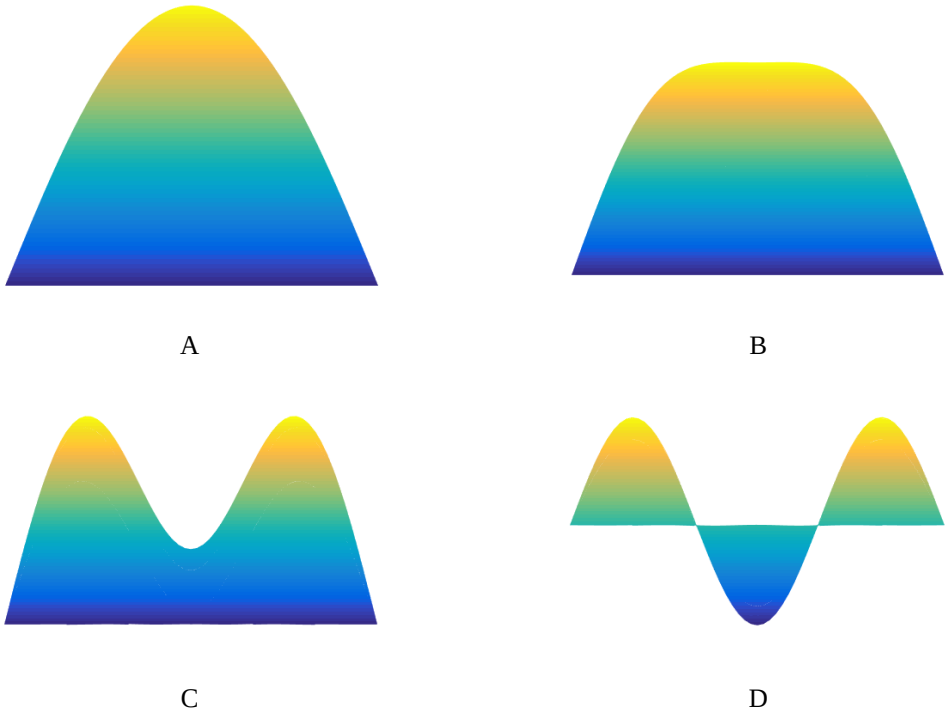

Figure 3.9 The deformation of the plate at point A, B, C, D in Figure 3.8

To discuss the convergence of the method with the number of domains, we look at Figure 3.8. 2×2 domains are not sufficient to get accurate results when $\bar{w}_{center}$ is larger than 0.5. With more domains, the results converge further along with the post-buckling curve. Figure 3.9 is the deformation of the plate at points A, B, C and D in Figure 3.8. It shows clearly that with 8×8 domains, the buckling passes from the first mode to the third mode.

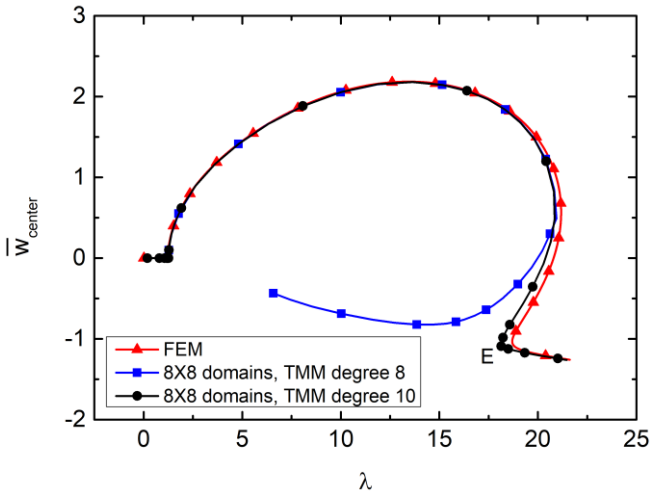

Figure 3.10 Comparison of results by FEM and TMM with degree 8 and 10

Figure 3.11 The deformation of the plate at point E in Figure 3.10

Figure 3.10 is the result by FEM and TMM with degree 8 and 10. With a larger degree of TMM, the post-buckling path converges to the FEM results. In Figure 3.11, one can see that the deformation of the plate has no great difference with that at point D. The system selects another bifurcation path and begins to enter another mode.

Table 3.2 and Figure 3.12 present the displacement loads when the displacement of center point $\overline{w}_{center} = 1$. They show that degree of TMM 6 is not sufficient to converge, even with 8×8 domains. To improve the reliability of the results, one can increase the degree of TMM or the number of domains. According to the previous study, it is better to compute the problem with smaller degree of TMM and large number of domains, because a large degree of TMM may lead to large conditioning number of the matrix. It also consumes more computing time than that if we increase

the number of domains. In Figure 3.12, the result by degree 20 and 2×2 domains is not good as that by degree 8 and 8×8 domains.

To find the load of FEM at $\bar{w}_{center}=1$, the data from $\bar{w}_{center}$=0.5 to 1.3 by ANSYS are fitted with a polynomial of degree 10. From TMM calculating, the reference load at $\bar{w}_{center}=1$ is $\lambda=2.98261\pm0.00001$. The discrepancy between FEM and TMM is about 3.35×10^{-5}.

Table 3.2 Displacement load values when the displacement of center point $\bar{w}=1$, convergence with mesh refinement and with the degree

Number of	Degree of TMM					
subdomains	6	8	10	12	15	20
2×2	3.14120	2.91440	3.00396	2.98004	2.98231	2.98268
3×3	2.95625	2.98184	2.98279	2.98261	2.98263	2.98263
4×4	2.96247	2.98271	2.98263	2.98262	2.98262	2.98262
6×6	2.97156	2.98261	2.98262	2.98262	2.98262	2.98260
8×8	3.00378	2.98261	2.98262	2.98262	2.98261	2.98260

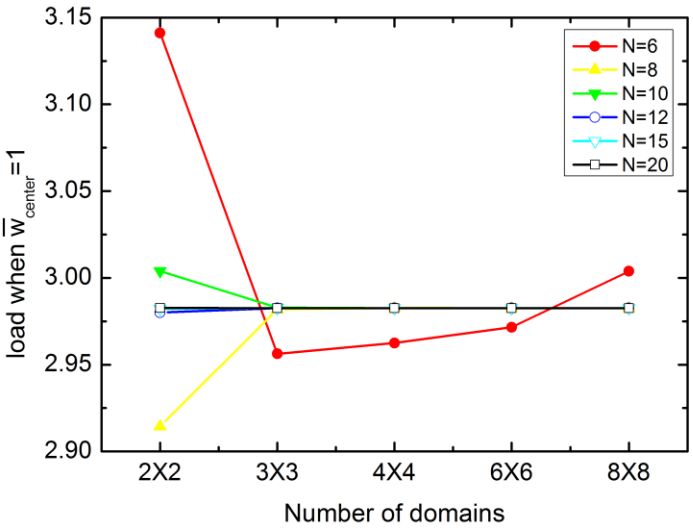

Figure 3.12 Displacement load values when the displacement of center point is 1

3.5 Conclusion

In this chapter, the boundary meshless method TMM (Taylor Meshless Method) is combined with ANM (Asymptotic Numerical Method) to solve nonlinear thin plate problems. The detailed procedure of this double Taylor series method consists of two parts: first, nonlinear partial differential equations are linearized by ANM, producing a set of linear equations in each iteration; next, these linearized partial differential equations are solved by TMM. The approximate solution obtained by TMM is used as the initial solution of next ANM iteration.

The buckling of thin plate with movable edges is studied. This double Taylor series method can compute buckling problems with much smaller perturbations than that in FEM. A bending test of thin plate with immovable edges is carried out to verify the boundary conditions and convergence of the method before buckling analysis. The results are in good agreements with that in FEM. Comparing with FEM solutions, the number of domains for buckling of thin plate with immovable edges is discussed.

The study shows that this new method is very efficient to solve a quasi-perfect bifurcation response and this does not require a strong numerical expertise. This double Taylor series method leads to an efficient path following technique that can be easily extended to other hyper-elastic models or to Newtonian fluids.

Chapter 4 Application of TMM to wrinkling of membranes under shear loading

4.1 Introduction

Over the past decades, different kinds of thin film structures are designed and playing more and more important roles in the fields of aerospace, automobile, construction and others. When the largest displacement w_{max} is much larger than the thickness h, the structure is defined as a membrane structure. Membrane structures have advantages in weight and storage requirements. Generally, the internal stresses of a thin plate under transverse loads consists of bending stress and membrane stress. However, a membrane structure cannot support compressive stress because the bending stress is so small that it can be ignored compared with the membrane stress [101]. When a compressive stress is applied, the structure becomes unstable and generates wrinkles. The existence of wrinkled regions has a great influence on the strength and reliability of the structure. The deformation and final state may not be uniquely determined. It is essential to have a clear understanding on the wrinkle phenomenon. Thus many material and mechanical researchers are recently interested in the prediction of the behavior of the membrane.

Previous numerical studies of membranes mostly use finite element models based on thin- membrane elements or shell elements [102]. Membrane elements have simple construction format, hence they have the advantage of computational cost. However, they ignore bending effect so that they cannot obtain accurate transverse deformation. Shell elements have overcome shortcomings of membrane elements and made models close to practical structures. Nevertheless, complicated mesh generation is still needed. By using Taylor Meshless Method, one will reduce the size of the discrete problem, what is necessary in cases where there are many wrinkles. Another

difficulty is the presence of a number of bifurcating solutions, especially corresponding to various wavenumbers, which is due to the very weak bending stiffness encountered for very thin membranes. Here ANM will give a more secure path following technique to compute the bifurcating curves in such a difficult situation. The ANM-TMM method described in the previous chapter will be applied to an iconic problem of membrane wrinkling under shear loading. Indeed this bifurcation problem is so difficult that these authors have been obliged to add a significant tensile load to increase the membrane stiffness and, in this way, to stabilize the response in order to be able to achieve the computation. Here the challenge will be to minimize this artificial tensile load and the imperfection discussed in the chapter 3.

This chapter presents a numerical study of rectangular membranes submitted to a shear loading. The objective is to simulate the generation of membrane wrinkles using TMM. A three-step analysis is introduced in detail. Some parametric studies are shown in this chapter, regarding the imperfection, tension load and subdomain sensitivity in order to know the contribution of each parameter to the wrinkling results.

4.2 Modelling of the membrane boundary value problem

To analyze the behavior of the wrinkled membrane, the membrane should be modeled numerically. In Chapter 3, the procedure of solving thin plate problems has been well established based on partial differential equations. In the development of the wrinkles, bending stiffness, although very small, plays an important role in the shape and amplitude of the wrinkles. By using the previous model that includes bending stiffness, the process of wrinkling is more accurately simulated.

The imperfection is an important factor affecting the final wrinkling results. Similar to the study of buckling of thin plate, generally a perfect membrane cannot be analyzed directly because the deformation will be discontinuous at the buckling point. Pure in-plane loads will not bring about mechanism on a perfect membrane. In practical simulation, imperfections are usually introduced to avoid bifurcation and get

continuous response.

There are many ways to distribute imperfections to perfect membranes. In FEM, for example, the imperfections can be imposed at selected or all interior nodes of the originally membrane mesh. The imperfection amplitudes, which are small in comparison to the thickness of the membrane, are regulated by a parameter to avoid element distortions. However, the imperfections should be large enough to provide sufficient bending-to-membrane coupling.

Another way to impose initial imperfections is seeding several eigenmodes onto the finite element model using a scaling factor to control the proportion between the imperfections and the membrane thickness. An eigenvalue buckling analysis has to be carried out before the membrane wrinkling to obtain eigenmodes.

In this study, the small out-of-plane deformation is produced by imposing transverse pressure onto the membrane. In this way, magnitudes of the imperfections are controlled by transverse loads. The deformation is generated on the whole membrane without pre-eigenvalue processing.

When solving buckling problems in Chapter 3, imperfections and in-plane loads are imposed from zero at the same time. For membrane wrinkling problems, imperfections, tension loads and shear loads should be imposed respectively. This is because at first few steps of Asymptotic Numerical Method, imperfections and tension are close to 0, leading to the presence of many localized modes and divergence of the results.

The x-axis is parallel to the bottom edge, y-axis is perpendicular to the bottom edge, and z-axis is normal to the neutral plane, as defined in Figure 4.1. The membrane analyzed in this chapter is a rectangular membrane with an aspect ratio of about 3:1. The material shown in Table 4.1 is Kapton coming from the data in [103] and [104]

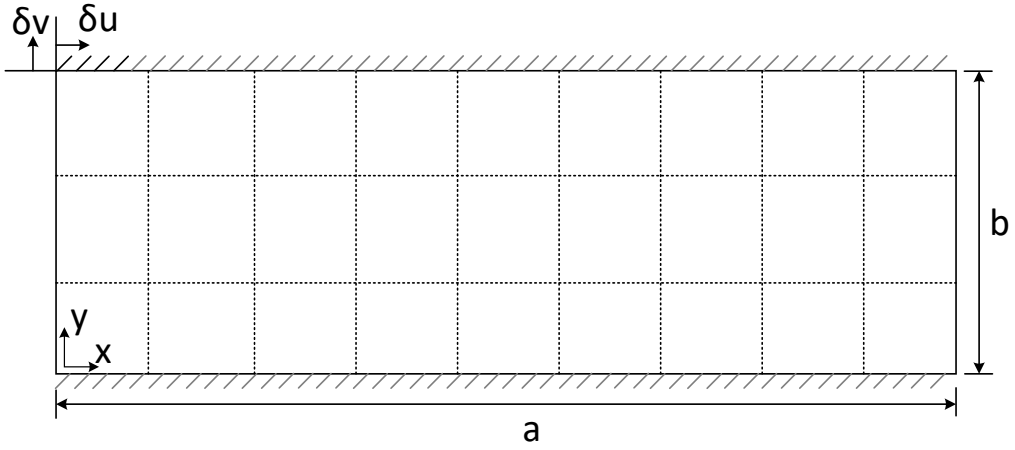

Figure 4.1 Rectangular membrane with tension δv and shear load δu

Table 4.1 Material property

Width (mm)	a	380
Height (mm)	b	128
Thickness (mm)	h	0.025
Young's modulus (MPa)	E	3500
Poisson's ratio	υ	0.3

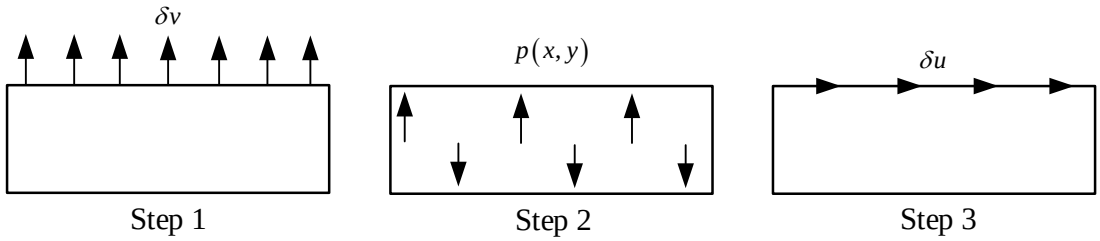

Figure 4.2 Steps of the algorithm

The loading process consists of three steps as in Figure 4.2:

The first step of the simulation is pre-tensioning the membrane by moving the top edge by a small displacement δv in y-direction. All degrees of freedom of the bottom edge are constrained. The left and right edges are simply supported. The fixed top edge is subjected to a prescribed displacement. A pre-stress is produced to increase the out-of-plane stiffness of the thin membrane and avoid local buckling

behavior. The initial pre-stress will affect the final amount of the wrinkles. This will be discussed later in this chapter. As the pressure p in Von-Karman equations cannot be zero, it is set to a very small value $p = 10^{-20}$.

The second step consists in producing imperfection by imposing transverse pressure onto the membrane. Here the membrane is splitted into several domains in both directions. The pressure will be positive and negative alternately in x-direction to produce sinusoidal deformation in transverse direction. The pressure remains consistent in y-direction. Note that the angle between the deformation and x-axis is 90°, which is different from the final wrinkles. Nevertheless, this treatment is better than pseudorandom imperfections produced on nodes or imposing pressure on a single direction. An imperfection sample is shown in Figure 4.3.

In the third and final step, the top edge is moved horizontally by a displacement δu while all other boundary conditions are the same as in the first and second steps. The shear displacement is gradually increased until the membrane is fully wrinkled. The pressure is set to the small value 10^{-20} as in the first step.

Figure 4.3 An imperfection sample

The plate is simply supported on vertical edges and clamped on horizontal edges with a displacement along the top edge as given by Eq.(4.1). These conditions are modeled using the method in Chapter 3. Previous study indicates that the convergence of the computation needs a moderate degree of Taylor series and a large number of subdomains [68]. The degree of Taylor series is chosen as $N = 8$ that is reasonable when the subdomains are sufficient, giving consideration to computational efficiency and accuracy. The degree of ANM is chosen as 10. The accuracy factor in ANM is 10^{-8}.

$$\begin{array}{llll} w=0 & \partial w/\partial y=0 & u=0 & v=0 \quad (0\le x\le a, y=0) \\ w=0 & \partial w/\partial y=0 & u=\delta u & v=\delta v \quad (0\le x\le a, y=b) \\ w=0 & M_x=0 & \sigma_x=0 & \tau_{xy}=0 \quad (x=0\,\&\,a, 0\le y\le b) \end{array} \tag{4.1}$$

4.3 Numerical Results

The material properties, geometric parameters and boundary conditions are introduced into the model in Chapter 3. Numerical simulations aim to find the important influencing factors of wrinkling of thin membranes with this new meshless method. Because of TMM's advantage on convergence with small loads, as illustrated in buckling tests of thin plates, the smallest tension and imperfections are searched, which can bring out bending stiffness and initiate the out-of-plane buckled deformations contributing to membrane wrinkling. Different combinations of tension loads, imperfections and number of subdomains are considered to test the sensitivity of the model to the wrinkling results.

Different numbers of subdomains are used as it has great influence on the convergence and final number of wrinkles. The ratio of the number of subdomains in x and y-directions is 3:1, which is roughly consistent with the aspect ratio of the membrane. The pre-tensioning displacement is ranged from 0 to 0.08mm. Different kinds of imperfections, defined as transverse deformation of the center point, are considered from 0 to 0.008mm.

4.3.1 Generation of membrane wrinkles

The generation of membrane wrinkles is demonstrated in this section. The membrane is splitted into 33 domains in x-direction and 11 in y-direction with a pre-tension of $\delta v = 0.02mm$ in the first step. The selection of the number of subdomains and tension load will be discussed later in this chapter. The membrane is tensioned in y-direction, keeping a flat state. Then the imperfection is produced by imposing transverse pressure, generating 0.001mm out-of-plane deformation at the center of the membrane. By imposing alternating pressure in x-direction, the

membrane generates alternating deformation as shown in Figure 4.4. Because of simply supported boundary conditions on side edges and bending stiffness produced by the pre-tension, the deformation near side edges is larger than that inside the membrane.

Figure 4.4 Imperfection of the membrane for wrinkling, tension load 0.02mm, imperfection 0.001mm.

Wrinkle generation is associated with mode jumps in terms of the interaction of a set of bifurcation points. There are several equilibrium paths after each bifurcation points. The deformation patterns have many possibilities when the membrane has many wrinkles. When the first equilibrium point exist, the wrinkles increase up to a certain number without bifurcations by increasing the shear displacement. Then, because of the selected imperfections and tension loads, the bifurcation paths converge to a single path. In this study, the observation focuses on this period from the beginning until the membrane is full wrinkled.

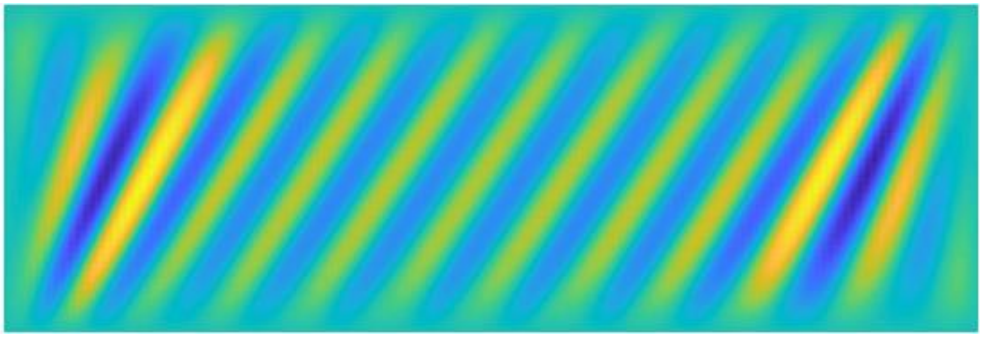

Figure 4.5 Full wrinkled membrane, 33×11 domains, tension load 0.02mm, imperfection 0.001mm.

Figure 4.5 shows the whole wrinkled patterns in the membrane. The wrinkles in the central region cross the whole membrane, making an angle of 45° with x-axis. There are two localized wrinkles in the triangular regions of the upper left and bottom right corners near the side edges. In this study, only wrinkles crossing the whole

membrane are counted.

4.3.2 Sensitivity with respect to the number of subdomains

When the deformation of structures becomes complex, two common approaches can be used to maintain the accuracy of the simulation: a larger degree of Taylor series or the multi-domain technique. A very large degree leads to high computational costs and large conditioning number of the matrix, which may decrease the stability of the computation. In this study, it is obvious that a single Taylor series is not sufficient to approximate the whole wrinkled membrane. Therefore, the membrane is divided to several subdomains with independent Taylor series in each part. Two neighboring domains are coupled by physical constraints.

The present parametric study is accomplished by varying the number of subdomains in which the membrane is divided. To avoid the influence of distortion, domains in x-direction and y-direction keep a quantitative ratio of 3:1, making each domain roughly a square. The results from wrinkling analysis are presented in Table 4.2, related to the final number of wrinkles corresponding to a shear load $\delta u = 0.15mm$. The problem cannot be simulated if the number of subdomains is less than 17×6. The simulation can be proceeded with 21×7 domains and predict 8 wrinkles shown in Figure 4.6. Three additional sets of domains are tested to investigate the effect of number of domains on the final wrinkle number. 33×11, 45×15 and 63×21 predict the same number of wrinkles, indicating that the results become independent when the number of domains is enough. In order to achieve a compromise between the computational efficiency and the accuracy of the results, the optimal mesh is at least three domains in x-direction to describe one wrinkle. In consideration of computational time and convergence of the solution, the set of 33×11 is selected in previous sections.

Table 4.2 Sensitivity of the response (number of wrinkles) to the number of sub-domains. Pre-tension $\delta v = 0.02$ mm, imperfection 0.001mm.

Number of domains	Number of wrinkles
15×5	Not converging
17×6	Not converging
21×7	8
33×11	11
45×15	11
63×21	11

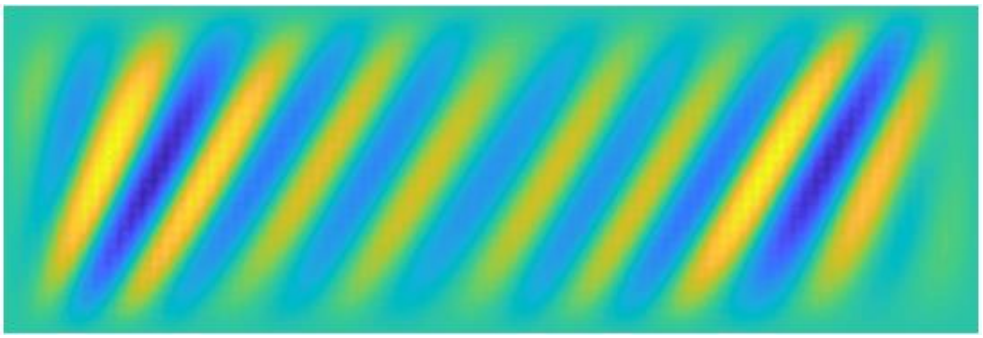

Figure 4.6 Full wrinkled membrane. Subdomains: 21×11, tension load 0.02mm, imperfection 0.001mm, shear load 0.15mm.

4.3.3 Sensitivity with respect to tension loads

The uniaxial tension load in y-direction provides an initial out-of-plane stiffness to the membrane, which is an important factor in determining the membrane wrinkles and computational stability. To test the sensitivity of tension loads, all the cases in this section are applied with an imperfection of 0.001mm and 33×11 subdomains.

4.3.3.1 A global look

Table 4.3 shows the final number of wrinkles for $\delta u = 0.15mm$ with different tension loads. Patterns are shown in Figure 4.7. The simulation cannot be proceeded without this pre-tensioning treatment. With 0.0005mm tension load, the membrane generates three main wrinkles and some minor local ones. In the range of 0.001mm to 0.02mm, the tension load has a strong effect on the number of wrinkles. After 0.02mm, the membrane keeps generating 11 wrinkles at the end of the computation. By

increasing the tension load, the angle between wrinkles and the bottom edge decreases to 45°.

Table 4.3 Number of wrinkles with different tension loads.

Tension load(mm)	Number of wrinkles
0.0005	3
0.001	4
0.01	10
0.02	11
0.05	11
0.08	11

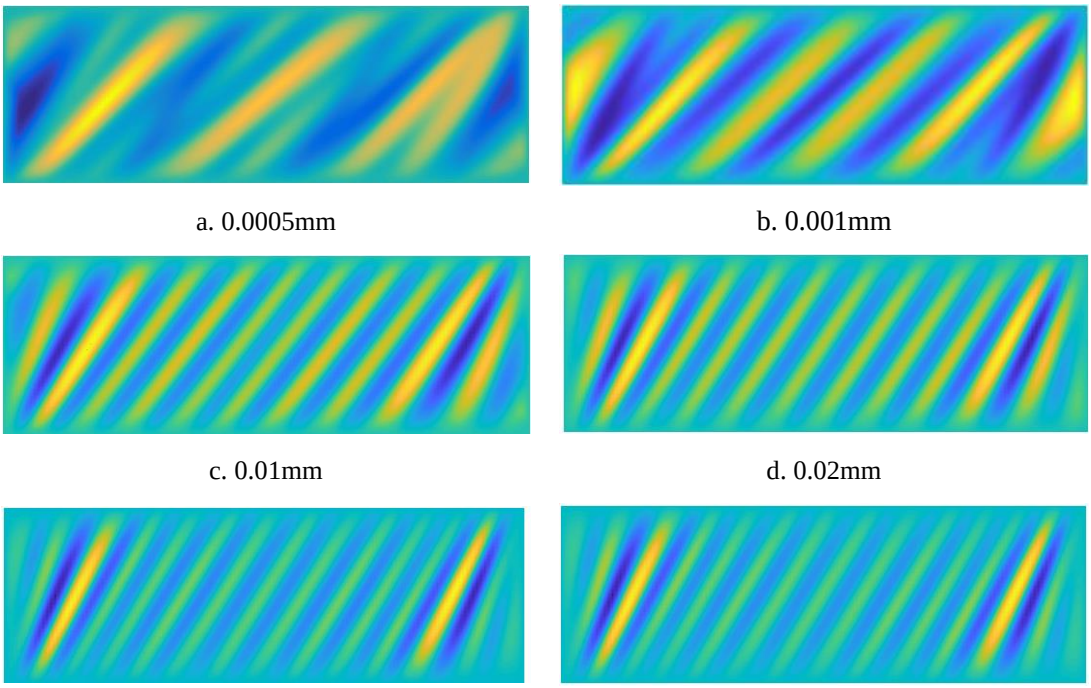

a. 0.0005mm b. 0.001mm

c. 0.01mm d. 0.02mm

e. 0.05mm f. 0.08mm

Figure 4.7 Wrinkle patterns with different tension loads.

The buckling curves of cases with a wide range of tension loads are shown in Figure 4.8. With a very small tension load, for example 0.0005mm or 0.001m, the membrane starts global buckling very early. A larger tension load leads to a larger critical shear load and a smaller maximum displacement, because of the increase of the global stiffness. Table 4.4 is the comparison of the maximum displacements and

amplitudes of center wrinkles when the shear load is 0.15mm.

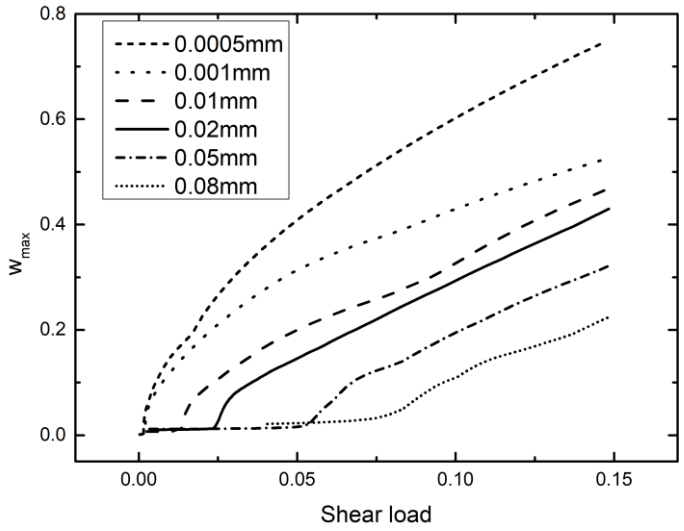

Figure 4.8 Shear load vs maximum displacement, tension loads from 0.0005mm to 0.08mm, imperfection 0.001mm.

Table 4.4 The maximum displacements and amplitudes of center wrinkles, shear load 0.15mm, imperfection 0.001mm.

Tension load(mm)	w_{max} (mm)	Amplitude of the central wrinkle(mm)
0.0005	0.7482	0.5461
0.001	0.5302	0.4081
0.01	0.4732	0.1893
0.02	0.4150	0.1686
0.05	0.3245	0.1186
0.08	0.2266	0.0643

4.3.3.2 A closer look

Now a closer look near the bifurcation point will be taken to observe the generation of membrane wrinkles. A zoom of the buckling curve with 0.05mm tension load in Figure 4.8 is shown in Figure 4.9. The further zoom of the buckling curve in Figure 4.9 indicates that the maximum displacement is monotonically increasing, which means the equilibrium continuation path is unique in the wrinkling process. The deformations of the membrane on selected points are plotted in Figure 4.10. The

membrane is quasi-flat when the shear load is smaller than 0.05mm. The first few wrinkles are generated near boundaries with 0.06mm shear load. The position of the maximum displacement moves towards the center area while the center area still keeps quasi-flat as shown in Figure 4.10(c) and Figure 4.10(d). From Figure 4.10(d) to Figure 4.10(e), the maximum position stops moving and wrinkles begin to appear in center area. In Figure 4.10(f), the membrane becomes stable and full wrinkled. Because of the boundary effect, the membrane starts wrinkling near boundaries and extends to the center area with the increase of the shear load. The amplitudes of the central wrinkles are much smaller compared with the largest one.

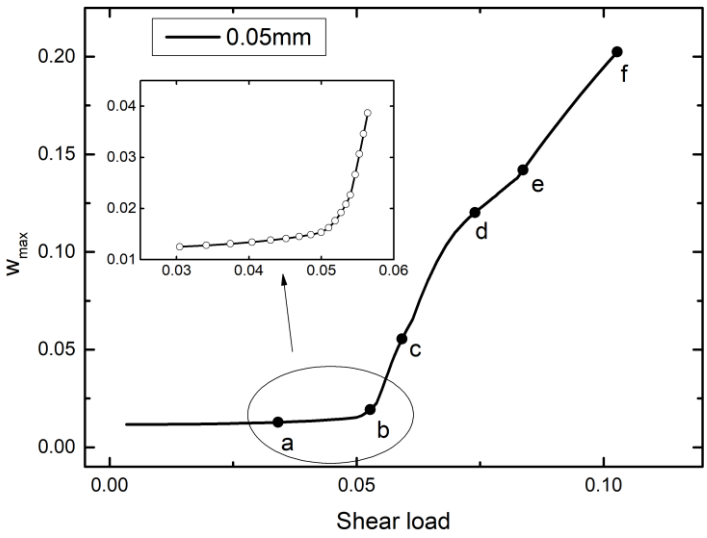

Figure 4.9 A zoom of the buckling curve, tension load 0.05mm.

In the FEM study by Wong [102] , the attempts to compute the full response in ABAQUS by an arc-length method are unsuccessful due to the complex localized instability, therefore they use transient dynamics to compute the solution in this case $\delta u = 0.05mm$. Using an arc-length method is difficult to find a stable branch in the equilibrium path of membrane wrinkling. By using ANM-TMM, however, the path-following technique can obtain the whole developing details of a wrinkled membrane as discussed in this section.

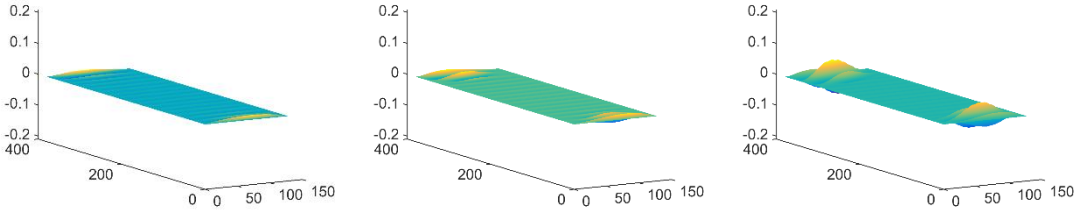

a. 0.0341mm b. 0.0527mm c. 0.0592mm

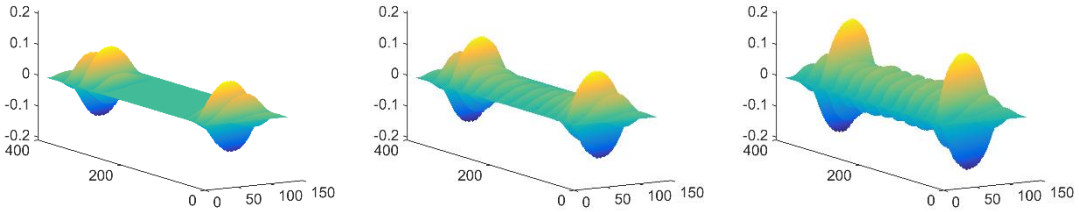

d. 0.0740mm e. 0.0837mm f. 0.1028mm

Figure 4.10 Deformations of the membrane with different shear loads, tension load 0.05mm.

4.3.3.3 Membrane wrinkling with a very small tension load

Another advantage of this method is that we were able to use a very small tension load to accomplish the simulation. The initial pretension in [102], which corresponds to the tension load in this thesis, is chosen as 0.05mm. This value is much smaller than that in his previous eigenvalue buckling analysis, from which the geometrical imperfections are obtained. However, the initial pretension still has to be large enough so that the membrane can avoid some localized modes and enter the global buckling period. In Figure 4.8, one can see that ANM-TMM works with tension loads much smaller than 0.05mm. In this section, the wrinkling development with a very small tension load 0.001mm will be discussed.

A zoom of the buckling curve with 0.001mm tension load in Figure 4.8 is shown in Figure 4.11. The further zoom of the buckling curve indicates that the maximum displacement has a slight decrease before the global buckling point. The computation follows another localized unstable branch then turns to the global one.

The deformations of the membrane on selected points are plotted in Figure 4.12. The membrane keeps quasi-flat before the critical shear load 0.0020mm. In Figure 4.12(d), four wrinkles are generated uniformly on the whole membrane. From Figure

4.12(e) to Figure 4.12(f), the deformation keeps increasing without any new wrinkle generated. The small tension load leads to a weak boundary effect, thus the wrinkles are generated simultaneously with approximately equal amplitudes. This is the main difference between this case and that in 4.3.3.2. Thus, the tension load has a very strong effect on all the aspects of the wrinkling process: first bifurcation load, number of wrinkles and spatial distribution of the amplitude of wrinkles.

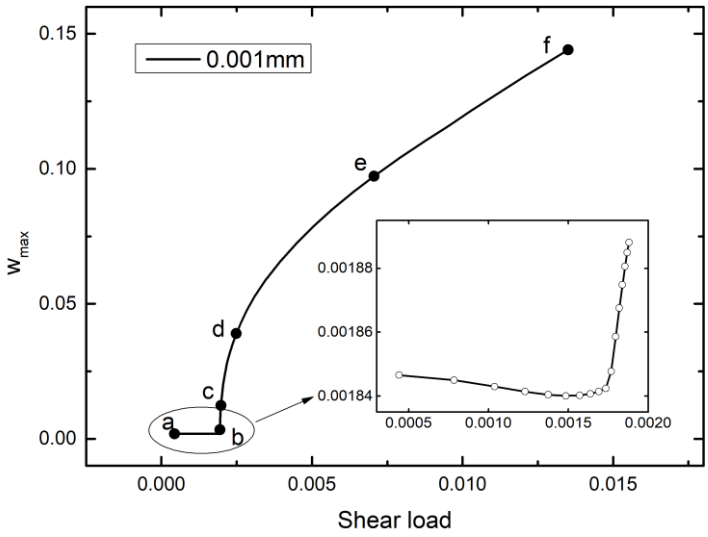

Figure 4.11 A zoom of the buckling curve, tension load 0.001mm.

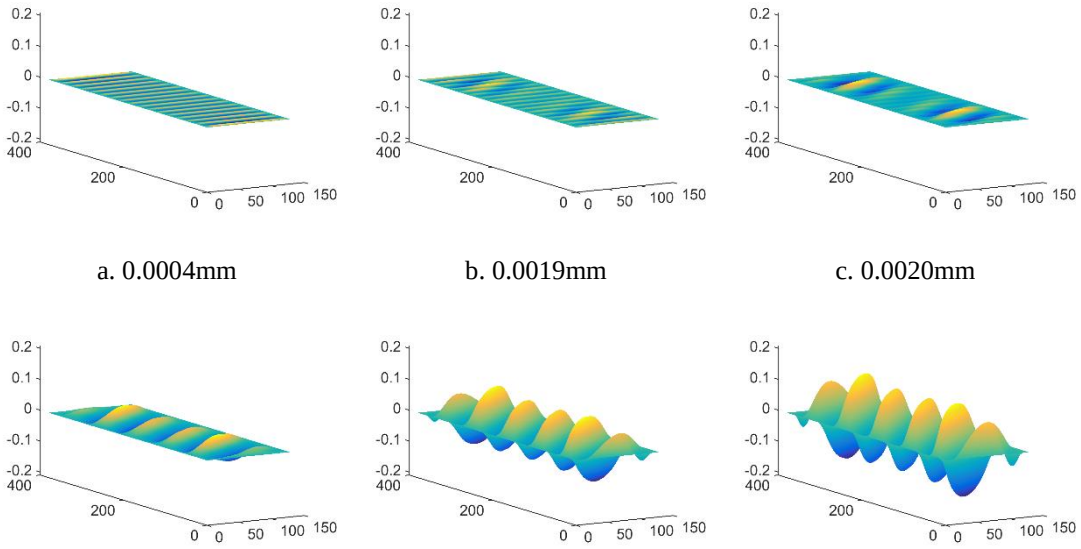

a. 0.0004mm b. 0.0019mm c. 0.0020mm

d. 0.0025mm e. 0.0071mm f. 0.0135mm

Figure 4.12 Deformations of the membrane with different shear loads, tension load 0.001mm.

4.3.3.4 Membrane wrinkling with a minimum tension load

The pre-tension process is an important step to stabilize the equilibrium path. If the tension load is too small, the simulation may not be accomplished as the algorithm could be trapped in the computation of local modes. It will be of important significance to find the limitation of ANM-TMM and study the behavior of the membrane with the smallest tension load.

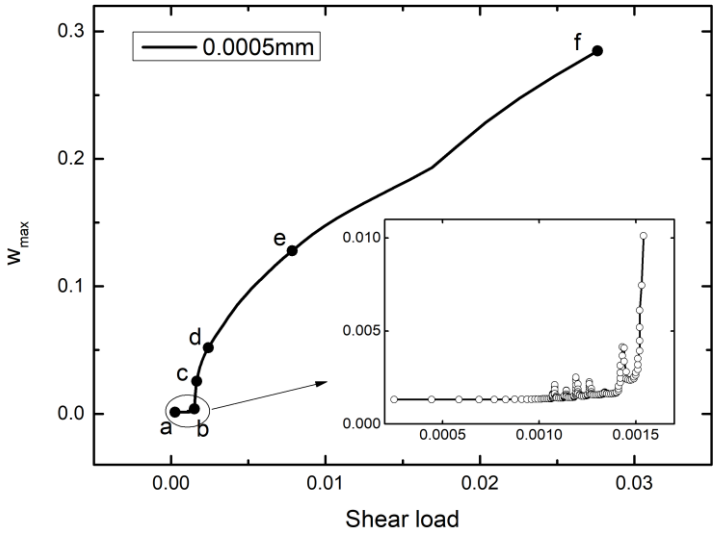

Figure 4.13 A zoom of the buckling curve, tension load 0.0005mm.

Figure 4.13 is a zoom of the buckling curve with 0.0005mm tension load in Figure 4.8. The membrane responses quickly with many localized buckling modes after the shear load is applied. The further zoom of the curve shows that the algorithm chooses an unstable branch automatically and then goes back to the fundamental equilibrium path. A stable bifurcated solution is reached after seeking for about 5 times. This phenomenon does not occur in the section 4.3.3.14.3.3.2 and 4.3.3.3 because the tension loads are large enough to stabilize the membrane and a stable equilibrium path can be sought very easily.

The deformations of the membrane on selected points in Figure 4.13 are plotted in Figure 4.14. At point b, the computation has left the fundamental equilibrium path and generated two wrinkles. From point c to point e, the main wrinkles grow up coupled with many localized minor ones. On the final pattern, another main wrinkle is generated in center area and the center displacement becomes positive, indicating a

mode jump between point e and point f.

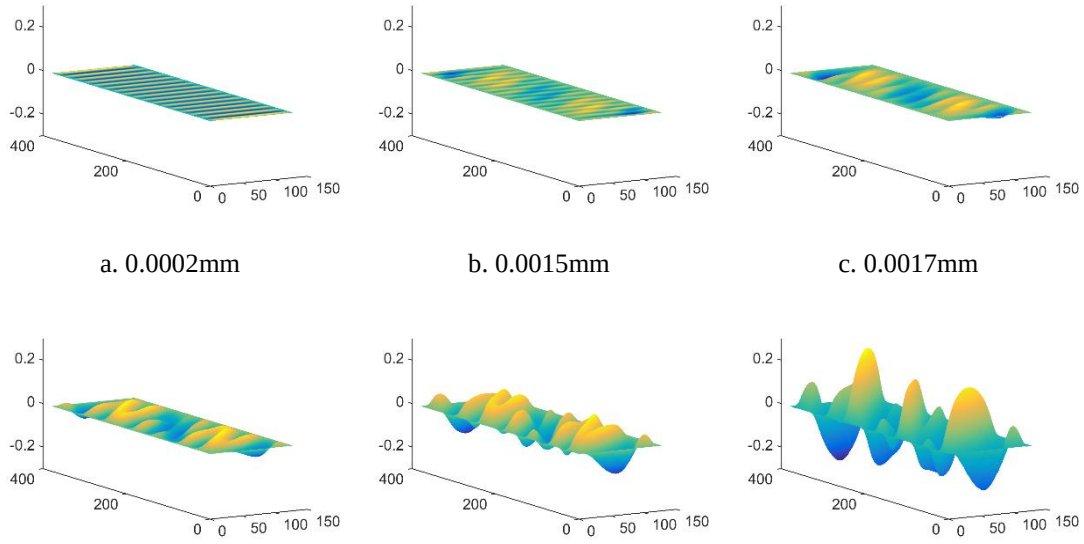

a. 0.0002mm b. 0.0015mm c. 0.0017mm

d. 0.0024mm e. 0.0078mm f. 0.0276mm

Figure 4.14 Deformations of the membrane with different shear loads, tension load 0.0005mm.

4.3.4 Imperfection sensitivity

Buckling problems cannot be analyzed directly because of the discontinuity at the bifurcation point. To obtain a response in the buckling analysis, an imperfection should be introduced. The response of some structures may highly affected by the imperfections applied to the original geometry. It is necessary to verify the imperfection sensitivity of the structure in membrane wrinkling simulation.

A moderate value $\delta v = 0.02$ mm is chosen as a tension load when testing the imperfection sensitivity. The imperfection is introduced into the original geometry according to Section 4.2. For each set of imperfections, a complete wrinkling simulation was carried out to observe the final number of wrinkles. Normally, the magnitudes of the perturbations are small in comparison with the membrane thickness. The imperfection, which is defined as the out-of-plane deformation at the center of the membrane, is ranged from 0.00006mm to 0.008mm.

The results from this study are presented in Table 4.5. In a wide range, the amplitudes of imperfections are independent with the final number of wrinkles. The

particular magnitude of the chosen imperfection is not critical. In practice, the optimal ratio of the imperfection and thickness is between 0.02 and 0.1. The smallest imperfection that can proceed the simulation is very small ($0.0001\text{mm}, 0.004h$). In comparison, the simulations are generally proceeded with imperfections of larger than $0.01h$ in FEM. The number of wrinkles begins to decrease when the imperfection is larger than 0.005mm ($0.2h$). This means that the number of wrinkles is sensitive to imperfections in the range larger than $0.2h$.

Table 4.5 Sensitivity of the response (number of wrinkles) to the imperfection. Pre-tension $\delta v = 0.02$ mm, number of sub-domains: 33×11.

Imperfection(mm)	Imperfection/h	Number of wrinkles
0.0001	0.004	11
0.0005	0.02	11
0.001	0.04	11
0.002	0.08	11
0.003	0.12	11
0.005	0.20	10
0.008	0.32	9

The largest imperfection that can use to generate reliable wrinkle patterns is smaller than that in FEM. This is because the different methods of imposing imperfections. In ABAQUS, imperfections are introduced by imposing geometric deformation directly on nodes or a linear superposition of buckling eigenmodes from the static analysis. In this study, a transverse pressure is imposed to the membrane to produce out-of-plane deformation. The stress distribution before wrinkling analysis is slightly different from that in ABAQUS. When imperfections are large, the influence of the pressure is not negligible.

4.4 Conclusion

This chapter is an extension of the previous work on the use of TMM for large deflection of thin plates. In this chapter, the membrane wrinkling problem is studied

with Taylor meshless method. Based on equilibrium equations and solution process established in Chapter 3, the wrinkle patterns are observed by imposing tension loads, imperfections and shear loads successively.

The imperfections are introduced by imposing transverse pressure, instead of pseudo-random geometric displacements on nodes or seeding initial buckling modes of a perfect membrane. This is an easy way to avoid stress concentration and localized buckling modes.

Different tension loads and imperfections are imposed to test their influence on final wrinkle patterns. The results indicate that imperfections should be large enough so that they can provide sufficient bending-to-membrane coupling. In a range, the magnitude of imperfections has no influence on the final wrinkling results.

The tension loads provide a small bending stiffness to the membrane, which should be considered to accurately calculate out-of-plane deformation. The study indicates that tension loads has a great influence on the final number of wrinkles.

TMM can accomplish convergent simulations with very small imperfections and tension loads in comparison with finite element methods. The approach of wrinkled membrane analysis by TMM has been well established. The future work includes detailed study on wrinkle amplitude and wavelength in membrane wrinkling problems.

Conclusions and future works

In this work, the behavior of thin plates and membranes are investigated by using a boundary collocation meshless method – Taylor Meshless Method (TMM), in which the PDEs are approximated by Taylor series and the boundaries are discretized with a least square collocation. Various parameters that govern the bending, buckling and wrinkling behaviors of thin structures are identified by numerical simulations.

First, the basic techniques of TMM is introduced. The degrees of freedom of the problem are reduced significantly by seeking independent coefficients in the truncated Taylor series that constructs shape functions. The effectiveness and efficiency of TMM are verified by solving a 2D Laplace equation.

Then, TMM is used to study Kirchhoff plates and laminated sandwich plates. Techniques in TMM help to reduce the degree of freedoms significantly so that one can increase the degree of the polynomials to a very high level. Different cases are considered to test the effectiveness and efficiency of the method. The error shows exponential convergence with the increase of degree of polynomials.

Next, TMM is combined with Asymptotic Numerical Method (ANM) to solve large deflection problems of thin plates. The nonlinear equations are expanded in the form of power series, which leads the problem to a series of linear equations. The step length is determined automatically by a reliable path following technique. The accuracy and efficiency of ANM-TMM is verified through these examples and the method can be easily extended to other nonlinear problems.

Based on the work of bending problems, the buckling of thin plates are studied. This approach fully takes the advantage of the path following technique. Thus the buckling process can be illustrated much more accurate than that by other methods. The performance of the approach is investigated by a series of benchmark buckling problems.

Last, the membrane wrinkling problems are studied. Different tension loads and

imperfections are imposed to test their influence on final wrinkle patterns. The results show that TMM can accomplish convergent simulations with very small imperfections and tension loads in comparison with finite element methods. The tension load has a strong effect on the amplitudes and number of global wrinkles while the imperfection affects the number of wrinkles only when it is large enough. The approach of wrinkled membrane analysis by TMM has been well established.

As revealed in this work, TMM is an efficient and robust method for a variety of linear and nonlinear elastic problems. Nevertheless, it will be of great significance to extend the application of TMM to many other engineering fields. Some further explorations could make TMM a more practical numerical tool:

1) As the algorithm for computing shape functions and introducing boundary conditions needs to be optimized, the computational efficiency can be improved with the help of techniques such as Automatic Differentiation.

2) Based on the resolution established in Chapter 3 and Chapter 4, a toolbox for thin structure problems can be developed to simplify the procedure in the pretreatment and optimize the interaction.

3) The numerical work on thin plate problems provides a good foundation for studying thin shells. It will also be interesting to extend the application of TMM to more challenging problems, involving fluid-solid coupling, contact and even vibration.

References

[1] M. Huang, B. Liu, T. Xu, Numerical calculation method, Science Press, Beijing, 2005.

[2] J. Ghaboussi, X. S. Wu, Numerical methods in computational mechanics, CRC Press, Boca Raton, 2016.

[3] R. J. LeVeque, Finite difference methods for ordinary and partial differential equations: steady-state and time-dependent problems, SIAM, Seattle, 2007.

[4] T. Liszka, J. Orkisz, The finite difference method at arbitrary irregular grids and its application in applied mechanics, Computers & Structures 11 (1980) 83-95.

[5] R. W. Clough, Thoughts about the origin of the finite element method, Computers and Structures 22 (2001) 2029-2030.

[6] C. Ray W, Early history of the finite element method from the view point of a pioneer, International Journal for Numerical Methods in Engineering 60 (2004) 283-287.

[7] O. C. Zienkiewicz, Y. K. Cheung, The finite element method in structural and continuum mechanics, McGraw-Hill, London, New York, 1967.

[8] X. Liu, Meshless methods, Science Press, Beijing, 2011.

[9] X. Zhang, Y. Liu, Meshless methods, Tsinghua University Press, Beijing, 2004.

[10] G. R. Liu, Meshfree methods: moving beyond the finite element method, CRC Press, 2009.

[11] R. A. Gingold, J. J. Monaghan, Smoothed particle hydrodynamics: theory and application to non-spherical stars, Monthly Notices of the Royal Astronomical Society 181 (1977) 375-389.

[12] L. B. Lucy, A numerical approach to the testing of the fission hypothesis, The Astronomical Journal 82 (1977) 1013-1024.

[13] J. J. Monaghan, Why particle methods work, SIAM Journal on Scientific and Statistical Computing 3 (1982) 422-433.

[14] J. J. Monaghan, An introduction to SPH, Computer Physics Communications 48

(1988) 89-96.

[15] J. Monaghan, R. A. Gingold, Shock simulation by the particle method SPH, Journal of Computational Physics 52 (1983) 374-389.

[16] J. Lattanzio, J. Monaghan, H. Pongracic, M. Schwarz, Controlling penetration, SIAM Journal on Scientific and Statistical Computing 7 (1986) 591-598.

[17] R. Gingold, J. Monaghan, The Roche problem for polytropes in central orbits, Monthly Notices of the Royal Astronomical Society 191 (1980) 897-924.

[18] G. Phillips, J. Monaghan, A numerical method for three-dimensional simulations of collapsing, isothermal, magnetic gas clouds, Monthly Notices of the Royal Astronomical Society 216 (1985) 883-895.

[19] W. K. Liu, S. Jun, Y. F. Zhang, Reproducing kernel particle methods, International Journal for Numerical Methods in Fluids 20 (1995) 1081-1106.

[20] W. K. Liu, Y. Chen, Wavelet and multiple scale reproducing kernel methods, International Journal for Numerical Methods in Fluids 21 (1995) 901-931.

[21] W. K. Liu, Y. Chen, R. A. Uras, C. T. Chang, Generalized multiple scale reproducing kernel particle methods, Computer Methods in Applied Mechanics and Engineering 139 (1996) 91-157.

[22] J. S. Chen, C. Pan, C. T. Wu, W. K. Liu, Reproducing kernel particle methods for large deformation analysis of non-linear structures, Computer Methods in Applied Mechanics and Engineering 139 (1996) 195-227.

[23] Z. Lin, F. Liu, D. Wang, Y. Gu, Reproducing kernel particle method for two-dimensional time-space fractional diffusion equations in irregular domains, Engineering Analysis with Boundary Elements 97 (2018) 131-143.

[24] D. Wang, P. Chen, Quasi-convex reproducing kernel meshfree method, Computational Mechanics 54 (2014) 689-709.

[25] P. Lancaster, K. Salkauskas, Surfaces generated by moving least squares methods, Mathematics of Computation 37 (1981) 141-158.

[26] T. Belytschko, Y. Krongauz, M. Fleming, D. Organ, W. K. S. Liu, Smoothing and accelerated computations in the element free Galerkin method, Journal of Computational and Applied Mathematics 74 (1996) 111-126.

[27] B. A. Szabo, I. Babuška, Computation of the amplitude of stress singular terms for cracks and reentrant corners, Fracture mechanics: nineteenth symposium, San Antonio, 1988.

[28] B. Nayroles, G. Touzot, P. Villon, Generalizing the finite element method: diffuse approximation and diffuse elements, Computational Mechanics 10 (1992) 307-318.

[29] T. Belytschko, Y. Y. Lu, L. Gu, Element-free Galerkin methods, International Journal for Numerical Methods in Engineering 37 (1994) 229-256.

[30] T. Belytschko, L. Gu, Y. Lu, Fracture and crack growth by element free Galerkin methods, Modelling and Simulation in Materials Science and Engineering 2 (1994) 519.

[31] T. Belytschko, Y. Lu, L. Gu, M. Tabbara, Element-free Galerkin methods for static and dynamic fracture, International Journal of Solids and Structures 32 (1995) 2547-2570.

[32] Y. Lu, T. Belytschko, M. Tabbara, Element-free Galerkin method for wave propagation and dynamic fracture, Computer Methods in Applied Mechanics and Engineering 126 (1995) 131-153.

[33] T. Belytschko, Y. Lu, L. Gu, Crack propagation by element-free Galerkin methods, Engineering Fracture Mechanics 51 (1995) 295-315.

[34] T. Belytschko, M. Tabbara, Dynamic fracture using element-free Galerkin methods, International Journal for Numerical Methods in Engineering 39 (1996) 923-938.

[35] M. Fleming, Y. Chu, B. Moran, T. Belytschko, Enriched element-free Galerkin methods for crack tip fields, International Journal for Numerical Methods in Engineering 40 (1997) 1483-1504.

[36] P. Krysl, T. Belytschko, The element free Galerkin method for dynamic propagation of arbitrary 3-D cracks, International Journal for Numerical Methods in Engineering 44 (1999) 767-800.

[37] G. Li, T. Belytschko, Element-free Galerkin method for contact problems in metal forming analysis, Engineering Computations 18 (2001) 62-78.

[38] I. Singh, K. Sandeep, R. Prakash, Heat transfer analysis of two-dimensional fins using meshless element free Galerkin method, Numerical Heat Transfer: Part A: Applications 44 (2003) 73-84.

[39] X. Chen, G. Liu, S. Lim, An element free Galerkin method for the free vibration analysis of composite laminates of complicated shape, Composite Structures 59 (2003) 279-289.

[40] A. Huerta, Y. Vidal, P. Villon, Pseudo-divergence-free element free Galerkin method for incompressible fluid flow, Computer Methods in Applied Mechanics and Engineering 193 (2004) 1119-1136.

[41] A. Singh, I. V. Singh, R. Prakash, Meshless element free Galerkin method for unsteady nonlinear heat transfer problems, International Journal of Heat and Mass Transfer 50 (2007) 1212-1219.

[42] E. Onate, S. Idelsohn, O. Zienkiewicz, R. Taylor, A finite point method in computational mechanics. Applications to convective transport and fluid flow, International Journal for Numerical Methods in Engineering 39 (1996) 3839-3866.

[43] E. Onate, S. Idelsohn, O. Zienkiewicz, R. Taylor, C. Sacco, A stabilized finite point method for analysis of fluid mechanics problems, Computer Methods in Applied Mechanics and Engineering 139 (1996) 315-346.

[44] R. Löhner, C. Sacco, E. Onate, S. Idelsohn, A finite point method for compressible flow, International Journal for Numerical Methods in Engineering 53 (2002) 1765-1779.

[45] H. Dalayeli, H. Hashemolhosseini, M. Farzin, B. Soltani, Improvement of the flow formulation by recovery of the hydrostatic pressure using the finite point method, International Journal for Numerical Methods in Engineering 65 (2006) 1403-1418.

[46] E. Oñate, F. Perazzo, J. Miquel, A finite point method for elasticity problems, Computers & Structures 79 (2001) 2151-2163.

[47] C. A. Duarte, J. T. Oden, An hp adaptive method using clouds, Computer Methods in Applied Mechanics and Engineering 139 (1996) 237-262.

[48] T. Liszka, C. Duarte, W. Tworzydlo, hp-Meshless cloud method, Computer Methods in Applied Mechanics and Engineering 139 (1996) 263-288.

[49] J. T. Oden, C. A. Duarte, Solution of singular problems using hp clouds, Mathematics of Finite Elements and Applications 9 (1996) 35-54.

[50] S. N. Atluri, T. Zhu, A new meshless local Petrov-Galerkin (MLPG) approach in computational mechanics, Computational Mechanics 22 (1998) 117-127.

[51] S. Atluri, T. L. Zhu, The meshless local Petrov-Galerkin (MLPG) approach for solving problems in elasto-statics, Computational Mechanics 25 (2000) 169-179.

[52] G. R. Liu, Y. Gu, A point interpolation method for two-dimensional solids, International Journal for Numerical Methods in Engineering 50 (2001) 937-951.

[53] J. Wang, G. Liu, Radial point interpolation method for elastoplastic problems, ICSSD 2000: 1st Structural Conference on Structural Stability and Dynamics, 2000.

[54] E. J. Kansa, Multiquadrics-A scattered data approximation scheme with applications to computational fluid-dynamics-I surface approximations and partial derivative estimates, Computers & Mathematics with applications 19 (1990) 127-145.

[55] K. Edward J, Multiquadrics-A scattered data approximation scheme with applications to computational fluid-dynamics-II solutions to parabolic, hyperbolic and elliptic partial differential equations, Computers & Mathematics with applications 19 (1990) 147-161.

[56] C. Franke, R. Schaback, Solving partial differential equations by collocation using radial basis functions, Applied Mathematics and Computation 93 (1998) 73-82.

[57] J. M. Melenk, I. Babuška, The partition of unity finite element method: basic theory and applications, Computer Methods in Applied Mechanics and Engineering 139 (1996) 289-314.

[58] T. Strouboulis, K. Copps, I. Babuška, The generalized finite element method, Computer Methods in Applied Mechanics and Engineering 190 (2001) 4081-4193.

[59] S. Beissel, T. Belytschko, Nodal integration of the element-free Galerkin method, Computer Methods in Applied Mechanics and Engineering 139 (1996) 49-74.

[60] A. Carpinteri, G. Ferro, G. Ventura, The partition of unity quadrature in meshless methods, International Journal for Numerical Methods in Engineering 54 (2002) 987-1006.

[61] X. Zhang, X. H. Liu, K. Z. Song, M. W. Lu, Least-squares collocation meshless method, International Journal for Numerical Methods in Engineering 51 (2001) 1089-1100.

[62] G. R. Liu, Y. T. Gu, A meshfree method: meshfree weak-strong (MWS) form method, for 2-D solids, Computational Mechanics 33 (2003) 2-14.

[63] A. Sadeghirad, S. Mohammadi, Equilibrium on line method (ELM) for imposition of Neumann boundary conditions in the finite point method (FPM), International Journal for Numerical Methods in Engineering 69 (2007) 60-86.

[64] D. S. Zézé, M. Potier-Ferry, N. Damil, A boundary meshless method with shape functions computed from the PDE, Engineering Analysis with Boundary Elements 34 (2010) 747-754.

[65] Y. Tampango, M. Potier-Ferry, Y. Koutsawa, S. Belouettar, Convergence analysis and detection of singularities within a boundary meshless method based on Taylor series, Engineering Analysis with Boundary Elements 36 (2012) 1465-1472.

[66] Y. Tampango, M. Potier-Ferry, Y. Koutsawa, S. Tiem, Coupling of polynomial approximations with application to a boundary meshless method, International Journal for Numerical Methods in Engineering 95 (2013) 1094-1112.

[67] J. Yang, H. Hu, M. Potier-Ferry, Solving large-scale problems by Taylor Meshless Method, International Journal for Numerical Methods in Engineering 112 (2017) 103-124.

[68] J. Yang, H. Hu, Y. Koutsawa, M. Potier-Ferry, Taylor meshless method for solving non-linear partial differential equations, Journal of Computational Physics 348 (2017) 385-400.

[69] A. H. D. Cheng, D. T. Cheng, Heritage and early history of the boundary element method, Engineering Analysis with Boundary Elements 29 (2005) 268-302.

[70] J. Yang, H. Hu, M. Potier-Ferry, Least-square collocation and Lagrange multipliers for Taylor Meshless Method, Numerical Methods for Partial Differential Equations 35 (2019) 84-113.

[71] A. E. H. Love, I. The small free vibrations and deformation of a thin elastic shell, Proceedings of the Royal Society of London 43 (1888) 352-353.

[72] S. P. Timoshenko, J. M. Gere, Theory of elastic stability, Courier Corporation, New York, 2009.

[73] Y. Xiong, A study on the Meshless Local Petrov-Galerkin Method for the Kirchhoff plate, Doctoral dissertation, Hunan University, 2004.

[74] J. T. Katsikadelis, The boundary element method for plate analysis, Academic Press, Oxford, 2014.

[75] S. Timoshenko, Theory of plates and shells, McGRAW-HILL, 2nd edition, New York, 1959.

[76] R. Seydel, Numerical computation of branch points in nonlinear equations, Numerische Mathematik 33 (1979) 339-352.

[77] E. Riks, An incremental approach to the solution of snapping and buckling problems, International Journal of Solids and Structures 15 (1979) 529-551.

[78] B. Cochelin, A path-following technique via an asymptotic-numerical method, Computers & Structures 53 (1994) 1181-1192.

[79] B. Cochelin, N. Damil, M. Potier-Ferry, Asymptotic-numerical methods and Padé approximants for non-linear elastic structures, International Journal for Numerical Methods in Engineering 37 (1994) 1187-1213.

[80] S. Baguet, B. Cochelin, On the behaviour of the ANM continuation in the presence of bifurcations, Communications in Numerical Methods in Engineering 19 (2003) 459-471.

[81] E. Boutyour, H. Zahrouni, M. Potier-Ferry, M. Boudi, Bifurcation points and bifurcated branches by an asymptotic numerical method and Padé approximants, International Journal for Numerical Methods in Engineering 60 (2004) 1987-2012.

[82] Y. Guevel, H. Boutyour, J. M. Cadou, Automatic detection and branch switching

methods for steady bifurcation in fluid mechanics, Journal of Computational Physics 230 (2011) 3614-3629.

[83] B. Cochelin, M. Medale, Power series analysis as a major breakthrough to improve the efficiency of Asymptotic Numerical Method in the vicinity of bifurcations, Journal of Computational Physics 236 (2013) 594-607.

[84] M. Potier-Ferry, N. Damil, B. Braikat, J. Descamps, J. M. Cadou, H. L. Cao, A. E. Hussein, Traitement des fortes non-linéarités par la méthode asymptotique numérique, Comptes Rendus de l'Académie des Sciences-Series IIB-Mechanics-Physics-Chemistry-Astronomy 324 (1997) 171-177.

[85] A. Tri, H. Zahrouni, M. Potier-Ferry, High order continuation algorithm and meshless procedures to solve nonlinear Poisson problems, Engineering Analysis with Boundary Elements 36 (2012) 1705-1714.

[86] A. Tri, H. Zahrouni, M. Potier-Ferry, Bifurcation indicator based on meshless and asymptotic numerical methods for nonlinear Poisson problems, Numerical Methods for Partial Differential Equations 30 (2014) 978-993.

[87] P. Assari, H. Adibi, M. Dehghan, A meshless method based on the moving least squares (MLS) approximation for the numerical solution of two-dimensional nonlinear integral equations of the second kind on non-rectangular domains, Numerical Algorithms 67 (2014) 423-455.

[88] J. A. Kołodziej, A. Zielinski, Boundary collocation techniques and their application in engineering, WIT Press, Southampton, Boston, 2009.

[89] G. Fairweather, A. Karageorghis, The method of fundamental solutions for elliptic boundary value problems, Advances in Computational Mathematics 9 (1998) 69.

[90] R. Schaback, Error estimates and condition numbers for radial basis function interpolation, Advances in Computational Mathematics 3 (1995) 251-264.

[91] A. D. Cheng, M. Golberg, E. Kansa, G. Zammito, Exponential convergence and H-c multiquadric collocation method for partial differential equations, Numerical Methods for Partial Differential Equations: An International Journal 19 (2003) 571-594.

[92] C. J. Alves, On the choice of source points in the method of fundamental solutions, Engineering Analysis with Boundary Elements 33 (2009) 1348-1361.

[93] P. R. Antunes, Reducing the ill conditioning in the method of fundamental solutions, Advances in Computational Mathematics 44 (2018) 351-365.

[94] K. Balakrishnan, P. A. Ramachandran, Osculatory interpolation in the method of fundamental solution for nonlinear Poisson problems, Journal of Computational Physics 172 (2001) 1-18.

[95] D. Nath, M. Kalra, P. Munshi, One-stage Method of Fundamental and Particular Solutions (MFS-MPS) for the steady Navier-Stokes equations in a lid-driven cavity, Engineering Analysis with Boundary Elements 58 (2015) 39-47.

[96] M. Jankowska, J. Kołodziej, A study of elastic-plastic deformation in the plate with the incremental theory and the meshless methods, Journal of Mechanics of Materials and Structures 11 (2016) 41-60.

[97] A. Griewank, A. Walther, Evaluating derivatives: principles and techniques of algorithmic differentiation, SIAM, 2008.

[98] P. G. Ciarlet, A justification of the von Kármán equations, Archive for Rational Mechanics and Analysis 73 (1980) 349-389.

[99] N. Damil, M. Potier-Ferry, A new method to compute perturbed bifurcations: application to the buckling of imperfect elastic structures, International Journal of Engineering Science 28 (1990) 943-957.

[100] H. J. Al-Gahtani, M. Naffa'a, RBF meshless method for large deflection of thin plates with immovable edges, Engineering Analysis with Boundary Elements 33 (2009) 176-183.

[101] S. Kumar, S. Upadhyay, A. C. Mathur, Wrinkling simulation of membrane structures under tensile and shear loading, Journal of Vibration Analysis 3 (2015) 17-33.

[102] Y. W. Wong, S. Pellegrino, Wrinkled membranes III: numerical simulations, Journal of Mechanics of Materials and Structures 1 (2006) 63-95.

[103] Y. W. Wong, S. Pellegrino, Wrinkled membranes I: experiments, Journal of Mechanics of Materials and Structures 1 (2006) 3-25.

[104] S. Inoue, Prediction methods of wrinkling in thin-membrane, Proceedings of International Symposium on Space Technology and Science, Tokyo, 2009.

[105] S. R. Idelsohn, E. Oñate, F. D. Pin, The particle finite element method: a powerful tool to solve incompressible flows with free-surfaces and breaking waves, International Journal for Numerical Methods in Engineering 61 (2004) 964-989.

Résumé en français de la thèse

Présentation rapide du chapitre 1.

Cette thèse a pour objet la simulation numérique de certaines équations aux dérivées partielles non-linéaires dont on sait qu'elles sont maintenant très largement utilisées dans un grand nombre de domaines. On s'intéressera plus particulièrement à la discrétisation spatiale de ces équations. Les méthodes de discrétisation les plus utilisées sont la méthode des différences finies (FDM) et la méthode des éléments finis (FEM). Pour la mécanique des solides et des matériaux, la méthode des éléments finis est de loin la plus importante, avec des logiciels commerciaux comme ABAQUS, ANSYS, MSC/NASRAN ou IDEAS.

Dans la FDM, on résout l'équation sous la forme forte (méthode de collocation) et on approche les dérivées par des différences comme dans la formule (1.1). L'équation est appliquée en un ensemble de nœuds et ce maillage est structuré, c'est-à-dire qu'on doit connaitre les voisins de chaque nœud pour pouvoir calculer les dérivées. Dans la FEM, l'équation est satisfaite au sens faible (méthode de Galerkin), c'est-à-dire en moyenne pondérée, l'approximation des inconnues et de l'équation étant définie sur des petits morceaux appelés éléments. Cet ensemble de nœuds et d'éléments doit être structuré pour obtenir la continuité du champ et assurer la convergence de la méthode. Ces méthodes fonctionnent bien, ce qui explique leur immense succès. En particulier la méthode des éléments finis est suffisamment souple pour permettre la modélisation de structures très complexes comme un avion ou une voiture, tout en prenant en compte des comportements variés et fortement non-linéaires. Les reproches habituellement adressés à ces deux méthodes sont, d'une part le trop grand nombre de degrés de libertés qui est dû à une approximation trop pauvre sur chaque élément (en général linéaire ou quadratique), d'autre part l'exigence d'un maillage très structuré qui est gênante par exemple lorsque de très grandes déformations requièrent une

opération de remaillage en cours de calcul.

Une autre approche est la méthode des éléments frontières (BEM), basée sur une transformation de l'équation aux dérivées partielles en équation intégrale de frontière. L'avantage obtenu est évident : on aura seulement la frontière à discrétiser, ce qui conduit à des modèles avec beaucoup moins de degrés de liberté. C'est très intéressant à notre époque, où les méthodes de réduction de modèle sont à la mode. La contrepartie, c'est qu'on ne sait construire l'équation intégrale de frontière que pour certains cas où les solutions fondamentales sont connues explicitement, en gros les systèmes linéaires, elliptiques et à coefficients constants. C'est pourquoi la BEM a des applications, en particulier en acoustique, mais il y en a beaucoup moins que pour les deux premières méthodes.

Les méthodes sans maillage (meshless ou meshfree) ont été développées pour éviter la construction d'un maillage structuré qui s'avère coûteuse en termes de « temps-ingénieur » et qui est une exigence forte en cas de très grandes déformations du domaine au cours du calcul. Ici on cherche donc à créer des fonctions de forme et à discrétiser les équations uniquement à partir d'un nuage de points sans aucune autre structure que la position des points. Les premiers travaux sur les méthodes sans maillage datent des années 1970 et on a assisté à une véritable explosion à partir des années 1990. De nombreuses versions de ces méthodes ont été proposées, certaines reposant sur le concept de noyau (kernel) comme la méthode SPH (smooth particle hydrodynamics, voir les équations (1.2) (1.3)), d'autres sur les moindres carrés mobiles (MLS : moving least squares, voir les équations (1.4) (1.6)), d'autres encore sur le concept de fonctions radiales. Certainement les méthodes les plus populaires sont celles déduites du concept MLS. Quant à la discrétisation des équations, on retrouve les deux approches de formulation forte ou formulation faible, avec une double difficulté : avec une discrétisation par collocation, la convergence est moins assurée qu'avec une méthode de Galerkin, mais l'application de la formulation faible demande de calculer des intégrales, ce qui n'est pas facile avec des fonctions qui ne sont pas des polynômes de bas degré et de plus cette intégration reste coûteuse. Après

plus de 25 ans de recherches intensives, il y a quelques beaux succès des méthodes sans maillage, par exemple pour des études de déferlement de vagues qui sont difficiles à traiter avec d'autres méthodes [105], mais pour l'instant, ces méthodes restent assez coûteuses et très peu utilisées dans les calculs pratiques et les principaux codes de calcul commerciaux.

Dans cette thèse, on s'intéresse à la méthode de Taylor sans maillage (Taylor Meshless Method, TMM) développée par Zézé [64], Tampango [65] et Yang [70]. Dans cette méthode, on propose de résoudre analytiquement l'équation aux dérivées partielles par la méthode des séries de Taylor. Cette résolution analytique permet de diminuer fortement le nombre de degrés de liberté comme dans la méthode des équations frontières (BEM), mais à la différence de la méthode BEM, TMM s'applique aisément à des équations non-linéaires, ce qui avait été fait grâce à l'algorithme de Newton ou de Newton-Raphson. Ici on couplera « Taylor Meshless Method » avec la méthode asymptotique numérique (ANM) pour pouvoir traiter des problèmes de plissement de membranes qui sont ingérables avec les codes de calcul existants lorsque la membrane est faiblement tendue.

Organisation de la thèse

L'objectif de la thèse est d'appliquer la « Taylor Meshless Method » à des problèmes d'instabilité de plaques en grands déplacements, en particulier à des problèmes de plissement d'une membrane très souple.

Le chapitre 2 décrit la technique de construction des fonctions de forme, puis l'applique aux problèmes de flexion linéaire des plaques, ce qui n'avait pas encore été fait.

Le couplage de la méthode asymptotique numérique (ANM) avec la discrétisation par TMM est présenté au chapitre 3 dans le cas du modèle classique des plaques de Föppl-von Karman.

Enfin le chapitre 4 aborde un problème particulièrement complexe étudié précédemment par Wong et Pellegrino [102, 103]. Il s'agit d'une plaque souple et

mince soumise à un chargement de cisaillement pour laquelle les méthodes classiques de type Newton-Raphson ou Riks n'ont pas permis d'obtenir de solution satisfaisante, la difficulté principale étant le suivi de courbe pour une membrane peu tendue (slack).

Présentation rapide du chapitre 2.

Ce chapitre présente la procédure désormais bien établie de la « Taylor Meshless Method », puis il en fait une première application aux problèmes de flexion linéaire des plaques élastiques. La clé est le calcul de la solution générale de l'équation aux dérivées partielles (PDE) sous forme de polynômes de degré élevé par la méthode des séries de Taylor : on demande que la série de Taylor du résidu de l'équation s'annule jusqu'à l'ordre p-2, ce qui définit explicitement une solution particulière et la solution générale de l'équation homogène associée sous une forme polynomiale. Cette construction désormais bien établie est décrite au paragraphe 2.2. Ensuite on applique les conditions aux limites et les conditions de transmission dans le cas d'une discrétisation en plusieurs sous-domaines, avec une série de Taylor par sous-domaine. Plusieurs méthodes ont été proposées pour traduire ces conditions et nous avons retenu la méthode de collocation-moindres carrés qui est la plus simple et est au moins aussi efficace que les méthodes basées sur les multiplicateurs de Lagrange. Le test présenté à la figure 2.4 rappelle la robustesse de la méthode alors que la figure 2.5 montre la convergence exponentielle avec le degré de l'approximation polynomiale.

Les paragraphes 2.5 et 2.6 décrivent l'application de la procédure TMM à la flexion des plaques isotropes et anisotropes. On se limite ici à un seul sous domaine et donc à une seule série de Taylor, ce qui peut être un peu pénalisant pour retrouver de très hautes précisions. Le point le plus important est la procédure de calcul des solutions polynomiales qui reposent sur les formules de récurrence présentées au tableau 2.1. Les tests présentés concernent les cas suivants.

1. Flexion d'une plaque circulaire encastrée sous pression uniforme.
2. Flexion d'une plaque carrée en appui sous pression uniforme.

3. Flexion de plusieurs plaques anisotropes stratifiées en appui et soumises à une force sinusoïdale.

Ces tests montrent qu'on peut obtenir une très bonne précision sur les déplacements et sur les contraintes dans la plaque pour des degrés élevés (entre 10 et 15), même avec une seule série de Taylor.

Présentation rapide du chapitre 3.

On étudie dans ce chapitre le fonctionnement d'une plaque en grands déplacements, et on a choisi le modèle de plaques de Föppl-von Karman. Il s'agit d'un modèle non-linéaire qui, contrairement au modèle de Love-Kirchhoff, introduit un couplage entre la réponse en membrane et la réponse en flexion. Dans ce chapitre et le suivant, nous appliquerons notre modèle numérique à des problèmes de bifurcation de structures très minces sous des chargements de compression.

On dispose de nos jours d'un grand arsenal de méthodes pour traiter numériquement des problèmes de bifurcation. On sait par exemple calculer directement les points de bifurcation sur une courbe de réponse non-linéaire, mais la procédure la plus simple est d'appliquer une méthode de continuation et d'analyser les résultats. De telles procédures (Newton, Newton-Raphson, Riks…) sont disponibles dans les codes de calculs existants et ils impliquent d'introduire une perturbation en force ou en géométrie lorsque la structure est parfaitement symétrique. Dans cette thèse, nous avons appliqué la méthode asymptotique numérique (ANM) qui présente plusieurs avantages pour traiter ce type de problème : tout d'abord le suivi de courbe est plus facile car le pas de calcul est défini a posteriori de manière automatique ; ensuite, et c'est une conséquence du point précédent, la méthode fonctionne avec des forces de perturbation plus petites, ce qui permet de traiter des structures presque parfaitement symétriques ; enfin les longueurs des pas de calcul diminuent automatiquement à l'approche d'une bifurcation, ce qui permet de détecter à l'œil des bifurcations éventuelles, simplement en regardant les courbes de réponse obtenues par le processus

de continuation.

La méthode proposée consistera à associer la méthode asymptotique-numérique (ANM) à une discrétisation spatiale par TMM (Taylor Meshless Method), ce qui sera appliqué au modèle de Föppl-von Karman en flèche-fonction de contrainte (3.1). Plus précisément l'application d'ANM transforme ce système non-linéaire en une suite d'équations linéaires à coefficients variables (3.7) (3.8) (3.9), ces dernières étant discrétisées ensuite par TMM. On aura donc une double série de Taylor : d'abord une série par rapport au chargement ou plus précisément par rapport à la longueur d'arc (3.6), puis une série par rapport aux deux variables d'espace x et y. Les problèmes linéaires issus d'ANM se ramènent à la résolution de deux systèmes linéarisés (3.11) à l'ordre 1, puis (3.14) aux ordres suivants : c'est ces deux types de problèmes qui seront résolus par TMM.

La procédure TMM appliquée aux équations de Föppl-von Karman est décrite brièvement à la section 3.3.2. Elle découle de la formule de récurrence (3.16), les coefficients de Taylor apparaissant dans chaque terme de (3.16) s'exprimant simplement à partir des coefficients de Taylor des termes calculés aux ordres précédents comme dans les formules (3.17) ou (3.18). Une fois que ces séries à deux niveaux (ANM et TMM) ont été calculées, la fin du pas ANM est obtenue d'une manière classique en demandant que le dernier terme de la série soit assez petit, voir l'équation (3.20) : c'est ce calcul de longueur de pas a posteriori qui fait la force de la méthode ANM pour les problèmes de bifurcation, un très petit pas pouvant venir juste après un pas très long.

La formulation en fonction de contraintes des équations de Föppl-von Karman est élégante et permet un traitement assez facile des séries de Taylor par rapport aux variables d'espace, mais il est fréquent qu'on doive écrire des conditions aux limites en termes des composantes horizontales du déplacements u et v. Dans le paragraphe 3.3.3, on a donc exprimé ces déplacements à partir de la fonction de contrainte, voir l'équation (3.28) ou sa traduction en termes de coefficients de Taylor (3.29). A noter qu'il apparait alors un déplacement rigide, c'est-à-dire trois inconnues

supplémentaires notées u, v et β dans l'équation (3.35). La manière d'écrire les conditions aux limites et les conditions de transmission est aussi précisée dans ce paragraphe 3.3.3.

Plusieurs applications numériques sont ensuite discutées concernant des plaques rectangulaires. Elles sont ensuite comparées avec les résultats obtenus avec le code par éléments finis ANSYS. Le premier exemple est le flambage d'une plaque carrée en compression bi-axiale en appui. Dans ce cas, on a essayé de prédire le point de bifurcation avec l'imperfection la plus faible possible : les figures 3.3 et 3.4 montrent que le suivi de courbe par ANM-TMM permet de suivre la bifurcation avec une force de perturbation extrêmement faible, beaucoup plus faible qu'avec le code d'éléments finis. Après le calcul d'une plaque en flexion, on s'est intéressé au comportement post-bifurcation d'une plaque en appui sous chargement uni-axial. A la première bifurcation, on obtient un mode sinusoïdal à une bosse et on passe progressivement à un mode à trois bosses (figures 3.9 et 3.11) qui demande une discrétisation plus fine (ici, 16 sous domaines et un degré 10). La méthode proposée permet donc de prévoir ce comportement complexe avec un maillage grossier et un suivi de courbe très précis.

Présentation rapide du chapitre 4.

Dans ce chapitre, la méthode décrite au chapitre précédent sera appliquée à un problème de plissement de membranes. Les membranes et les films très minces sont un sujet d'importance croissante, soit pour des raisons de recherche fondamentale (compréhension des instabilités), soit pour des raisons technologiques (réduction de poids, structures ultralégères…). Le problème choisi est le plissement d'une membrane très mince soumise à un chargement de cisaillement. Ce problème très simple est une source de difficultés pour le calcul numérique, en particulier pour des chargements très faibles car la rigidité quasi nulle en flexion rend la structure extrêmement sensible à la moindre compression. Wong et Pellegrino [102] ont étudié

ce problème avec un code de calcul commercial. Vu les difficultés numériques rencontrées, ils ont choisi d'ajouter un chargement de tension assez important en sorte que la rigidité géométrique due à cette tension compense la trop faible rigidité de flexion. Nous rediscutons ici ce problème de plaque mince en cisaillement pour essayer d'expliquer l'influence de cette tension additionnelle et, si possible, de comprendre le comportement de cette structure lorsque cette tension est très faible.

Le problème de membrane de Wong et Pellegrino est décrit à la Section 4.2. On considère une membrane rectangulaire (rapport d'aspect a/b≈3) très mince (b/h≈5000) et soumise à un chargement principal de cisaillement. Ce problème apparemment très simple s'est avéré ingérable par les méthodes de continuation à longueur d'arc imposée. Il avait été traité par une approche pseudo-dynamique, mais il avait fallu introduire une imperfection géométrique, ce qui est classique dans l'étude numérique des bifurcations, mais aussi une pré-tension qui stabilise le calcul, mais risque de modifier fortement le comportement de la membrane. L'influence de cette pré-tension est donc un enjeu important qui sera discuté dans ce chapitre. Ici l'imperfection géométrique sera produite par une force transversale et non par un défaut initial de planéité, le point important étant la très faible valeur de cette imperfection pour résoudre presque parfaitement le problème de bifurcation.

Les résultats numériques sont présentés à la section 4.3. Il apparait clairement que la procédure de continuation fonctionne et permet de calculer les solutions plissées, même avec une imperfection très faible, et un maillage relativement grossier de 33×11 sous-domaines. L'algorithme de continuation a donné des résultats cohérents même pour des pré-tensions extrêmement faibles (cf Figure 4.8), alors que les résultats de la littérature mentionnent tous la difficulté à faire fonctionner un algorithme de continuation et qu'ils préfèrent en général l'approche pseudo-dynamique et se limitent à des chargements assez grands. Ici on obtient la courbe de réponse pour des cisaillements faibles alors que la membrane est très peu tendue.

Un résultat un peu surprenant est présenté à la Table 4.3 et à la Figure 4.7: pour des

pré-tensions très faibles (0.5μm et 1μm), les modes de déformations n'ont que 3 ou 4 plis alors que la littérature en trouve au moins 10 ou 11 avec des tensions plus importantes. Ces résultats de la littérature ne sont donc pas représentatifs d'une membrane chargée presque uniquement en cisaillement, cette pré-tension transversale modifiant fortement les modes de déformation et les courbes de réponse (Figure 4.8). Une contribution importante de cette thèse, avec le pilotage ANM et la discrétisation TMM, est donc de pouvoir faire ces calculs de structures très molles conduisant à des modèles mathématiques ayant beaucoup de solutions.

L'évolution des formes déformées en fonction du chargement de cisaillement est présentée pour plusieurs valeurs de la pré-tension. Les figures 4.9 et 4.10 présentent le cas d'une pré-tension de 0.05 mm étudié par Wong et Pellegrino : la première bifurcation se produit pour un cisaillement $\delta \approx 0.05$ mm et correspond à un mode très localisé aux bords. Une seconde bifurcation pour $\delta \approx 0.08$ mm déclenche l'apparition de plis plus petits au centre du rectangle, les simulations de Wong et Pellegrino (voir leur Figure 9) présentant la suite de l'histoire pour $0.1 \text{ mm} \leq \delta \leq 2.6$ mm. Pour une pré-tension très faible de 0.001 mm, la bifurcation a lieu beaucoup plus tôt, le nombre de plis est bien plus faible (4 à 6) et les amplitudes des oscillations sont plus uniformes, sans concentration près des bords. Enfin on a simulé l'apparition des plis avec une membrane initialement très molle (pré-tension de 0.0005 mm) : la courbe de réponse (Figure 4.13) oscille fortement dès le début du calcul, avec un nombre très important de pas ANM, signe de la présence de solutions multiples et de nombreuses quasi-bifurcations dues à l'état presque mou de la membrane, les plis correspondant à cet état très mou étant très irréguliers, cf Figure 4.14. Enfin, on discute l'influence de la petite imperfection transversale ajoutée pour déclencher la bifurcation. Dans le cas traité au Tableau 4.5, l'algorithme de continuation fonctionne pour un défaut supérieur à 0.1 μm (en valeur adimensionnelle 1/250) et prédit 11 plis à condition que le défaut ne soit pas trop grand.

En résumé, la méthode de continuation proposée a permis de résoudre ce problème de membrane très difficile, en particulier au début du chargement où la membrane est

très molle. Il est apparu que la pré-tension introduite par Wong et Pellegrino a une très forte influence sur la réponse de la membrane et qu'il y a des différences importantes entre une membrane avec une pré-tension quasi-nulle et celle avec une pré-tension de 0.05mm utilisée par ces auteurs.

Conclusions

Dans cette thèse, on a étudié le comportement des plaques minces et des membranes en utilisant une méthode de collocation-frontière sans maillage (TMM), dans laquelle l'EDP est résolue analytiquement au sens des séries de Taylor et les conditions au bord sont discrétisées par collocation-moindres carrés. Divers paramètres régissant le comportement en flexion, flambage ou plissement sont identifiés.

Tout d'abord, on rappelle les techniques de base de TMM. Ainsi, on réduit fortement le nombre de degrés de liberté en construisant des fonctions de forme solutions de l'EDP. L'efficacité de TMM est illustrée dans le cas d'une équation de Laplace 2D.

Ensuite TMM est utilisé pour étudier les plaques de Kirchhoff et les plaques composites stratifiés. La réduction du nombre de degrés de liberté permet d'augmenter le degré jusqu'à un ordre élevé. Différents tests démontrent l'efficacité de la méthode qui converge exponentiellement avec le degré des polynômes.

Puis on combine TMM avec la méthode asymptotique numérique (ANM) pour étudier des problèmes de flexion de plaques en grands déplacements. On développe les équations non linéaires sous forme de séries entières, ce qui conduit à une suite de problèmes linéarisés. La longueur de pas est déterminée a posteriori à partir des propriétés de convergence des séries. La précision et l'efficacité d'ANM-TMM sont vérifiées à travers quelques exemples de flexion ou de flambage et la technique peut être étendue à d'autres modèles non linéaires.

Notre modèle numérique permet de simuler des phénomènes de flambage, grâce à la technique de continuation. On sait que la méthode de pas adaptatifs d'ANM permet de

détecter des points de bifurcation de manière très précise et avec des imperfections extrêmement petites. Nous vérifierons cette propriété pour divers benchmarks de flambage.

Enfin on s'intéresse au plissement des membranes avec un benchmark de cisaillement d'une membrane rectangulaire très mince qui s'était avérée quasiment impossible à modéliser par d'autres modèles de continuation, même en rajoutant une traction transversale. Nos tests montrent qu'ANM-TMM permet de le faire avec des imperfections très petites et aussi pour des valeurs très petites de la traction transversale. On a vu que cette traction a une influence importante sur la réponse et le nombre de plis obtenus.

Notre travail a montré que TMM est un outil robuste et efficace pour discrétiser divers problèmes d'élasticité linéaire et non-linéaires. Il serait donc important d'étendre les applications de TMM à d'autres domaines des sciences de l'ingénieur. Quelques travaux complémentaires pourraient être menés pour approfondir nos résultats /

1. L'algorithme de calcul des fonctions de forme pourrait être optimisé et généralisé, par exemple avec la technique de Différentiation Automatique.
2. A partir des travaux décrits aux chapitres 3 et 4, une « toolbox » destinée aux structures minces pourrait être développée pour simplifier le prétraitement et la définition des données.
3. Nos études sur les plaques minces forment une bonne base pour l'étude des coques minces. Il serait aussi intéressant d'étendre le champ d'application de TMM à des problèmes difficiles, par exemple les couplages fluides-structures, la mécanique du contact ou les vibrations.

METHODE SANS MAILLAGE DE TYPE TAYLOR POUR PLAQUES MINCES

RESUME : Une nouvelle classe de méthodes sans maillage – Taylor Meshless Method (TMM) – a été introduite. Elle repose sur une solution explicite des équations aux dérivées partielles dans le domaine à l'aide des développements en séries de Taylor. Parce que la PDE est résolue analytiquement dans le domaine, on est réduit à un problème de frontière discret dont la taille est plutôt petite. L'efficacité de TMM a été vérifiée en résolvant certaines PDEs. TMM est utilisé pour résoudre les problèmes de plaques de Kirchhoff et de plaques sandwich laminées. L'erreur montre une convergence exponentielle avec l'augmentation du degré de polynômes. TMM est combiné à la Méthode Asymptotique-Numérique (ANM) pour résoudre les problèmes de grands déplacements de plaques minces. La longueur du pas est déterminée automatiquement par une technique fiable de suivi de courbe. Cette méthode en double série peut facilement être étendue à d'autres problèmes non linéaires. Le processus de flambement peut être illustré de manière beaucoup plus précise que celle d'autres méthodes. La performance de l'approche est examinée par une série de problèmes de flambement de référence. Les problèmes de plissement de membrane sont étudiés. Les résultats montrent que TMM peut réaliser des simulations convergentes avec de très petites imperfections et des charges de tension comparées aux méthodes par éléments finis. L'approche de l'analyse de la membrane ridée par la TMM a été bien établie.
Mots clés : Méthode sans maillage, Série de Taylor, Collocation

TAYLOR MESHLESS METHOD FOR THIN PLATES

ABSTRACT: A new class of meshless method – Taylor Meshless Method (TMM) – has been introduced that relies on an explicit solution of the partial differential equations inside the domain with the help of Taylor series expansions. Because the PDE is solved analytically in the domain, one is reduced to a discrete boundary problem whose size is rather small. The effectiveness and efficiency of TMM have been verified by solving some PDEs. TMM is used to solve Kirchhoff plate and laminated sandwich plate problems. The error shows exponential convergence with the increase of degree of polynomials. TMM is combined with Asymptotic-Numerical Method (ANM) to solve large deflection problems of thin plates. The step length is determined automatically by a reliable path following technique. This double series method can be easily extended to other nonlinear problems. The buckling process can be illustrated much more accurately than that by other methods. The performance of the approach is investigated by a series of buckling benchmark problems. The membrane wrinkling problems are studied. The results show that TMM can accomplish convergent simulations with very small imperfections and tension loads in comparison with finite element methods. The approach of wrinkled membrane analysis by TMM has been well established.
Keywords : Meshless method, Taylor series, Collocation

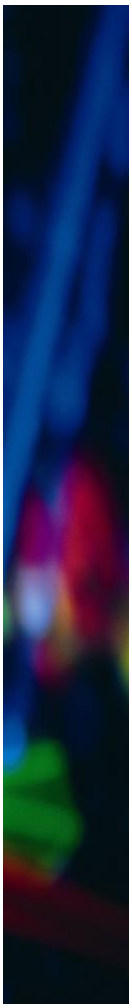

Arts et Métiers Sciences et Technologies

HESAM UNIVERSITÉ